AD-A036 080 ROYAL AIRCRAFT ESTABLISHMENT FARNBOROUGH (ENGLAND) F/G 13/7
METAL SEALS: RESULTS OF A THEORETICAL AND EXPERIMENTAL STUDY OF--ETC(U)
JUN 76 L E RUSKELL

UNCLASSIFIED RAE-TR-76070 DRIC-BR-53653 NL

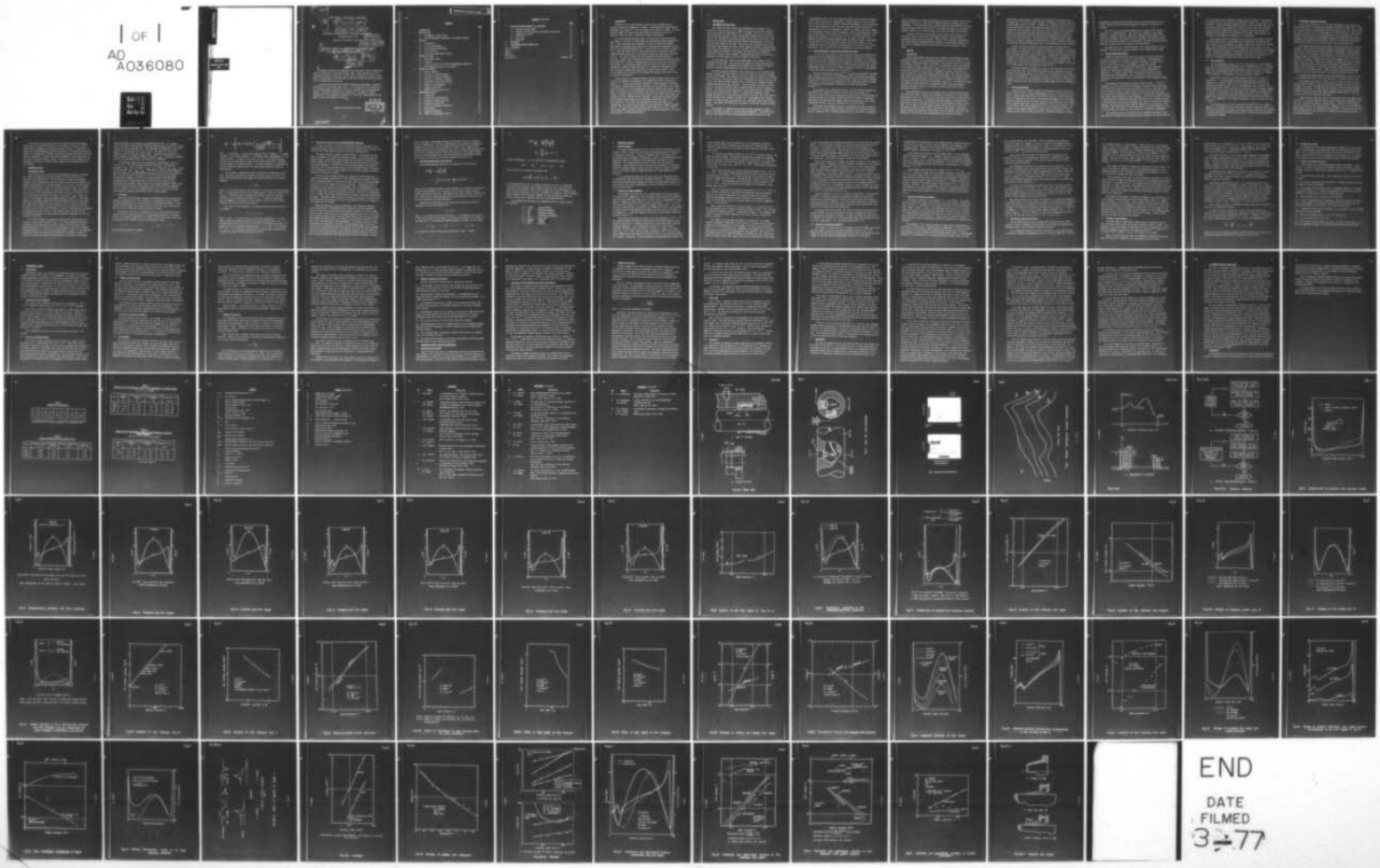

END

DATE FILMED 3-77

UDC 621-762.7 : 629.13.065.2 : 621.89.013

(9) Technical rept.,

(14) RAE-TR-76070

ROYAL AIRCRAFT ESTABLISHMENT

Technical Report 76070

(18) DRIC

Received for printing 9 June 1976

(19) BR-53653

(6) METAL SEALS: RESULTS OF A THEORETICAL AND EXPERIMENTAL STUDY OF THEIR ELASTOHYDRODYNAMIC LUBRICATION.

by

(10) L. E. C. Ruskell

(12) 94 p.

(11) Jun 76

SUMMARY

This Report describes an experimental and theoretical study of elastohydrodynamic lubrication in reciprocating metal seals. Their lubrication was not satisfactory under all conditions, and the aim of the work was to gain a fundamental understanding of the hydrodynamic conditions between the seal and counterface to determine why this was so.

A rig was constructed which enabled simultaneous measurement of pressure distribution and film shape under a seal. On the theoretical side, solutions of the elastohydrodynamic equations are given and compared with the experimental results. The Report concludes with a discussion of the physical factors responsible for the unsatisfactory behaviour of the seals; some suggestions are made as to how these might be overcome.

Departmental Reference: EP 697

CONTENTS

CONTENTS (concluded)

1 INTRODUCTION

The mass of an aircraft hydraulic system tends to decrease as the operating pressure and temperature increase. Increased pressure means smaller components and flowrates[1,2], with an optimum in the range 45 to 60MPa. Increased operating temperature means that less equipment is required to cool the hydraulic fluid, and there is therefore a smaller mass penalty.

The reciprocating elastomeric seals currently used in aircraft systems are limited to a pressure of about 30MPa and a maximum operating temperature of 130°C. Metal seals have been considered in order to realize the possible advantages of extending these limits and of increasing the operational life of seals, thus reducing maintenance costs. Aircraft seals are currently changed on an 'on condition' basis, that is, when trouble occurs; in practice, lives of 12000h have been achieved on civil aircraft, though very much less on military aircraft. Two types of dynamic seal are required in aircraft hydraulic actuators: a piston seal to maintain the differential pressure across the piston, and a gland seal to prevent leakage between the jack rod and the end closure of the cylinder. A conventional piston ring can be used as a piston seal since, although its leakage is higher than that of a conventional elastomeric seal, this is internal leakage and fluid does not escape from the system. Very little leakage can be tolerated from a gland seal, however, and a piston ring is therefore not suitable.

Walsh, Westcott and Lydiard[3] studied a possible design of metal seal, but found its performance unsatisfactory for reasons which will be discussed in section 2.1. The work was therefore extended to a more fundamental investigation aimed at understanding in detail the operation of these seals, the ultimate objective being to use the knowledge thus gained to improve their design. This Report describes how this investigation was carried out and the results obtained, discusses possible reasons for the shortcomings of the present seal design, and suggests how these problems might be overcome. Parts of the work have already been published: descriptions of the experimental techniques used[4,5,6] form a small proportion of the whole and have been included in this Report for completeness, but theoretical work which has been published elsewhere[7] has been omitted. The work has also been written up and submitted as a Ph.D. Thesis[8] which covers similar ground to this Report but, with the exception of the results and discussion, in much greater detail.

2 PREVIOUS WORK

2.1 Development of metal seals

Fig.1 shows the type of metal seal considered by this study. It is basically a truncated metal cone, clamped and statically sealed by O-rings at one end and having an interference fit on a hydraulic jack rod at the other. This interference provides a radial sealing force between the lip of the seal and the jack rod when the pressures are equal on both sides of the seal. The sealing force increases with increasing internal system pressure, which acts upon the outer surface of the seal. Due both to the interference and to the differential area between the outer surface (which is exposed to pressure) and the contact area between seal and rod, the radial stress at the sealing surfaces always exceeds the pressure to be sealed; the sealing force is therefore sufficient to prevent static leakage. Terminology which will be used later to describe the various parts of the seal is given in the figure.

The seal shown has a step at the outside edge of the contact lip (as indicated in the figure). This feature was absent from earlier seals and was introduced for the more fundamental work described in this Report in order to define the contact length between seal and jack rod more precisely.

The seals tested and reported in Ref.3 were found to give extremely high values of breakout friction (that is, the force required to initiate stroking), of the order of 1000N. The leakage, on the other hand, was found to be virtually zero until wear on the lip had reduced the interference fit between seal and rod to zero after about 150 000 stroking cycles, at which point leakage increased dramatically and failure was considered to have occurred. The life of the seal could be increased to 165 000 cycles by flame plating the lip with tungsten carbide. By varying the seal proportions[5] it was possible both to increase the friction still further and to reduce it to within more acceptable limits. Leakage was apparent for seals having low values of friction, and a thin film of oil was visible on the surface of the jack rod. This suggested that a hydrodynamic oil film can exist under the seal lip, resulting in much lower friction values. Seal shapes associated with low dynamic friction also gave low breakout friction.

In an attempt to reduce friction in the boundary lubrication regime a number of possible coatings for the seal lip were examined[9]. It was found that the very hard tungsten carbide coating gave good results provided that the

coating remained intact, but that rapid wear ensued if the coating was damaged. At the other extreme silver plating gave a slightly higher friction and wear rate, but did not break up. However, potential improvements in seal performance due to these coatings were much less than those which had been achieved by operating the seal in the hydrodynamic, instead of boundary, lubrication regime. It was therefore decided to make a fundamental study of the hydrodynamic lubrication of these seals, and to determine the effect of operating parameters, seal material and geometry on the lubricant film. Of course even when a seal normally operates in the hydrodynamic regime the boundary regime is unavoidable in some parts of its duty cycle (for example when stroking begins). Thus suitable coatings could eventually become important, but further work on them was deferred until studies of the elastohydrodynamic regime were complete.

2.2 Elastohydrodynamic lubrication of flexible surfaces

It is now well established that the successful operation of dynamic seals depends upon an elastohydrodynamic film of lubricant between the seal and its counterface to prevent excessive friction and wear; in addition, if a lubricant film can form in both stroking directions leakage is reduced because the sealed fluid can be carried in both directions. Early studies simplified this elastohydrodynamic problem to that of a flexible cylinder rolling and sliding against a plane; this model approximates to an O-ring seal.

Optical interferometry techniques[10,11] and capacitance methods[12] have been used to measure the lubricant film thickness between the cylinder and counterface, and hydrodynamic pressure has been measured using piezo-electric pressure transducers[12]. Theoretical considerations of the problem are similar to those of classical elastohydrodynamic lubrication, and they have been well reported[11,13].

The problem of the sliding rubber cylinder may be considered solved, but few workers have tackled the problem of shapes other than O-rings, the difficulties caused by pressure differentials across the seal, and the effect of confining the seal in a housing. Dowson and Swales[12] carried out some model experiments with square-section rubber blocks and concluded that their elastohydrodynamic behaviour was quite different from that of cylinders.

Simultaneous measurements of pressure distribution and film thickness in an actual seal were first reported by Field and Nau[14], who studied the piston seal of a hydraulic jack. Pressure was measured by a piezo-electric transducer

and film thickness by a capacitance method; the seal was of square cross section. Theoretical work by the same authors[15] showed qualitative agreement with the experiments. The results were quite different from those which had been obtained with an O-ring; further work by Field[16] on a U-seal has shown its elastohydrodynamic behaviour to be different again from O-ring and square section seals.

Thus while much work has been done on seal models, particularly of the O-ring, far less is known about other shapes of seal, or how well models represent actual operating conditions. Since different shapes of elastomeric seal show different elastohydrodynamic behaviour, it was thought unlikely that any of the previously reported research would be directly relevant to metal seals.

3 TEST RIG

3.1 Introduction

The main experimental requirement is to measure the hydrodynamic pressure distribution and the oil film thickness between the seal and the jack rod. The techniques of Dowson and Swales[12] mentioned in the previous section were thought to be the most suitable. Field and Nau[14] had successfully applied these methods to the study of a rubber piston seal; using a seal of this type enabled them to mount their transducers in the wall of a hydraulic cylinder. Since there is little difference in principle between elastomeric gland seals and piston seals their work was considered to be applicable to both types. In contrast the metal seal of the type being studied is more difficult to arrange as a piston seal and there is not much need for its development in this role. A difficult problem in studying the metal gland seal is therefore to mount the instrumentation inside the hydraulic jack rod. The manner in which this was done will be described in section 3.2.

The instrumented jack rod is a straight cylinder running through a hollow test block with a seal at either end, and there is therefore no net hydrostatic force acting on the rod. One end of the test block houses the test seal and the other end a labyrinth seal. Stroking is achieved by means of a driving jack, and stroke reversal is by limit switches and an electrohydraulic selector valve. There are two types of relative motion between a gland seal and a jack rod: outstrokes, in which a point on the jack rod moves from inside to outside the sealed cylinder; and instrokes, where motion is in the opposite direction. The interior of the test block can be pressurized, and the pressure cycle is

controlled by limit switches. Pressure can be applied on outstrokes only, on instrokes only, or on both strokes. Pressure is supplied to the test block via a double-ended hydraulic actuator. Pressure from a hydraulic power pack is fed into one end of the actuator; the other end contains the test fluid, and this is connected to the test block. Test fluid can thus be isolated from the working fluid of the main pressure supply enabling different fluids to be tested in contact with the seal without the necessity for dismantling and cleaning the whole of the main power pack. The main purpose of changing fluids in these tests was to simulate temperature variations using oils of different viscosities, but obviously different fluids might need to be investigated for other purposes.

Profiles of pressure distribution and film shape are displayed on an oscilloscope. To enable the trace to move in opposite directions for outstrokes and instrokes the horizontal trace deflection is achieved by means of a displacement transducer connected to the driving jack. Stroking speed is measured by an inductance transducer and displayed on a digital voltmeter; the sampling of this voltmeter is controlled by a microswitch which is in turn activated by the driving jack. By adjusting the position of the microswitch sampling can be done at the same instant that the probes pass under the seal.

Friction is measured by means of a load cell situated between the driving jack and the test jack. The results inevitably contain components due to the friction of both seals; however the friction of the labyrinth seal is assumed to be very low and neglected. No provision was made for measuring leakage directly; equipment to do this has been developed, but many hours' testing is required to obtain a reliable result, and this was not thought feasible for this fundamental study.

3.2 Pressure measurement

A piezo-electric pressure transducer was mounted inside the jack rod as shown in Fig.2 in order to measure hydrodynamic pressure. Pressure acts on the end of a piston which projects onto the surface of the rod, and the resultant force is transmitted by the piston to the pressure-sensitive face of the transducer; the clearance between the piston and the rod is sealed at the rod surface with a flexible epoxy resin to prevent leakage of fluid into this space. Without the piston, with fluid impinging directly on the pressure transducer, the volume of fluid trapped inside the rod would be very large relative to the volume of fluid in the oil film; the predicted compression flow due to typical

hydrodynamic and system pressures would then be of the same order as the oil volume. This would obviously cause inaccurate readings, so the piston is necessary.

The cable from the transducer passes down the centre of the rod and is connected to a charge amplifier. The total input impedance to the charge amplifier, including transducer, cables and connectors, must exceed $10^{14}\Omega$ for satisfactory response. The connector on the transducer could not be cleaned once the rod had been assembled, so a sheath made of a high resistance silicone rubber was moulded around the junction to exclude moisture.

The pressure probe is self-calibrating, since system pressure acts as a reference, and this can be measured statically with a simple Bourdon gauge.

3.3 Film thickness measurement

Changes in capacitance between the seal and an insulated brass insert in the jack rod are used to deduce oil film thickness. The capacitance changes are measured by a frequency modulation technique: the probe forms part of an oscillator circuit, and changes in capacitance produce corresponding changes in the frequency of oscillation. These frequency changes are converted by a demodulator to a dc output proportional to capacitance. To obtain a signal which is directly proportional to film thickness rather than capacitance, and to eliminate the effect of stray capacitances, the demodulator output is processed by a small analogue computer network.

The mounting of the capacitance probe is shown in Fig.2. In order to assemble the rod both probes were first mounted on tapered plugs; these were then pressed into tapered holes drilled radially in the rod. The axial length of the capacitance probe is 0.5mm, giving the same axial resolution as the pressure probe. Circumferentially, however, the film thickness is averaged over about 10mm. After assembly and final grinding, a Talysurf profilometer was used to check whether the capacitance probe was flush with the rod surface (a stylus is traversed across the surface of interest, and vertical motion of the stylus is converted into an electrical signal which is amplified and recorded on a chart recorder). This showed that the probe had suffered a permanent depression into the rod of 0.75μm, so this had to be allowed for in subsequent measurements.

Two methods were used to calibrate the film thickness measuring system. The first was to measure all the various circuit parameters and thence calculate

the relationship between demodulator output and film thickness. The second was to calibrate directly by measuring the demodulator output due to a known film thickness. Careful measurement showed the radial clearance between the jack rod and a flange of the seal housing to be between 70μm and 74μm. The clearance calculated from the demodulator output was between 72μm and 75μm after due allowance had been made for the depression of the probe. This agreement was considered to be adequate confirmation of the calibration.

When system pressure was applied it was found that the measured clearance increased between jack rod and flange; whilst deformation of flange and rod under pressure are to be expected, it seemed possible that some of this increase might be due to depression of the capacitance probe into the jack rod. By changing the system pressure from 0 to 13.8MPa the radial clearance was increased by 7μm. Treating the flange as a compound cylinder and the jack rod as a simple cylinder the corresponding expected change in clearance was calculated to be about 5μm. This gives a probe depression of about 2μm at 13.8MPa.

3.4 Test conditions

All the experimental results refer to a brass seal with a silver-plated lip. Two such seals were manufactured, and are designated A and B. A Talyrond showed seal B to be the more nearly cylindrical, and so this seal was used for almost all the experiments; seal A was used to examine the effect of changing the seal geometry. The dimensions of seal B are given in Table 1.

Three test fluids were used: DP47, OM160 and diesel fuel. DP47, or Silcodyne 'H', is a chlorinated silicone polymer capable of operating at temperatures in excess of 200°C, and is the fluid with which the seals are ultimately intended to be used. As all the experiments were conducted at an ambient temperature of 22°C, the other two fluids were used to simulate changes in viscosity at both ends of the temperature range. OM160 is a straight mineral oil having a viscosity about six times greater than that of DP47 at ambient temperature; the viscosity of diesel fuel is about 20 times less than that of DP47 at that temperature. The relevant properties of the test fluids are given in Table 2.

The stroking speed of the test jack could be varied from 0 to 250mm/s. However, at low speeds the motion was found to contain a large oscillatory component and this prevented a steady state being attained. Readings were therefore not taken at speeds below 60mm/s; the oscillatory component becomes negligible at approximately 50mm/s.

3.5 Preliminary experimental results

At zero system pressure an oil film and hydrodynamic pressure generation were observed both on outstrokes and instrokes using DP47 or OM160 fluid. There was no such evidence of hydrodynamic lubrication using diesel fuel, and few tests were made with this fluid to avoid damage to the sliding surfaces. When system pressure was applied lubrication was maintained on the outstrokes but on the instrokes records showed no hydrodynamic pressure and negligible film thickness. Subsequent investigations were therefore confined to the outstroke and system pressure was reduced to zero on the instroke to avoid unnecessary wear.

Fig.3 shows typical oscilloscope traces of pressure distribution and film thickness. The transition from system pressure to atmospheric pressure can be clearly seen on the outstroke, where significant hydrodynamic pressure generation occurs. On the instroke, system pressure is zero, and a very small hydrodynamic pressure is visible at the instroke inlet. An oil film can be seen on outstrokes, although it appears that electrical breakdown occurs at the outlet, where the film is thin. Electrical breakdown can be seen over almost the whole contact during instrokes. The outstroke film shape is remarkable in that the film at inlet and outlet is relatively much thinner than at the centre of the contact, but no cavitation occurs. This is contrary to expected hydrodynamic behaviour, and this point will be dealt with in more detail in section 4.1.

Increasing the system pressure caused large distortions of the seal, and it was decided that seals A and B were unsuitable for pressures above 14MPa.

Film thickness was found to vary by a factor of about two when the jack rod was rotated relative to the seal, and this is thought to be due to out-of-roundness of the seal. Although the basic features of the lubrication remained unchanged with rotation, it was necessary to ensure that the angular position of the rod remained constant when making systematic measurements of, say, the variation of inlet film thickness with speed.

It was found that the jack rod had to stroke about twice the length of the seal lip[5,6] at constant speed in order to attain steady-state conditions in the oil film. This was determined by viewing traces at different stroke lengths until two successive traces were identical. Changes in the oil film are propagated axially at about the average oil velocity, which in this case is about half the stroking speed, so the criterion for reaching the steady state has some theoretical foundation.

The purpose of this section has been to describe general experimental observations of a qualitative nature on the behaviour of the seal. Before presentation of systematic, quantitative results, however, it is pertinent to examine the elastohydrodynamic problem theoretically. A particularly important theoretical consideration is whether the observed pressure distribution and film shape are compatible. Normally the rapidly diverging oil film found under the seal would be associated with a region of cavitation: in fact, pressure in the diverging film actually increases. This problem will be discussed under the next heading.

4 THEORETICAL STUDY

4.1 Hydrodynamic theory

The oscilloscope traces of Fig.3 show hydrodynamic pressure increasing in a region of diverging oil film and regions of relatively thick film associated with high pressures. This is contrary to expected hydrodynamic behaviour, where diverging oil films are usually associated with cavitation and pressures are highest in the thinner regions of an oil film. For most hydrodynamic situations this is true, and it has been shown by Blok[17] and Theyse[18] that if the film shape is similar to that shown in Fig.3, with minima at the inlet and outlet and a maximum inbetween, then if rupture of the fluid is not to occur the film thickness at the centre of the contact $h_{max} < 3h_0/2$; h_0 is the film thickness at which the pressure gradient $dp/dx = 0$. The author, however, has considered slightly different hydrodynamic conditions and shown that under some circumstances there need be no limit to the film thickness at the centre of the contact, and that the pressure in this region can be high relative to that in the thin film region at the inlet. The theoretical arguments are examined rigorously in Ref.7; it is sufficient here to state that the circumstances necessary for these unusual hydrodynamic conditions to exist are satisfied in the seal.

Four distinct shapes of pressure distribution can be defined that are relevant to seals, and are shown in Fig.4. All these pressure distributions correspond to film shapes which are thin at inlet and outlet with a central maximum inbetween. A distribution of the type shown in curve I will hereafter be designated mode I, a curve II distribution mode II, and so on. The important difference between these pressure distributions is the number of points of inflection on them, the position of these points in relation to the pressure

maxima and minima, and the number of such maxima and minima. For example, curve I has only one such point of inflection between pressure peaks and troughs, whereas the other curves have more. The film shape corresponding to mode I is subject to the constraint that $h_{max} < 3h_0/2$. For modes II, III and IV, however, it can be shown that $h_{max} > 3h_0/2$. The pressure distribution of Fig.3 conforms to the shape of a mode II solution, h_{max} is therefore unlimited, and the two experimental results can therefore be compatible.

The difference between the film thicknesses corresponding to modes II, III and IV is in the film thickness minimum at the inlet. Denoting this minimum by h_{min} , then: for mode II $h_{min} < h_0$; for mode III $h_0 < h_{min} < 3h_0/2$; and for mode IV $3h_0/2 < h_{min} < h_{max}$. Each mode has certain salient features which may enable it to be identified qualitatively from the oil film profiles as well as from the pressure distribution. Thus in practice the film shapes corresponding to modes I, II and III are characterized by film thickness minima which are of similar magnitude at inlet and outlet; mode I can be identified by the relatively small central film thickness maximum. Modes II and III are extremely difficult to distinguish qualitatively from film thickness alone, but mode IV can be distinguished from II and III by the fact that the inlet minimum is generally much larger than the outlet minimum.

4.2 Elasticity

Deflections of the surfaces bounding the hydrodynamic oil film modify the pressure distribution, and a full treatment of the problem therefore requires the simultaneous solution of the elasticity and hydrodynamic equations. In the present case this means calculating the deflections of the metal seal and the jack rod due to an arbitrary pressure over their surfaces.

An analytical solution is available[19] for the stresses and deflections of a solid circular cylinder subjected to a discontinuous pressure on its curved surface. By using the complex Fourier integral transform the radial deflections at the surface of a cylinder subject to the pressure loading

$$p = 0 \quad , \quad x < 0 \quad ; \qquad p = p_0 \quad , \quad x \geq 0$$

are given by the indefinite integral

$$\frac{Eu}{R} = -p_0\left[\frac{(1-\nu)}{2} + \frac{2(1-\nu^2)}{\pi}\int_0^\infty \frac{\sin\left(\frac{zx}{R}\right)dz}{z\left[z^2\left\{\frac{I_0(z)}{I_1(z)}\right\}^2 - z^2 - 2(1-\nu)\right]}\right]$$

where p is pressure, x the distance along the axis of symmetry, z a dummy variable, E the elastic modulus, u the radial surface displacement, R the jack rod radius, ν Poisson's ratio, and I_0 and I_1 are modified Bessel functions of the first kind, of orders zero and one respectively. Evaluation of this integral is described in Ref.8. An arbitrary pressure distribution can then be idealized as shown in Fig.5, and the surface deflections found by superposition.

Finite element techniques were used to calculate the deflections of the seal. The seal is divided into a number of discrete elements joined at the nodes, and by minimizing strain energy the analysis produces a set of linear equations

$$\underline{f} = D\underline{v}$$

where $\underline{f}$ is a column vector of nodal forces, $\underline{v}$ a vector of nodal displacements, and D a square matrix known as the stiffness matrix. Loading is applied in the vector $\underline{f}$, sufficient nodal constraints are applied to prevent rigid body movements, and the equations are solved for $\underline{v}$. A computer program which employs axisymmetric isoparametric cubic elements, such as are described by Zienkiewicz[20], was written for this purpose.

The 'elastic' film thickness h is obtained from the deflections by the relationship

$$h = u + v + c - i$$

where u and v are the rod and seal deflections respectively, i is the radial interference between seal and rod at some fixed datum point, and c is the undeformed profile of the seal lip relative to this fixed datum caused, for example, by wear and machining imperfections; h, u, v and c are functions of x, and i is a constant. The profile of an actual seal is measured with a Talysurf and used in the theoretical calculations.

4.3 Iterative solution of the elastohydrodynamic equations

A computer program was written to solve the equations discussed in the preceding sections; there is still the problem of coupling them so that both the elasticity and hydrodynamic equations are satisfied simultaneously.

Two common iterative schemes are shown in Fig.6. The solution for the seal is achieved in two stages and uses both schemes. In the first stage the inverse scheme is employed; an initial guess at the pressure distribution is modified manually by the programmer to bring the deflections and film thickness into better agreement. The efficiency of this process depends upon operator experience, but a reasonably good solution can be obtained in about five cycles. This is then used as the starting estimate for an entirely automatic iterative procedure in the computer program.

The most obvious automatic procedure is the direct method described, for example, by Stephenson and Osterle[21]. Film thickness gives a pressure distribution via Reynolds equation, this gives an elastic deflection, and the new shape is used as the film thickness for the next iteration. Although the region of convergence can be extended by under-relaxation, that is by weighting the new film thickness with that from the previous iteration, the method basically works only for light loads, when the deflections are small relative to the film thickness. At higher loads, when the deflections are larger, alternative methods must be sought. The simple scheme was found to diverge in the case of the metal seal. The method eventually adopted to close the loop and obtain the next estimate of film thickness is as follows.

Having obtained the starting approximation, the hydrodynamic pressure distribution and the corresponding elastic deflections are very sensitive to values of inlet and outlet minimum film thickness; therefore if the film thickness and elastic deflections are in reasonable agreement the values of inlet and outlet minima obtained from the inverse Reynolds equation must be quite accurate. The maximum film thickness has little effect on the pressure distribution, however, and is therefore known only approximately. The absolute values of elastic displacements are sensitive to pressure, but the deformed shape is not, so it follows that the differences between the maximum film thickness and its minimum values are also known accurately. The iterative procedure is to use values of inlet and outlet minima obtained from the inverse Reynolds equation as a datum for the elastic deflections, and thereby obtain a new film thickness. This is

used to calculate a hydrodynamic pressure distribution, which in turn gives a new set of deflections. To a first approximation the system has two degrees of freedom, and the inlet and outlet minima are adjusted until values of film thickness agree with the corresponding deflections to within some specified limit. Once a fully converged solution has been obtained the initial stage of manual iteration can be dispensed with, since by successively incrementing variables each solution can be used as a starting estimate for the next case.

4.4 Non-dimensionalization of the problem

The elastohydrodynamic equations to be normalized are of the form

$$e^{-\alpha p}\frac{dp}{dx} = 6\eta_0 U\left[\frac{h - h_0}{h^3}\right]$$

$$h = \int_{-\infty}^{\infty} K_1(x,z)p(z)dz + \oint_s K_2(x,s)p(s)ds + c - i$$

where the first integral denotes a linear operation on the pressure distribution to obtain the deflections of the jack rod and the second integral denotes a similar operation for the seal. The range of the second integration implies that $p(s)$ refers to the pressure acting over the entire surface of the seal, and includes atmospheric and system pressures.

Neglecting the deflections of the jack rod and replacing the second integration by a matrix multiplication,

$$\underline{v} = \frac{L}{E}K\underline{p}$$

where $\underline{v}$ is a vector of the seal deflections, L the length of the contact, E the elastic modulus of the seal, $\underline{p}$ the pressure acting over the surface of the seal, and K a dimensionless compliance matrix. Putting $P = p/E$ gives

$$\bar{H} = h/L \qquad X = x/L \qquad C = c/L \qquad \bar{I} = i/L \quad .$$

For a numerical solution the normalized equations at node i become

$$e^{-\alpha E P_i} \frac{dP}{dX_i} = \frac{6\eta_0 U}{EL}\left[\frac{\bar{H}_i - \bar{H}_0}{\bar{H}_i^3}\right]$$

$$\bar{H}_i = \sum_{j=1}^{m} k_{ij} P_j + C_i - \bar{I}$$

where the elements of K are a function of the geometrical groups

$$R/L \ , \quad t_1/L \ , \quad t_2/L \ , \quad L_1/L \ , \quad L_2/L \ .$$

The solution of the equation thus depends upon

$$p_s/E, \frac{\eta_0 U}{EL} , \alpha E, \frac{i}{L} , \frac{c_1}{L} , \frac{c_2}{L} , \ldots, \frac{c_n}{L} , \nu$$

and the geometrical groups. In theory the profile can vary in a completely arbitrary manner along the entire length of the seal, but in practice this variation is very limited. Most of the variables are ratios of lengths, so for given relative proportions of the seal the number of variables is greatly reduced. Other variables such as friction, leakage and total sealing load, which are derived from the basic equations, may also be non-dimensionalized.

The dimensionless parameters are summarized below for a given relative seal geometry:

$\bar{U} = \eta_0 U/EL$		speed parameter
$\bar{P} = p_s/E$		pressure parameter
$\bar{G} = \alpha E$		materials parameter
$\bar{I} = i/L$		interference parameter
$\bar{W} = w/EL$		total load
$\bar{Q} = \eta_0 Q/EL^2$		leakage
$\bar{F} = F/EL$		friction .

5 THEORETICAL RESULTS

5.1 General comments

The results presented below are for a seal having the dimensions of seal B shown in Table 1, except where the effect of varying geometrical proportions is discussed in section 5.6. Only the isothermal case is treated, and the lubricating fluid is assumed to be Newtonian. Values of the dimensionless parameters were chosen to correspond with experimental conditions for easy comparison. For reasons given in section 3.5 only seal outstrokes are discussed. Unless otherwise stated, solutions were obtained by the automatic iterative procedure; manual solutions are given where the automatic procedure would not converge or where a marked difference was found between the two solutions.

It has already been noted that the seal profile and interference vary circumferentially and are difficult to measure accurately. Standard profiles were therefore defined when studying the effect of varying speed, pressure, etc. Three profiles were used corresponding to Talysurf traverses of the seal lip, and are shown in Fig.7.

5.2 Variation of speed parameter

This parameter can vary over a wide range because of the large change in oil viscosity with temperature. For a brass seal lubricated by DP47 hydraulic fluid over the temperature range $-40^{\circ}C$ to $+200^{\circ}C$ and at stroking speeds of from 60mm/s to 250mm/s the speed parameter lies in the range 3×10^{-13} to 3×10^{-10}. The results given below are at a pressure parameter value of 6.85×10^{-5}; this value was chosen because it corresponds to 6.89MPa (1000 lb/in^2) system pressure for seal B, which is experimentally convenient and more results are available for comparison. It also lies roughly in the centre of the pressure range discussed in section 5.3.

Fig.8 shows the pressure distribution and film thickness at $\bar{U} = 5 \times 10^{-11}$. Both profiles exhibit the features which have already been discussed at some length: in particular, a rapidly diverging film is associated with a high and increasing pressure. In the terminology of section 4.1 it is a mode II solution: this means that at the centre of the film $h > 3h_0/2$, and at the inlet $h_{min} < h_0$. Fig.9 shows the speed increased to 10^{-10}. Both inlet and outlet pressure peaks are reduced, but the total load $\bar{W}$ and the film thickness $\bar{H}_0$ increase, as expected. In more conventional elastohydrodynamic contacts the

outlet pressure spike, which is mainly due to the exponential increase of viscosity with pressure, becomes more pronounced with increasing speed. It therefore seems reasonable to attribute the peak found under the seal to some other cause.

If the speed is increased further to 1.44×10^{-10}, as shown in Fig.10, the mode of solution changes. The pressure distribution no longer has a maximum near the inlet but merely the series of points of inflection of the third mode. The film thickness is qualitatively similar to that of mode II solutions, but at the inlet $h_0 < h_{min} < h_a$. For $\bar{U} > 1.8 \times 10^{-10}$ the automatic process does not converge.

Fig.11 shows the effect of reducing the speed parameter from 5×10^{-11} to 3.5×10^{-11}. The pressure spikes become sharper but the basic features of the distribution are preserved. As the speed is reduced still further the type of solution changes from the second to the fourth mode, as shown in Fig.12, where $\bar{U} = 2.5 \times 10^{-11}$. This mode persists as the speed is further reduced to 10^{-11} and 7.5×10^{-12}. The outlet pressure spike becomes very pronounced at these speeds (Figs.13 and 14).

Since the predicted outlet minimum film thickness at $\bar{U} = 7.5 \times 10^{-12}$ is about 0.25μm in dimensional terms under the experimental conditions studied, there did not seem to be any point in reducing the speed still further; effective hydrodynamic lubrication would obviously not be possible at this order of film thickness, given the sliding conditions and surface roughnesses likely to be encountered.

Fig.15 shows the variation of load with speed. At low speed the film is thin and changes little in absolute value with changes in speed. The total load is therefore reasonably constant. At high speed, changes in film thickness are larger and hence the elastic component of the total load due to deflection varies noticeably.

The change of solution mode with speed is interesting. The computer program is designed to seek mode II, if it exists. The transition from mode II to mode III is continuous (as is that to mode I, but this is not encountered except at $\bar{P} = 0$; see section 5.3). Therefore, at the higher end of the speed range there is no problem in moving gradually into mode III. The transition at low speed from mode II to mode IV, however, is discontinuous; the program only seeks a solution of this latter type if none can be found in the preferred mode

II (this process implies consciously abandoning mode II and starting the solution again). If this situation is altered, so that the program seeks mode IV from the outset, it is possible to obtain two solutions under the same set of conditions, as shown in Fig.16. Thus solutions are not necessarily unique; whether mode IV exists whenever mode II exists has not been determined. Mode II is the more important because it corresponds to the first stable state which the seal encounters as the jack rod starts stroking and the film grows.

The question remains as to whether the absence of mode II at low speeds is physically correct or whether it is due to numerical instability of the iterative solution. Experimentally, mode II solutions do exist in the relevant speed range, and approximate theoretical solutions of this type can be obtained by manual iteration. Fig.17 shows a manual solution at $\bar{U} = 10^{-11}$, and the corresponding fully converged automatic solution. Although this manual solution is very good, no way could be found to persuade the automatic process to converge on it. Convergence is always faster and easier in mode IV than in mode II, and it seems likely that the lack of mode II is due to an overwhelming numerical preference for mode IV, or instability in mode II, rather than physical reality. The existence of two modes at the same speed has also been detected experimentally and will be described in section 6.4.

Another problem is the lack of a solution at high speed. Using automatic iteration, all modes are numerically unstable, but manual solutions were obtained, and it seems physically unlikely that lubrication should suddenly cease as the speed is increased. It was not thought worthwhile to expend what would doubtless need to be a great deal of effort on this problem, which only occurs at the extreme end of the speed range.

Fortunately the film thickness $\bar{H}_0$ varies continuously with speed even though the mode of solution may change. Therefore, although the theoretical and experimental modes may be different, a single continuous curve may be used to represent the variation of film thickness with speed, and is shown in Fig.18. To a first approximation $\bar{H}_0$ is directly proportional to $\bar{U}$.

5.3 Variation of pressure parameter

The range of pressure which is of interest is from 0 to 60MPa; for a brass seal this gives a variation of pressure parameter from 0 to 2.75×10^{-4}. However it was found that at pressures above about 14MPa the predicted oil film became too thin for effective hydrodynamic lubrication to take place.

No experiments were performed above this pressure owing to gross distortion of the seal and very thin oil films, and the consequent risk of damage to the sliding surfaces. Theoretical calculations were therefore only made for pressure parameter variations in the range 0 to 1.37×10^{-4}.

Fig.19 shows the variation of film thickness with $\bar{P}$ at two different values of materials parameter $\bar{G}$. Automatic solutions could not be obtained for $\bar{P}$ less than 4×10^{-5}. Clearly, system pressure is an important variable which has a marked effect on the film thickness. For a seal with the dimensions used in the experiments effective lubrication is not predicted for $\bar{P}$ greater than about 1.5×10^{-4}.

The automatic solutions are mode II between $\bar{P} = 5.5 \times 10^{-5}$ and 8.2×10^{-5}. Below this range there is a gradual transition to mode III; above it, the solution jumps to mode IV. Fig.20 shows the pressure distributions at these pressures, and Fig.21 the corresponding film thicknesses. Although no automatic solution could be found at low values of $\bar{P}$, manual solutions were obtained. Because of the smaller amount of distortion at $\bar{P} = 0$, first mode solutions can exist. Fig.22 shows manual first and second mode solutions at this pressure for different profiles. The solution is extremely sensitive to profile and interference changes because the load is entirely due to elastic forces.

5.4 Variation of materials parameter

The probable variation of the parameter $\bar{G}$ is quite small. The elastic modulus of likely seal metals does not vary by more than a factor of about two, and if only DP47 is considered as the working fluid then $\bar{G}$ varies from about 2000 to 4000. However, in some of the experiments OM160 mineral oil was used, which has a higher viscosity-pressure coefficient than DP47, and so the effect of varying the materials parameter from that of an isoviscous fluid to that of steel lubricated by OM160 was studied. Fig.23 shows the resulting changes in film thickness; points corresponding to particular combinations of materials are indicated.

The parameter $\bar{G}$ is normally neglected in seals work by considering the lubricant to be isoviscous. Although viscosity enhancement is only of the order of a factor of two, and hence small compared with what may occur in point or line contacts, it does increase the film thickness significantly - at experimental values of $\bar{G}$ the increase over an isoviscous fluid is nearly 70 per cent with

DP47 and about 100 per cent with OM160. This is insufficient to change the lubrication regime; for example, it would not extend the hydrodynamic region significantly into the low-speed range, but it needs to be accounted for in any comparison between theory and experiment. The solutions given in Fig.23 are for $\bar{U} = 5 \times 10^{-11}$ and are all in the second mode.

Figs.18 and 19 show the effect of varying speed and pressure at two different values of $\bar{G}$ corresponding to experimental conditions; the curves differ only in absolute magnitude, there being no change in general form or slope with material variation.

The experimental seals were silver plated over the contact zone. For theoretical purposes the seal was treated as being made entirely of brass. The validity of this assumption was tested by repeating the case shown in Fig.9 for $\bar{U} = 10^{-10}$ and with a coating of silver 0.082mm thick over the contact zone. The film thickness $\bar{H}_0$ was reduced from 6.36×10^{-4} to 6.26×10^{-4}. This effect was considered negligible, given other uncertainties such as profile and interference, and was neglected.

If the jack rod is assumed to be rigid then for the case shown in Fig.8 $\bar{H}_0$ drops from 3.19×10^{-4} to 3.08×10^{-4}. This is also a small quantity, but since the problem had to be solved to obtain this figure, and since the computing time needed to produce jack rod deflections was small, the effect of the elastic rod was included in all the calculations.

The elastic modulus of the seal is incorporated in the materials parameter $\bar{G}$: Poisson's ratio for the seal, however, appears in the dimensionless compliance matrix, and this must be considered in conjunction with the materials parameter if changes in the latter are produced by varying the seal modulus E rather than by changing α . In practice the possible change of Poisson's ratio ν is small; changing ν from 0.35 (brass) to 0.295 (steel) changes the film thickness $\bar{H}_0$ for the case of Fig.8 from 3.19×10^{-4} to 3.09×10^{-4}.

5.5 Interference and profile effects

These variables have not been included under the next section on seal geometry: they are independent variables which do not affect the dimensionless compliance matrix, and are therefore discussed separately.

The interference between the seal and the jack rod is one quantity which is difficult to measure experimentally, and it is therefore important to see how

film thickness depends on this parameter. Initial limits on the interference tend to be set by rule of thumb. A minimum interference must always be present, making allowances for possible out of roundness and machining tolerances, and experience suggests that this should be at least 12μm on diameter. If the interference is too large excessive force will be required during assembly and damage to the seal will result. Again, experience shows that 30μm is about the maximum. This gives an interference parameter $\bar{I}$ in the range 8×10^{-4} to 2×10^{-3}.

Fig.24 shows the effect of varying the interference over this range. The order of the effect is similar to that of the materials parameter: it has a significant effect on film thickness (in this case nearly halving it) but not to the extent of changing the lubrication regime.

The interference on the seal will vary continuously throughout its life as wear occurs, and although the range given above is for reasonable design limits, in practice $\bar{I}$ may approach zero. No solutions have been undertaken in this region but it should be noted that film thickness does not grow indefinitely with decreasing $\bar{I}$, except when $\bar{P} = 0$, because a load is still provided by system pressure. The pressure component thus forms an ever greater proportion of the load as wear takes place.

No attempt has been made to quantify the changes in the seal profile, or to investigate them systematically: Fig.25 merely shows a plot of $\bar{U}$ against $\bar{H}_0$ for profiles 1 and 2 of Fig.7. Small changes in profile produce small but significant changes in film thickness, in this case of the order of 10 per cent. Since the profile varies circumferentially around the seal this suggests that experimentally a variation in measured film thickness is to be expected between different portions of the seal lip. The curve for profile 1 shows a slight discontinuity when the solution mode changes.

5.6 Changes in seal geometry

The large number of geometrical variables makes a systematic study of their influence impracticable over the entire range of possible designs. Each dimension in turn was therefore varied about the value corresponding to seal B, and its performance calculated for the operating values: $\bar{U} = 5 \times 10^{-11}$; $\bar{P} = 6.85 \times 10^{-5}$; $\bar{G} = 2060$; $\bar{I} = 1.42 \times 10^{-3}$; profile 2 was assumed.

Curve 1 of Fig.26 shows the effect of changing the thickness of the seal lip at the free end. Increasing t_1/L increases the film thickness

significantly, and $\bar{W}$ changes from 1.16 to 1.24×10^{-4} as t_1/L varies from 0.027 to 0.047: for seal B, $t_1/L = 0.04$. The increase in $\bar{H}_0$ which can be realized by changing t_1/L is limited by assembly problems, since normal stress along the contact is proportional to t and i .

The figure also shows in curve 2 that a small increase in film thickness can be obtained by thickening the root of the seal. This is to be expected, since it stiffens the shell and allows more of the load to be borne by hoop stress. In general, therefore, thickening the seal material increases film thickness; however, it seems likely that an optimum exists and that too thick a seal will affect the value of $\bar{H}_0$ adversely.

Increasing the step height from $L_2/L = 0.011$, as in seal B, to 0.013 decreases $\bar{H}_0$ from 3.19×10^{-4} to 3.09×10^{-4}. Although this effect is negligible, the trend is again to increase film thickness by increasing the amount of material on the seal.

An important variable is the ratio L_1/L ; reducing this leads to an appreciable increase in film thickness, see Fig.27. Reducing L_1/L decreases the load on the oil film up to a point; as it is reduced still further, however, elastic forces begin to increase the load again, and the result is an optimum value for maximum film thickness. This is clearly demonstrated by the figure. The position of this optimum would certainly depend on the value of other dimensions: in particular, thickening of the seal will increase the relative importance of elastic forces. The value of L_1/L is 0.717 for seal B.

Fig.28 shows the effect of changing the radius of the seal; this does not appear to be an important parameter.

A simple rule can be devised for scaling a seal up or down in size: provided that the relative proportions, including $\bar{I}$, remain constant the only dimensionless group which is affected is $\bar{U}$ (since L changes). From Fig.18, $\bar{H}_0$ varies roughly proportionally to $\bar{U}$. Thus to a first approximation

$$\frac{h_0}{L} \propto \frac{\eta_0 U}{EL} \quad \text{or} \quad h_0 \propto \frac{\eta_0 U}{E} \ .$$

Hence the actual film thickness remains virtually constant for a given set of operating parameters when the seal is scaled up or down in size.

5.7 Leakage and friction

For completeness Fig.29 shows dimensionless leakage and friction plotted against speed parameter, and Fig.30 shows them plotted against pressure parameter. From the purely theoretical point of view there is little to be said about these quantities; a fuller discussion will be deferred until the section on experimental results and to the comparison between theory and experiment.

5.8 Summary of theoretical results

(1) Film thickness $\bar{H}_0$ varies approximately linearly with speed. At low values of $\bar{U}$ mode IV solutions are obtained; there is a transition to mode II at higher speed and a further gradual change to mode III as $\bar{U}$ increases still further.

(2) Pressure peaks are predicted. These become more pronounced with decreasing speed.

(3) $\bar{H}_0$ varies inversely with system pressure. Automatic solutions could not be obtained at very low pressures.

(4) $\bar{H}_0$ increases with increasing values of materials parameter $\bar{G}$; because of the limited range of $\bar{G}$, however, this parameter does not affect the film thickness to the same extent as speed or system pressure.

(5) Film thickness varies inversely with interference.

(6) No way of quantifying profile changes is considered, and all that can be said is that changes in the seal profile modify the film thickness; for the profiles considered, the variation in $\bar{H}_0$ is about 10 per cent.

(7) Thickening the seal material increases $\bar{H}_0$, but whether or not an optimum exists has not been determined.

(8) There is an optimum value of L_1/L for a maximum $\bar{H}_0$.

(9) $\bar{H}_0$ decreases with the ratio R/L .

(10) If the entire seal is scaled up or down, the actual film thickness h_0 is virtually unchanged if values of the operational parameters remain the same.

6 EXPERIMENTAL RESULTS

6.1 Introduction

Experimental results are presented for systematic variations in operating parameters and for some variation in seal geometry. The range of theoretical operating parameters considered in the previous sections was chosen to correspond to the range of practical conditions; hence the experimental results cover the same operating region. Variations of seal geometry, however, were not possible in the experiments to the same extent as in the theory; reasons for this will be given in section 6.6. For reasons discussed in section 3.5 only outstrokes have been considered except in section 6.7, where instroke friction is also quoted briefly. Unless otherwise stated, the depression of the capacitance probe by pressure is taken into account.

6.2 Variation of speed parameter

The range of speed parameter covered at 22°C is from about 6×10^{-12} to 3×10^{-11} using DP47 fluid and from 3.5×10^{-11} to 1.4×10^{-10} using OM160.

Fig.31 shows a family of measured film shapes at 6.89MPa system pressure and at different values of $\bar{U}$; actual speeds are also given. Because two different fluids are used the materials parameter also varies (from 2060 for DP47 to 3030 for OM160). The corresponding pressure distributions are given in Fig.32; they are all in mode II. After recording film thickness the jack rod was rotated before measuring pressure so that readings were taken with the pressure probe in the same position relative to the seal lip as the capacitance probe prior to rotation.

Fig.33 summarizes the variation of film thickness with speed at this pressure.

6.3 Variation of system pressure

Fig.34 shows a family of measured film profiles over a range of system pressures and at a speed parameter value of 5×10^{-11}. The pressure has an appreciable influence on the shape of the film and the minimum film thicknesses. At 13.8MPa distortion is very large, and it was concluded that this was about the maximum pressure for which this seal was suitable. Fig.35 shows the observed pressure distributions corresponding to the film shapes of Fig.34. The basic features do not change significantly with system pressure. Fig.36 shows the maximum film thickness and the inlet minimum film thickness plotted against

pressure, summarizing Fig.34; it should be noted that at the highest pressure the total depression of the capacitance probe (see section 3.3) is about 2.75μm. The inlet minimum film thickness is obtained as the difference between an apparent film thickness of 2.95μm and a probe depression of 2.75μm; the value of inlet film thickness quoted at this pressure is thus subject to significant errors.

6.4 Change of solution mode

All the results for seal B correspond to mode II except at zero system pressure, when mode I is also obtained over some portions of the lip. With seal A, all four modes were observed; of particular interest is the existence of two modes under the same operating conditions. Fig.37 shows film profiles on two different stroking cycles, and modes II and IV are clearly discernible (see section 4.1). This situation occurs very infrequently, and is observed sometimes over a limited speed range on the first stroke of the rod, or when speed has been reduced during the stroke. Subsequent strokes give mode II lubrication.

The existence of two lubrication modes is predicted theoretically, and it is interesting to be able to obtain similar behaviour experimentally. The phenomenon is of little practical significance, however, as the existence of an alternative lubrication mode does appear to be a rather freak occurrence.

6.5 Variation of materials parameter

The most convenient way to vary $\bar{G}$ is to change α by using a different oil; unfortunately this means dismantling the seal and jack rod, which prevents repeatability. It is found theoretically that changing the oil from DP47 to OM160 makes little difference to the film thickness at the same value of $\bar{U}$; experimentally, possible changes in film thickness caused by reassembly would tend to mask those due to the variation of α. No attempt was therefore made to assess the effect of the materials parameter experimentally.

6.6 Seal geometry

The two seals A and B were nominally identical, and were found to have the same qualitative performance (for example, the same hydrodynamic modes with similar oil film shapes). However, small manufacturing imperfections and the resulting differences between the seals gave different quantitative behaviour. It is felt to be impossible to make two seals to within sufficiently close tolerances that their precise behaviour is the same. It follows that it is impossible to determine the quantitative effect of geometry changes by making a

series of seals of slightly different dimensions: the effect of unwanted variations in geometry would be inseparable from that of the deliberate variations. All that was done, therefore, was to change an existing seal.

Seal A was modified by removing metal from the outside (atmospheric) edge of the lip at the step, thereby reducing L and increasing the length of the unsupported section. Fig.38a shows the film thickness and pressure distribution at a system pressure of 6.89MPa, and Fig.38b at 13.8MPa, both with the lip length L reduced from 7.62mm to 5.03mm.

At 6.89MPa pressure the conditions in the contact were qualitatively the same as before, although the unsupported section did deflect towards the rod and the minimum film thicknesses were smaller. At 13.8MPa the pressure loading was too great and the unsupported section of the seal was forced into contact with the rod. Some of the pressure drop then occurred across this point of contact. When the seal was removed for inspection, scuffing was evident in this region.

When the length L was reduced further to 2.54mm no pressure or oil film were recorded, and it was concluded that elastohydrodynamic lubrication had ceased.

6.7 Leakage and friction

For a fundamental study of seal behaviour these two parameters are not of great importance; theoretically they are derived from more basic hydrodynamic parameters, and experimentally they are difficult to measure. For practical applications, however, leakage and friction are crucial, and it is therefore interesting to compare the behaviour of the metal seal with that of a conventional elastomeric type.

Direct measurement of leakage is inaccurate and requires prolonged testing[22]. However, when pressure and film thickness are available leakage can be calculated from the relationship

$$Q = \frac{Uh_0}{2} \quad .$$

Fig.39 shows how this quasi-experimental leakage varies with speed at 6.89MPa pressure and for the two different test fluids. Fig.40 shows these results replotted to demonstrate how leakage would vary with temperature at a constant stroking speed of 100mm/s using DP47 as the working fluid. It is

assumed that outstrokes and instrokes take the same time and that there is no instroke lubrication: that is, no leaked fluid is carried back into the test cylinder.

The leakage of the metal seal is obtained as a flowrate, but SBAC and MIL-Specs stipulate that leakage should not exceed one drop every 25 stroking cycles. This is difficult to convert to a flowrate with any accuracy, since many assumptions are involved; the range 1ml/h to 10ml/h has been taken as a satisfactory leakage level, and corresponds to a range of from low to acceptably high leakage. Comparison with the results of Field and Nau[14] at room temperature for a conventional square section rubber seal (also using the film thickness to calculate leakage) shows that the metal seal leaks less; this is to be expected since the rubber seal always gives thicker films under similar operating conditions. How the two types of seal would compare at other temperatures is uncertain, because the mechanical properties of rubber vary with temperature. Instroke lubrication would reduce the leakage of all seals still further.

Final judgement on the leakage performance of the metal seal cannot be made on the basis of simplified experiments but must await endurance testing in a service environment. Comparison with rubber seals under similar conditions suggests, however, that leakage will not be a problem.

Fig.41a shows the variation of measured outstroke friction with speed and system pressure for seal B; instroke friction at zero system pressure is also shown. The general form of these curves is characteristic of hydrodynamic lubrication, but a fuller discussion of their shape will be deferred until section 7.3, where they are compared with theoretical friction. It should be remembered that these friction values are for two seals, the presence of the labyrinth seal being neglected. These friction values are extremely low, and certainly acceptable from the practical point of view.

Also shown in Fig.41b are the corresponding curves for seal A, with L = 5.03mm. At 6.89MPa the behaviour is similar to before, but at 13.8MPa the shape of the curve is quite different, and this suggests that some transition region between boundary and elastohydrodynamic lubrication has been reached. This deduction is consistent with the observation of scuffing under these conditions.

Breakout friction, that is, the force required to initiate stroking, was also measured. Such measurements were difficult to make accurately because of

their transient nature, and repeatability was poor. As a rough guide, the breakout friction at a given pressure usually exceeded the dynamic friction by up to 100 per cent, the precise amount being dependent on the stroking speed. This order of breakout friction would be acceptable in practice.

6.8 Summary of experimental results

The main experimental findings may be summarized as follows:

(1) A hydrodynamic film of lubricant exists between the seal and jack rod on outstrokes; on instrokes such a film is only observed at high speed when no system pressure is applied to the seal.

(2) Film thickness is highly speed-dependent; if the depression of the capacitance probe is taken into account, the inlet minimum film thickness $\bar{H}$ is roughly proportional to $\bar{U}$.

(3) The maximum film thickness increases, and the minimum decreases, with increasing system pressure. Considerable distortion of the seal is evident due to pressure.

(4) Shortening the contact lip in relation to the overall length of the seal reduces the film thickness and results in large deflections of the shell. Hydrodynamic lubrication ceases with further shortening of the contact.

(5) The sliding friction is low by conventional seal standards.

(6) Quasi-experimental values of leakage deduced from film thickness measurements are also low; confirmation of this by measuring actual leakage awaits endurance testing.

(7) The different modes of lubrication examined theoretically are observed in the oil film under the seal.

(8) As predicted theoretically, two different hydrodynamic lubrication modes may exist under the same operating conditions.

7 COMPARISON BETWEEN THEORY AND EXPERIMENT

7.1 Pressure and film shape

Fig.42 compares theoretical and experimental pressure distributions and film profiles; the theoretical results both of pressure and film thickness have been modified to account for the finite resolving power of the transducers in the axial direction. Both sets of results have the same basic features, and the

agreement was considered fair, particularly in view of some of the uncertainties about seal dimensions. At other speeds or pressures the comparison of these shapes is similar to Fig.42 until changes of mode occur in the theoretical solution; direct comparison of the profiles then becomes impossible. However, the theoretical model is certainly capable of reproducing the unusual features of the experimental measurements over a significant part of the speed range.

7.2 Variation of film thickness with speed and pressure

Fig.43 shows a comparison between theoretical and experimental values of inlet and maximum film thicknesses at different speeds. Because the solution mode changes at low speed, the theoretical curve for the inlet minimum has been extrapolated into this region and is shown as a dotted line. The maximum film thickness is also shown dotted where the solution is in the fourth mode. Note that at the higher end of the speed range the transition from mode II to mode III is marked by a crossover of $\bar{H}_0$ and $\bar{H}_i$. The transition between OM160 and DP47 fluids is indicated by a discontinuity in the curves, which are for different values of $\bar{G}$ on either side of the transition. In the experimental points allowance is made both for the depression of the capacitance probe and its finite resolving power in the direction of stroking. The slope of the lines is in fair agreement, but the measured minimum film thicknesses are lower than those calculated. It has been shown theoretically that film thickness is quite sensitive to geometrical factors such as lip thickness and interference, which are difficult to measure, and vary around the seal. Thus by assuming errors in measurement and inserting different seal dimensions into the theoretical calculations the theoretical curve could, if desired, be made to correspond exactly with the experimental points. It can be inferred from sections 5.5 and 5.6 that the dimensional changes required to achieve this would be small.

Fig.44 shows the change in film thickness with pressure at a speed of $\bar{U} = 5 \times 10^{-11}$. Comparison of results here is difficult because h_0 cannot be measured experimentally and because the required minimum film thickness is only available theoretically when the solution is in the second or third mode. The theoretical values of $\bar{H}_0$ have been plotted together with the inlet minimum film thickness, where available.

Once again, although the absolute values are different where direct comparison of inlet film thickness is possible, and although the experimental results are sparse, the trends of the curves are qualitatively similar.

7.3 Leakage and friction

Because leakage was not measured directly, agreement between theoretical and experimental values depends on agreement between film thicknesses. Particularly at high speeds, therefore, the predictions of leakage are likely to be as accurate as experimental values deduced from film thickness; a comparison has already been made between theoretical and experimental film thicknesses.

Friction, however, was measured directly, and Fig.45 shows a comparison of friction values. The experimental results include the friction of the labyrinth seal, and are averaged around the circumference since it is impossible to isolate the friction contribution of a particular segment of the seal lip. The completely theoretical values of friction are shown as a line, and the points which are indicated as being derived from measured film thicknesses are obtained from the relationship

$$F = \frac{2\pi RLU\eta_0}{h}$$

where h is the inlet minimum film thickness.

Agreement is not good between the theoretical and experimental curves. At low stroking speeds the absolute magnitudes differ by about a factor of two; this could perhaps be accounted for by the friction component due to the labyrinth seal and circumferential variations in film thickness. However, as speed increases the experimental friction increases but the theoretical friction remains fairly constant, and the two curves therefore diverge. Friction which increases thus with speed may in general be consistent with hydrodynamic lubrication - the slope depends upon the relationship between speed and film thickness. But in this case, where film thickness varies approximately linearly with speed, the friction would be expected to remain virtually constant. This is demonstrated by the friction calculated from measured film thickness via the above equation. This is an approximate relationship because it assumes a parallel oil film; nevertheless, the general behaviour of these points more nearly resembles that of the theoretical curve than that of the directly-measured friction. The linear relationship between film thickness and speed does not depend upon assumptions concerning profile, interference, etc., used in the theoretical calculations, and the discrepancy between the slopes of the friction curves cannot therefore be due to these

factors. It therefore seems likely that the oil film is not wholly hydrodynamic and that some asperity contact takes place. This is visible experimentally as electrical breakdown on the film thickness traces.

It should be mentioned that the agreement between theory and experiment on friction is better for metal seals than for elastomers. The relatively thick films associated with elastomers give friction values due to viscous shear alone which are an order of magnitude or more below the measured values: this is also thought to be due to asperity contact[14].

In conclusion, the agreement between predicted and measured friction is poor, and it seems likely that this is due to localized breakdown of the hydrodynamic lubricant film; nevertheless, the actual friction values are acceptable for practical applications.

7.4 Total load

Table 3 shows a comparison between theoretical and experimental values of dimensionless load and actual load on the oil film at different values of speed parameter. These figures were obtained by integrating the pressure distributions. Agreement is very close despite the fact that at $\bar{U} = 2 \times 10^{-11}$ and $\bar{U} = 10^{-11}$ the theoretical solutions are mode IV and the measured distributions are mode II.

Table 4 shows the variation of load parameter with system pressure at constant speed. Once again agreement between theory and experiment is good, and this suggests that the pressure distributions are known fairly accurately. The result marked with an asterisk is for $\bar{U} = 10^{-11}$ and DP47 fluid, whereas the other results are for $\bar{U} = 5 \times 10^{-11}$ and OM160. This is because the appropriate theoretical solution was not available at $\bar{U} = 5 \times 10^{-11}$. However, load does not change a great deal with speed, and it is useful to quote this result for comparison purposes.

7.5 Discussion

When judging the comparison between theoretical and experimental results it is important to ask the question: does the theoretical model reproduce the basic behaviour of the seal with sufficient accuracy for the model to be used as a tool in the understanding of seal performance, even though there are discrepancies between results obtained by calculation and observation?

In some instances agreement between theory and experiment is very good, particularly considering the unreliability of the geometrical data. For example, pressure distributions agree well, and the variation of film thickness with speed and pressure is predicted reasonably accurately. In other cases the agreement is poor. The effects of inaccuracies in the manufacture of the seal have been tentatively advanced to account for some of these discrepancies. These imperfections mean that input data for the calculations are not truly representative of the seal, meaning that whilst the way in which film thickness varies may be correctly predicted, absolute values may not, and also that certain experimental effects such as averaging of the film thickness are observed. By making suitable assumptions about the magnitude of these inaccuracies the differences between theory and experiment could be largely eliminated.

The essence of the problem is that a fully controlled experiment is not practicable, since a seal cannot be manufactured to the accuracy required for such an exercise. Obviously one method of testing a theory is to set up a simplified model experiment in which all the relevant parameters are known. This is valid only when the initial assumptions are similar in both the real problem and the model. It will be argued below that the elastohydrodynamic conditions are a function of the seal geometry, and that the only way to reproduce them is in a seal; simplifying the geometry would merely establish that the correct governing equations had been selected for the model without reproducing the unusual conditions in the seal.

Given that a fully controlled experiment is not feasible, that agreement between theory and experiment is nevertheless fairly good, and that plausible hypotheses have been advanced to account for discrepancies which do occur, it is felt that the theoretical model is adequate for exploring the behaviour of the seal. The considerable effort needed to overcome some of the possible sources of inaccuracy described was not considered worthwhile.

8 DISCUSSION

The first experimental results were obtained before any real progress had been made with the theory. It was evident both that the seal performance was unsatisfactory and that its unusual features could not be explained without a theoretical model; such an explanation was an essential prerequisite to the elimination of undesirable characteristics and the design of a better seal.

No explanation has yet been offered as to why the oil film boundary should deform into an arched or bowed profile - intuitively it would be expected that the maximum deflection would occur somewhere near the maximum pressure: in fact the minimum deflection occurs at that point. Another problem is the cause of the pressure spike; although it looks similar to those calculated for some rolling contacts it behaves differently, becoming more pronounced as speed decreases. Finally, the lack of instroke lubrication is a serious shortcoming not having an obvious cause such as inlet starvation. The following arguments are postulated to explain these features.

The arched shape of the oil film is calculated using a complicated set of equations which give little intuitive guidance, but there is a simple physical explanation. Assume that the rod is stationary and there is no oil film under the seal. System pressure acting on the unsupported shell between the lip and the housing causes the shell to deflect towards the rod; this also happens owing to the interference fit between the seal and the rod. At the outside, or atmospheric, edge of the contact the seal and rod are touching. In the actual contact region, therefore, continuity of slope requires the seal to deflect away from the rod. Towards the free end hoop stress and pressure loading provide a restoring force which deflects the seal inwards, and the overall result is an arched profile. This will be modified by hydrodynamic pressure when the rod is stroked and an oil film begins to form, but a similar reasoning still applies.

In dry contact conditions, when the seal and rod are touching, the load is therefore especially heavy at the atmospheric edge of the lip. As an oil film forms, a high pressure must be present at this point to support the local load and separate the sliding surfaces: hence the pressure spike. The spike is thus primarily due to the elastic stresses in the contact which are in turn the result of the seal geometry. The high pressure only increases the oil viscosity by a factor of about two; the corresponding viscosity increase in a disk machine in conditions in which a pressure spike is observed is several orders of magnitude. Although the causes of this spike between the disks cannot strictly be divorced from the elasticity equations and the contact geometry, it only occurs when the influence of pressure on viscosity is large, and is thus primarily due to the exponential variation of viscosity with pressure. For a hypothetical isoviscous fluid, no pressure spike is predicted. For the seal, on the other hand, the predicted pressure spike changes little for an isoviscous fluid. The peak increases with decreasing speed and film thickness as the value of hydrodynamic pressure approaches the dry contact stress more nearly.

The failure to form a lubricating film on instrokes is also related to contact stress. To support the high local load near the outside edge of the contact the hydrodynamic pressure must be high, but fall off rapidly to atmospheric at the end of the contact. The theoretical and experimental results show that this happens during outstrokes, where the outside edge of the seal corresponds to the oil film outlet. There is thus a large negative pressure gradient at the outlet. Were an instroke film to form, a pressure peak would be required in the same position to support the local load. There would thus be a steep pressure gradient at the inlet and this would be the factor determining h_0. The steeper the pressure gradient the smaller the corresponding value of h_0. Thus the heavy local loading at the atmospheric edge of the lip restricts h_0. (It is now clear why a differentiation has been made between pressure peaks caused by pressure-dependent viscosity and those due to seal geometry: in a disk machine the spike always appears at the outlet, and reversal of the disk motion has no effect, but in the seal the position of the spike is fixed.)

It has been shown that the basic shape of the seal, and the way in which it is loaded under pressure, are responsible for the local load concentration, which in turn causes the somewhat unusual and unsatisfactory behaviour. It is possible to interpret the performance of the early seals in the light of this. The ratio L_1/L was sometimes over 4 (flexibility was then thought to be an advantage), as opposed to the value of about 0.7 for seals A and B. Pressure acting on the shell thus caused an enormous load at the outlet edge, and it is probable that the shell was forced into contact with the rod at higher pressures. Seals A and B are, of course, an improvement; but although a change in performance can be realized by modifying some of the dimensions, the heavy loading at a critical point is still an obstacle to any significant improvements such as limiting the distortion or instroke lubrication.

Given the unsatisfactory features of the seal, some of which were apparent from early experimental evidence, it is pertinent to ask whether there was any point in proceeding with such a detailed study as has been described. The answer is that a seal which exhibits elastohydrodynamic lubrication can, whatever its shortcomings, be used as a vehicle to study metal seals in depth. The results of this study have determined the root causes of these shortcomings and enabled methods of eliminating them to be devised. The improvements sought are to reduce the excessive distortion, allowing higher system pressures, to reduce local stress concentrations and hydrodynamic pressure peaks, and to obtain

instroke lubrication. A possible means of achieving these objects has been devised, and is discussed in the next section.

It would be useful to obtain some confirmation of the results from previous elastohydrodynamic work. The physics of the problem is simpler for a metal than a rubber seal: absorption of oil, incompressibility of the rubber, variation in elastic properties, etc., do not occur with metals. Mathematically, however, the metal seal is more complex, requiring more sophisticated methods both for finding the elastic deflections and solving (in the sense of finding the appropriate roots of) the hydrodynamic equations. A direct, quantitative comparison between metal seals and other types of elastic contact is impossible: conditions in the metal seal are unique.

For future work the obvious problem is to tackle the design of a new seal (see section 9). Having obtained a seal which operates satisfactorily in the hydrodynamic regime, the question of applying a suitable coating to the lip so that it operates successfully in conditions where the boundary lubrication regime is unavoidable must be considered. The high friction and wear of the original seals (in which hydrodynamic conditions were not attained) has been attributed to poor load distribution along the seal lip. A more even distribution of this load to promote hydrodynamic conditions would tend to reduce local loadings and reduce friction and wear problems; thus the remedy for poor elastohydrodynamic lubrication would also benefit the boundary regime. A promising possibility for improving boundary lubrication still further is a dry bearing material bonded to the inside of the lip in place of silver plating.

The hypotheses based on existing results which have been advanced to explain the seal behaviour will be tested by the redesigned seal. The theoretical problems associated with the new design are expected to be less, and the instrumented jack rod can be used to verify the predictions. If the desired seal characteristics are attained then work on endurance testing may begin.

The final conclusion is that whilst elastohydrodynamic lubrication can exist in the metal seals which were studied, with beneficial effects, the necessary conditions are frequently not met. The results of this work indicate why this is so, and how to remedy this; it is probable that, as a result, an improved seal with satisfactory elastohydrodynamic performance can be designed.

9 AN IMPROVED DESIGN OF METAL SEAL

The aim is to eliminate the high local stress at the instroke inlet and to distribute the load caused by interference and pressure loading more evenly along the contact: Fig.46 illustrates a method of achieving this. Fig.46a shows a section of part of the seal; the shell tapers fairly steeply towards the free end, and the length of the contact lip is no longer defined by a step. In Fig.46b the same seal section is shown in contact with a jack rod; they are an interference fit. If the taper is correct, the stress will rise gently at the instroke inlet, though care will be needed to prevent excessive stress at the outstroke inlet. As pressure is applied in Fig.46c, the extra load forces a greater proportion of the shell into contact with the rod, giving a greater load-bearing area, and the taper prevents the local stress from rising too quickly. This gentle rise in stress will tend to encourage the establishment of an instroke oil film, and prevent the large deflections and 'arching' which occurred in the original seal design.

The exact degree of tapering and interference required to obtain a smooth change in contact stress can be calculated using the finite element computer subroutines already developed during this work. It seems likely that there will be an optimum shell thickness and taper for a particular system pressure, and that therefore seals will be designed for a particular operating pressure. The full elastohydrodynamic computer program can be used to make predictions of the pressure distribution and film thickness under the seal. If the redesign has the expected result, the theoretical problem will be simpler than the one already solved for the existing type of seal: a near-parallel film with a single-peaked pressure distribution should be obtained. Once a satisfactory design has been arrived at, the predictions can be checked by manufacturing a seal and testing it using the instrumented jack rod. If these tests indicate that the lubrication is satisfactory, that is, that instroke lubrication occurs and gross distortion has been eliminated, then it should be possible to begin testing metal seals in a practical way to ascertain their leakage, friction, life, and so on; it is on these quantities that the usefulness of the final design must ultimately be judged.

10 CONCLUSIONS

An instrumented jack rod has been constructed which is capable of measuring pressure distribution and oil film thickness under a metal seal, and experimental

results have been obtained over a range of operating parameters. Theoretical work has used the finite element method to calculate the deflections of the seal and successfully integrated this into an automatic iterative elastohydrodynamic solution on a digital computer.

There is reasonable agreement between theoretical and experimental results. Using the theoretical model it is possible to predict the response of film thickness to changes in the dimensions of the seal and to variations in the operating parameters.

The understanding of seal behaviour gained from this work has helped to explain the shortcomings of the existing seal design and the theoretical model can be used to explore new seal designs.

Table 1

DIMENSIONS OF TEST SEAL B

L	L_1	L_2	t_1	t_2	R	i
7.62	5.46	0.083	0.305	1.01	15.827	0.0108

All dimensions are in mm; i is the radial interference between the seal and jack rod; other parameters are defined in Fig.1.

Table 2

PHYSICAL PROPERTIES OF TEST FLUIDS AT 22°C

Fluid	Absolute viscosity $N\ s\ m^{-2}$	Relative density	Pressure coefficient $nm^2\ N^{-1}$	Relative permittivity
DP47	0.082	1.04	21	2.891
OM160	0.43	0.90	30	2.327
Diesel	0.0039	0.84	~30	2.230

Table 3

THEORETICAL AND EXPERIMENTAL VALUES OF LOAD PARAMETER AT DIFFERENT SPEEDS

Seal B; $p_s = 6.89$MPa

Fluid	Speed parameter $\bar{U}$	Theoretical load parameter $\bar{W}$	Experimental load parameter $\bar{W}$	Experimental load $w/N\ m^{-1}$
OM160	10^{-10}	1.14×10^{-4}	1.22×10^{-4}	8.24×10^{4}
OM160	5×10^{-11}	1.07×10^{-4}	1.16×10^{-4}	8.21×10^{4}
DP47	2×10^{-11}	1.07×10^{-4}	1.16×10^{-4}	8.20×10^{4}
DP47	10^{-11}	1.05×10^{-4}	1.11×10^{-4}	8.07×10^{4}

Table 4

THEORETICAL AND EXPERIMENTAL VALUES OF LOAD PARAMETER AT DIFFERENT SYSTEM PRESSURES

Seal B; $\bar{U} = 5 \times 10^{-11}$; fluid OM160

Pressure p_s MPa	Theoretical load parameter $\bar{W}$	Experimental load parameter $\bar{W}$	Experimental load $w/N\ m^{-1}$
13.9	$2.08\ 10^{-4}$	$2.21\ 10^{-4}$	$1.49\ 10^{5}$
6.89	$1.07\ 10^{-4}$	$1.16\ 10^{-4}$	$8.21\ 10^{4}$
0	$*2.21\ 10^{-5}$	$1.90\ 10^{-5}$	$1.28\ 10^{4}$

* See text, page 34

SYMBOLS

C, C_i	dimensionless seal profile c/L
c, c_i	seal profile
$\underline{c}$	vector representing seal profile having elements c_i
D	global stiffness matrix
E	elastic modulus of seal or rod
F	seal friction
$\bar{F}$	dimensionless friction F/EL
$\underline{f}$	vector of nodal forces
$\bar{G}$	materials parameter αE
$\bar{H}, \bar{H}_i$	dimensionless film thickness h/L
$\bar{H}_0$	h_0/L
h, h_i	film thickness
h_0	film thickness at which $dp/dx = 0$
h_{min}	minimum film thickness
h_{max}	maximum film thickness
$\bar{I}$	dimensionless interference i/L
$I_0(x)$	modified Bessel function of the first kind of order zero
$I_1(x)$	modified Bessel function of the first kind of order one
i	radial interference between seal and rod
K	compliance matrix
k_{ij}	element of K matrix
L	length of seal lip
L_1	length of shell
L_2	step height
P, P_i	dimensionless pressure p/E
$\bar{P}$	dimensionless system pressure
p, p_i	pressure
p_s	system pressure
p_0	atmospheric pressure
$\underline{p}$	vector of pressures

SYMBOLS (concluded)

Q	leakage per unit width
$\bar{Q}$	dimensionless leakage $\eta_0 Q/EL^2$
R	radius of jack rod or seal
t	seal thickness
t_1	seal thickness at free end
t_2	seal thickness at root
U	jack stroking speed
$\bar{U}$	dimensionless speed parameter $\eta_0 U/EL$
u, u_i	radial deflections at surface of jack rod
v, v_i	radial deflections at surface of seal
$\underline{v}$	vector of radial deflections at surface of seal
$\bar{W}$	dimensionless load w/EL
w	load per unit width
X	dimensionless distance along seal x/L
x	distance along axis of symmetry of seal
α	viscosity-pressure coefficient
η	absolute viscosity
η_0	absolute viscosity at atmospheric pressure
ν	Poisson's ratio

REFERENCES

No.	Author	Title, etc.
1	R.H. Walsh	An investigation of the effects of working pressure on aircraft hydraulic systems. RAE Technical Report 69159 (1969)
2	J.N. Demarchi R.K. Haning	Lightweight hydraulic system hardware endurance test. US Naval Air Development Centre Technical Report NAVAIRDEVCEN-75085-30 (1975)
3	R.H. Walsh M.J. Westcott W.G. Lydiard	Metallic and composite seals for jack rods. Proc. Fourth Int. Conference on Fluid Sealing, Philadelphia, Paper No.3 (1969)
4	L.E.C. Ruskell	An investigation of the lubrication of high performance metallic seals. Unpublished RAE Technical Memorandum (1972)
5	L.E.C. Ruskell M.J. Westcott	High performance reciprocating seals for aircraft hydraulic systems. Proc. Sixth Int. Conference on Fluid Sealing, Munich, Paper No.H7 (1973)
6	L.E.C. Ruskell M.J. Westcott	Ref.5 reprinted in Tribology, 7, 21 (1974)
7	L.E.C. Ruskell	Reynolds equation and elastohydrodynamic lubrication in metal seals. Proc. R. Soc. Lond. A. 349, 383-396 (1976)
8	L.E.C. Ruskell	The elastohydrodynamic lubrication of metal seals. Ph.D. Thesis, University of Reading (1975)
9	J.K. Lancaster	Selection of materials for thin-lipped seals operating in chlorinated silicone hydraulic fluid. RAE Technical Report 74051 (1974)
10	H. Blok H.J. Koens	The 'breathing' film between a flexible seal and a reciprocating rod. Proc. I. Mech. Engrs. Symposium on Lubrication and Wear, 221 (1963)

REFERENCES (continued)

No.	Author	Title, etc.
11	A.D. Roberts P.D. Swales	The elastohydrodynamic lubrication of a highly elastic cylindrical surface. Brit. J. Appl. Phys. 2, 1317 (1969)
12	D. Dowson P.D. Swales	The development of elastohydrodynamic conditions in a reciprocating seal. Proc. Fourth Int. Conference on Fluid Sealing, Philadelphia, Paper No.1 (1969)
13	D. Dowson P.D. Swales	An elastohydrodynamic approach to the problem of the reciprocating seal. Proc. Third Int. Conference on Fluid Sealing, Cambridge, Paper No.F3 (1967)
14	G.J. Field B.S. Nau	An experimental study of reciprocating rubber seals. Proc. I. Mech. Engrs. Symposium on Elastohydrodynamic Lubrication, Leeds, Paper No.C5/72 (1972)
15	G.J. Field B.S. Nau	A theoretical study of the elastohydrodynamic lubrication of reciprocating rubber seals. Trans. ASLE, 18, 48 (1975)
16	G.J. Field	Private communication (1974)
17	H. Blok	Inverse problems in hydrodynamic lubrication and design directions for lubricated flexible surfaces. Proc. Int. Symposium on Lubrication and Wear, Houston, Texas, 1 (1963)
18	F.H. Theyse	The inverse hydrodynamic theory and its application in the design of controlled leakage seals between moving parts. Proc. Third Int. Conference on Fluid Sealing, Cambridge, Paper No.F2 (1967)
19	C.J. Tranter J.W. Craggs	The stress distribution in a long circular cylinder when a discontinuous pressure is applied to the curved surface. Phil. Magazine, 36, 241 (1945)

REFERENCES (concluded)

No.	Author	Title, etc.
20	O.C. Zienkiewicz	The finite element method in engineering science. McGraw-Hill: London (1971)
21	R.R. Stephenson J.F. Osterle	A direct solution of the elastohydrodynamic lubrication problem. Trans. ASLE, 5, 365 (1962)
22	M.C. Fielding L.E.C. Ruskell M.J. Westcott	The automatic measurement of leakage from hydraulic seals. RAE Technical Report 72148 (1972)

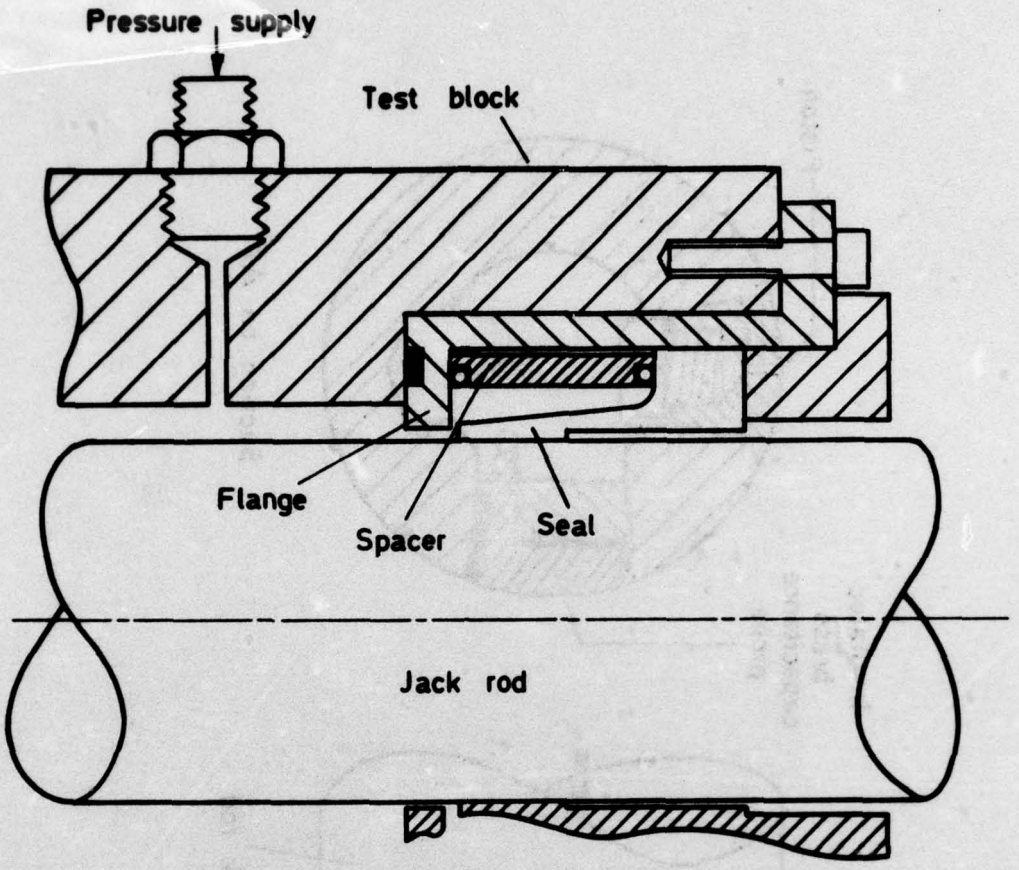

a Seal in housing

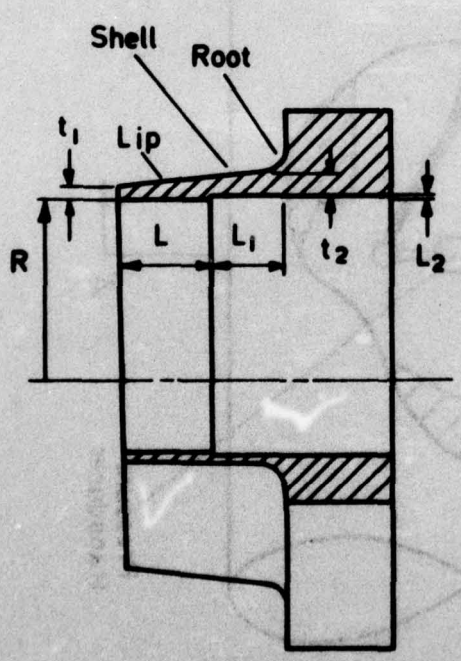

b Section of seal

Fig.1a&b Metal seal

T.R.76070

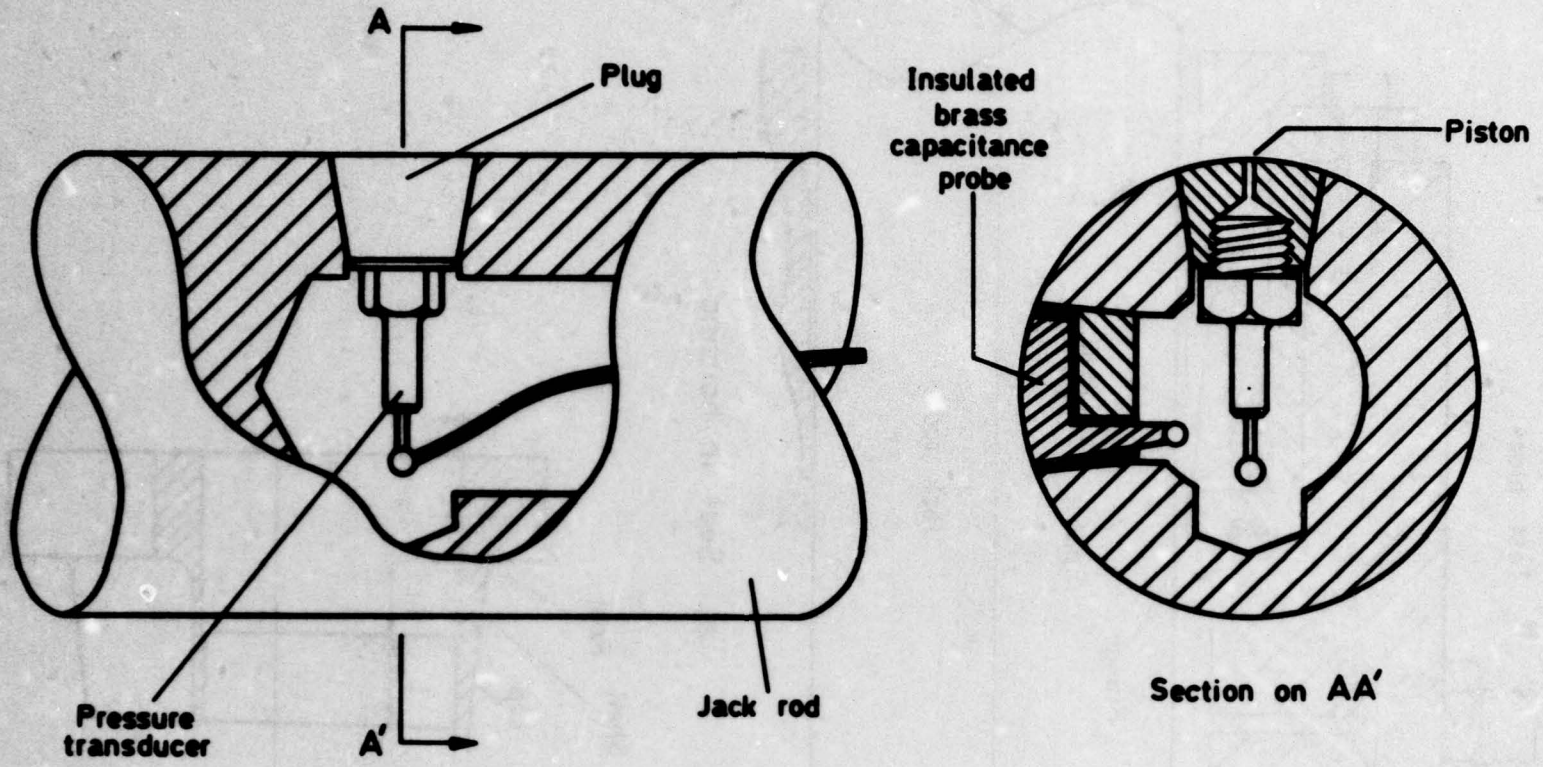

Fig. 2 Jack rod instrumentation

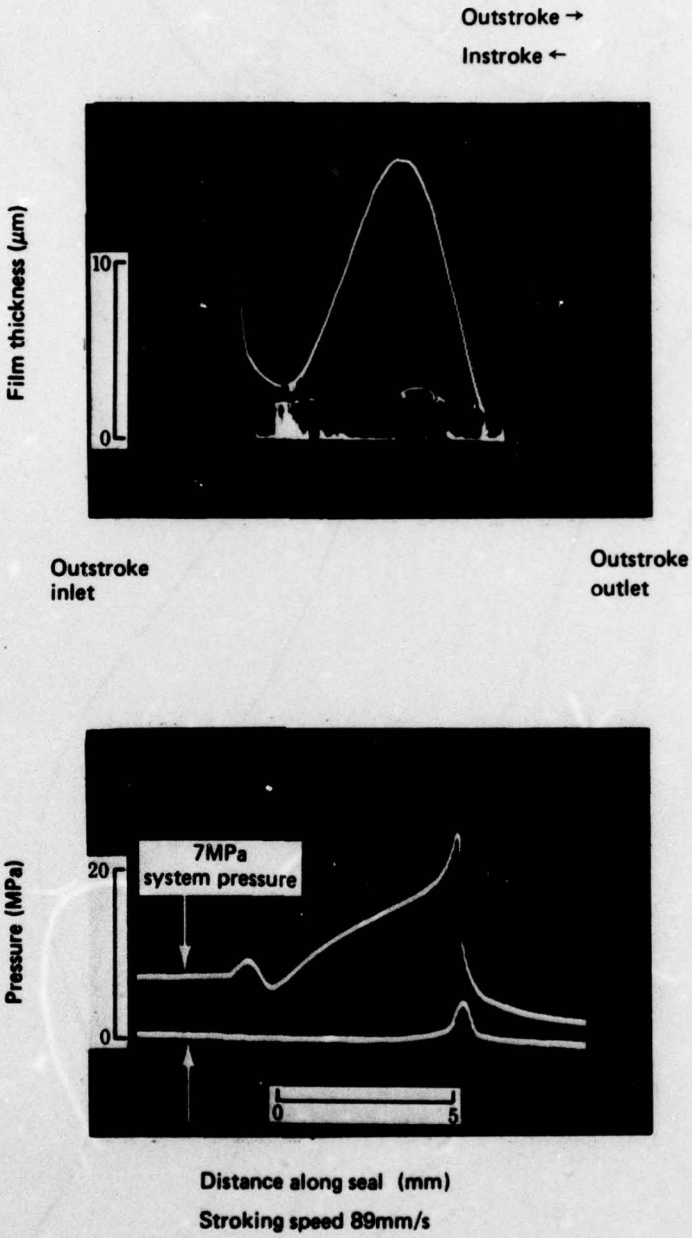

Fig.3 Pressure and film thickness traces

Fig. 4

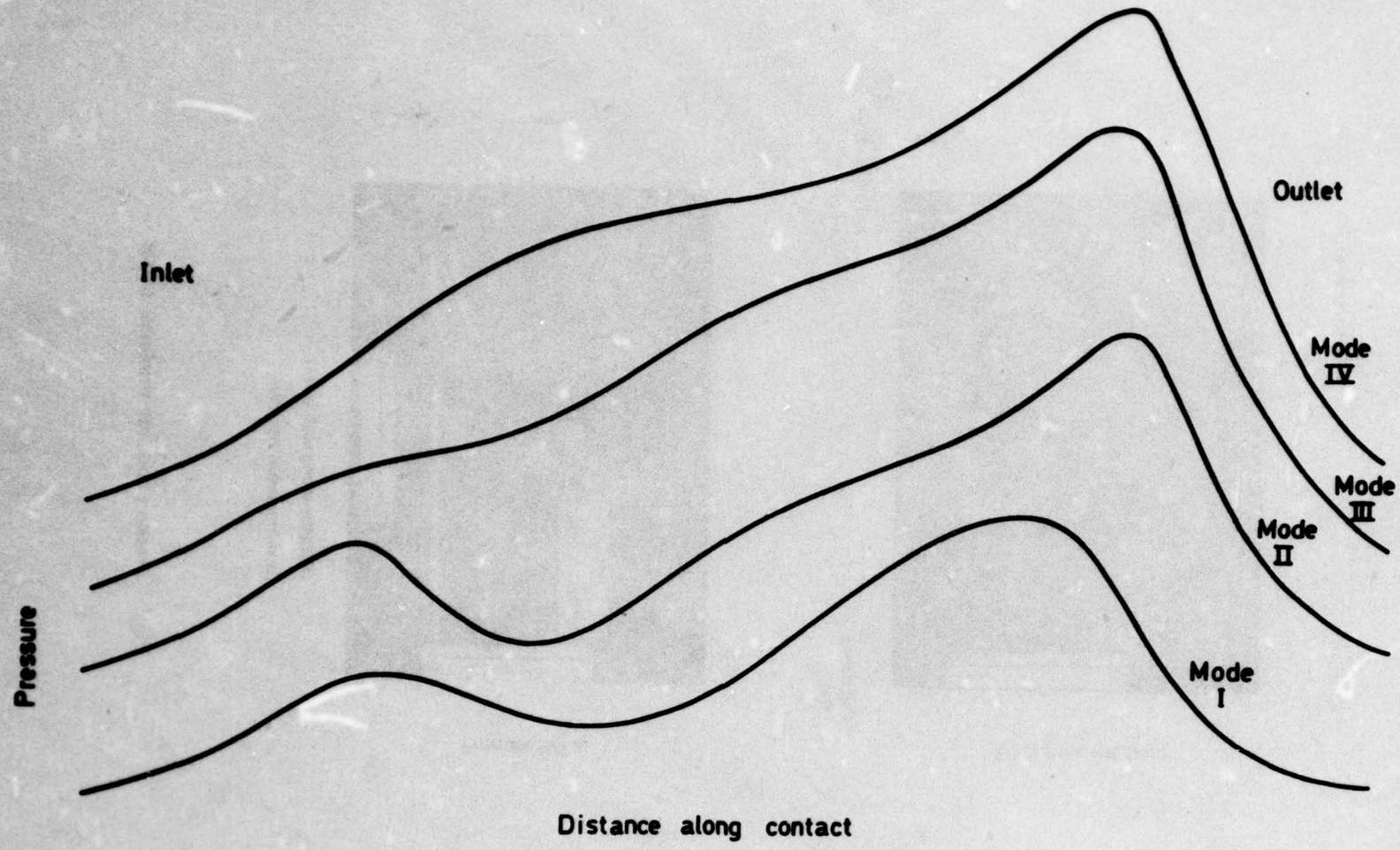

Fig. 4 Complex hydrodynamic pressure distributions

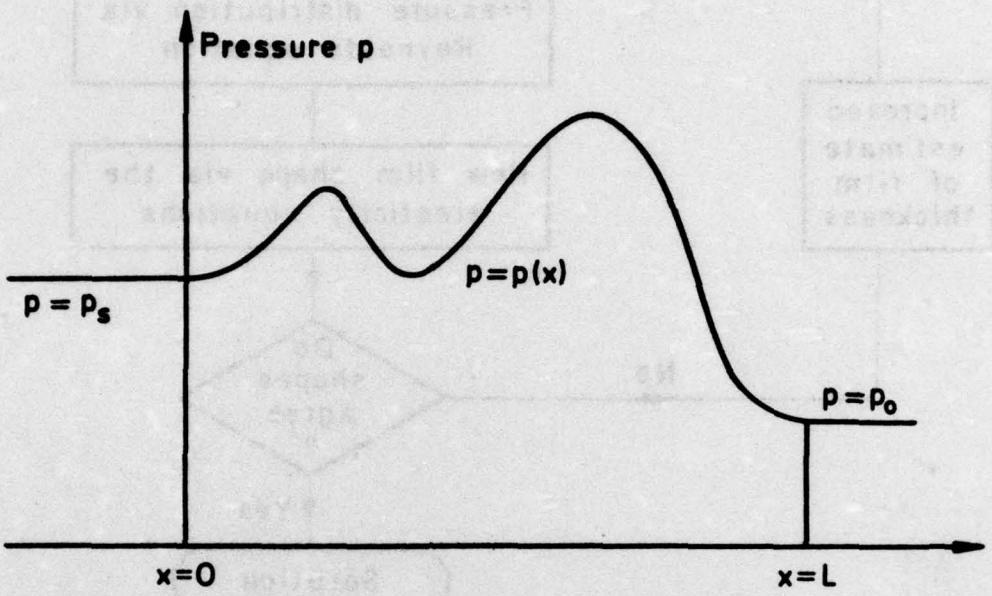

a Pressure acting on jack rod

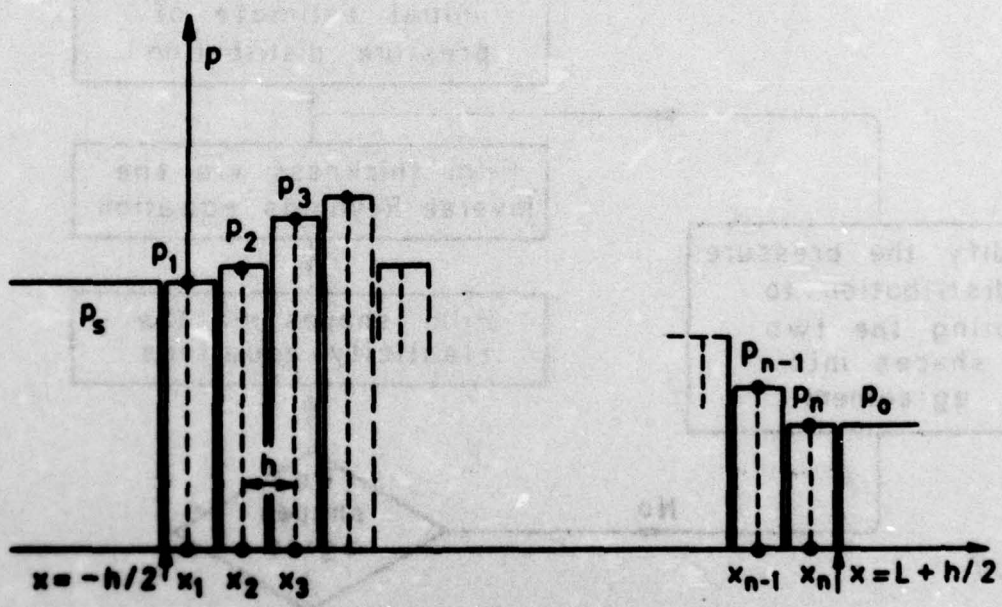

b Idealization of pressure

Fig.5 a&b

Fig. 6 a&b

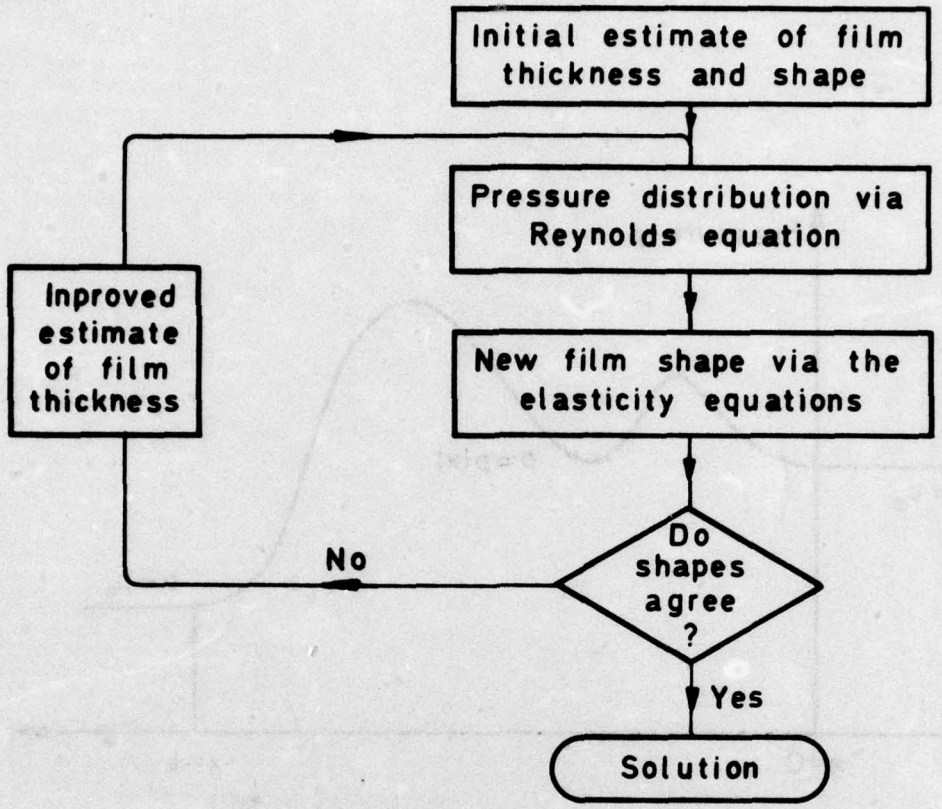

a Forward elastohydrodynamic solution

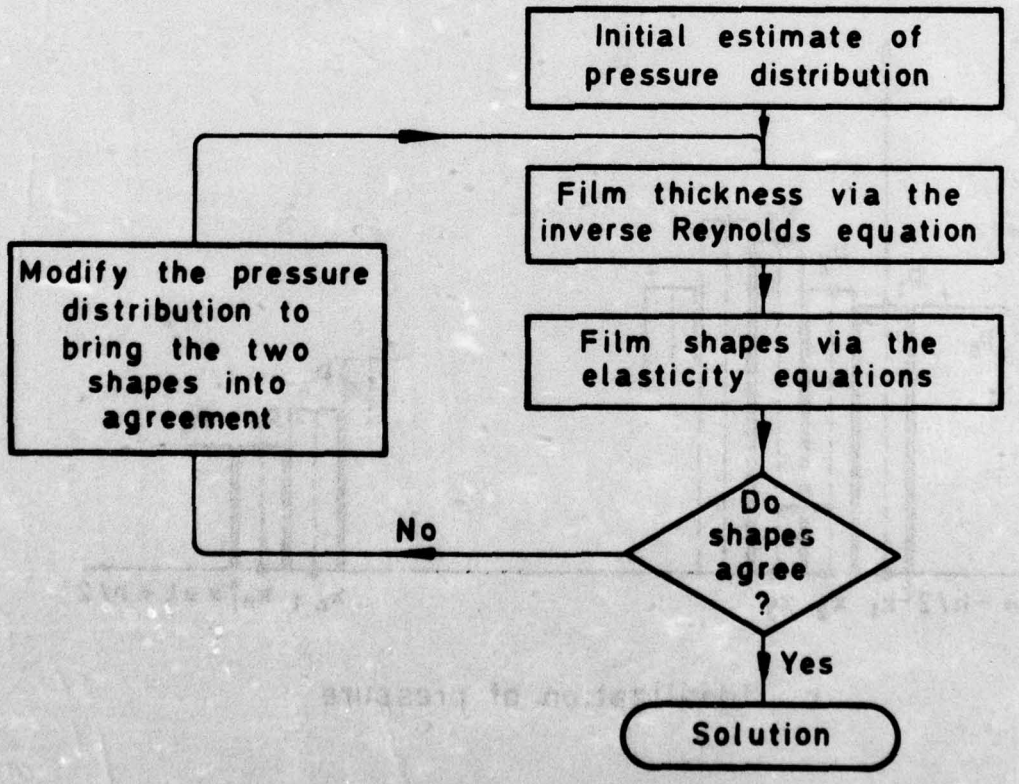

b Inverse elastohydrodynamic solution

Fig. 6 a&b Iterative schemes

TR 76070

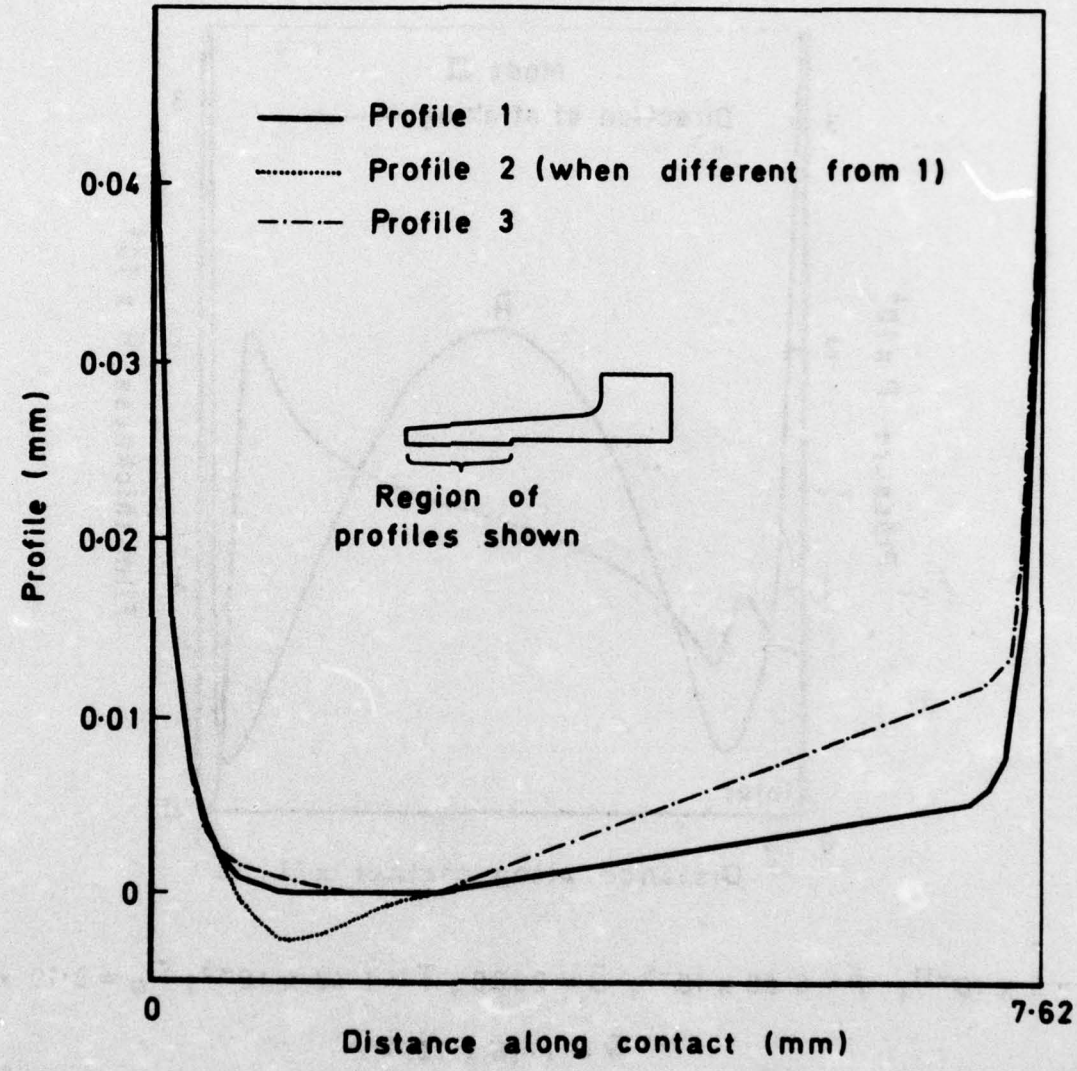

TR 76070

Fig. 7 Undeformed lip profiles from talysurf traces

Fig. 8

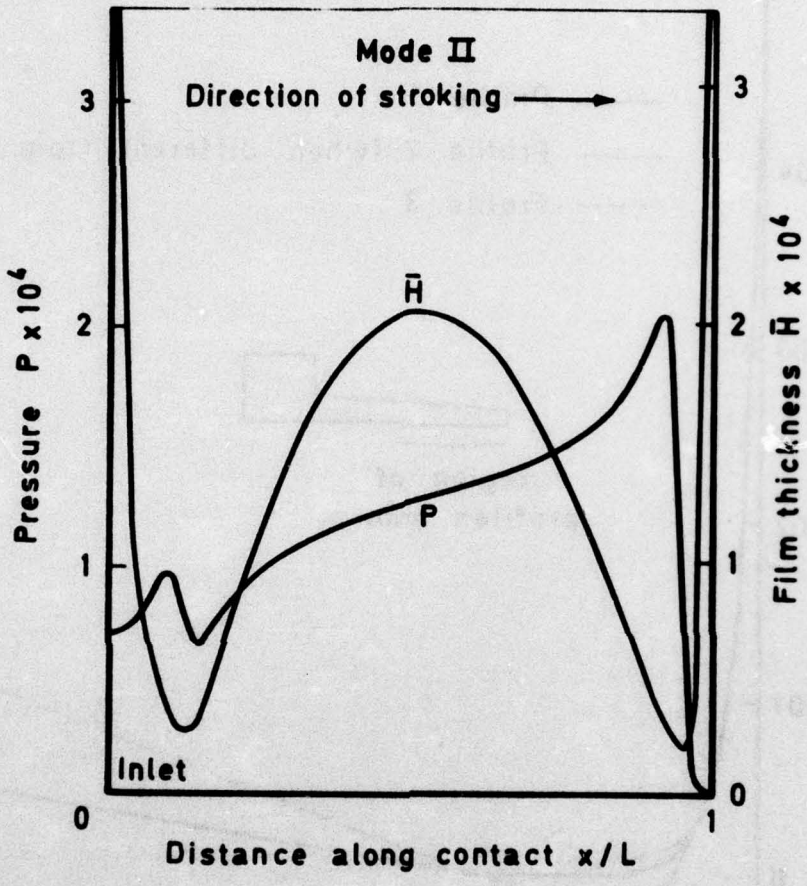

TR 76070

$\bar{U} = 5 \times 10^{-11}$; $\bar{P} = 6{\cdot}85 \times 10^{-5}$; $\bar{G} = 2060$; $\bar{T} = 1{\cdot}42 \times 10^{-3}$; $\bar{H}_0 = 3{\cdot}19 \times 10^{-4}$;

$\bar{W} = 1{\cdot}16 \times 10^{-4}$

other parameters as for seal B, profile 2 (Table 1 and Fig.7)

Fig. 8 Dimensionless pressure and film thickness

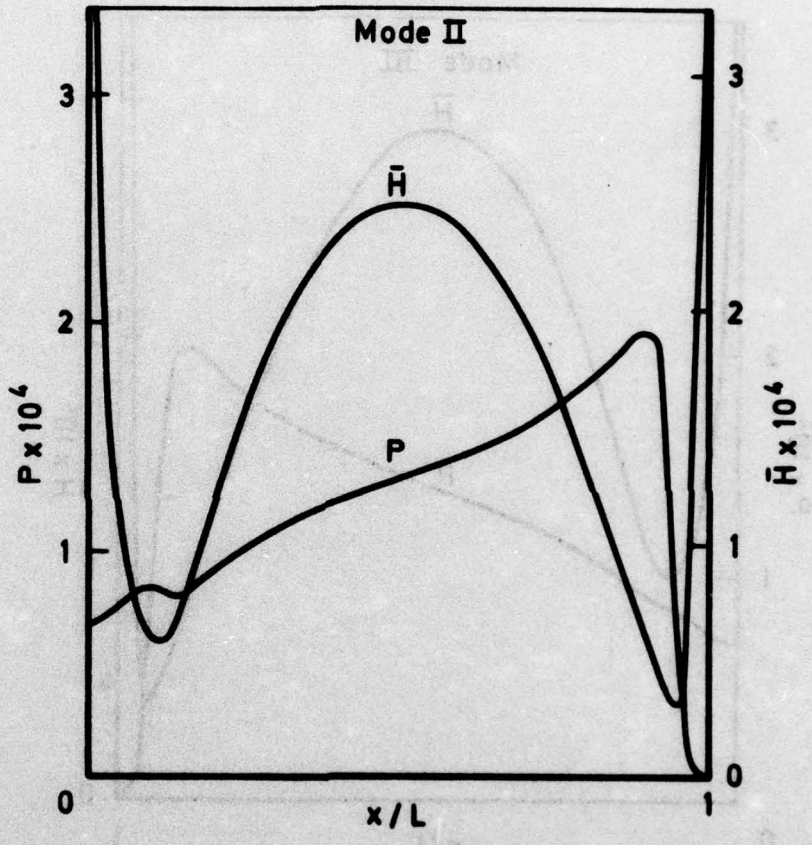

$\bar{U} = 10^{-10}$; $\bar{H}_0 = 6{\cdot}36 \times 10^{-4}$; $\bar{W} = 1{\cdot}22 \times 10^{-4}$;
other parameters as in Fig. 8

TR 76070

Fig. 9 Pressure and film shape

Fig.10

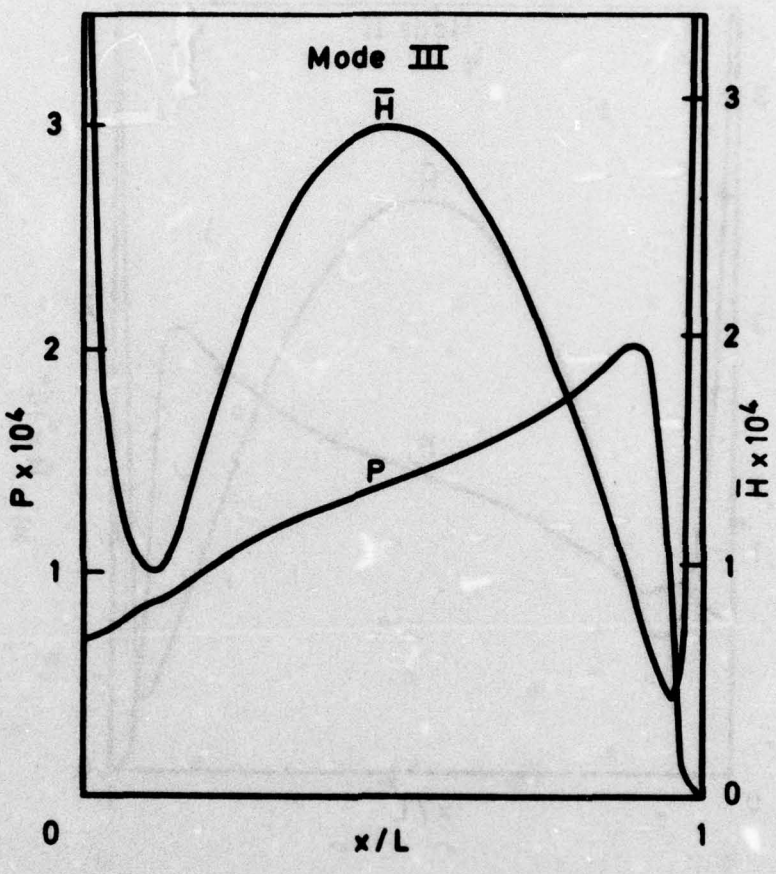

$\bar{U} = 1{\cdot}44 \times 10^{-10}$: $\bar{H}_0 = 8{\cdot}63 \times 10^{-4}$: $\bar{W} = 1{\cdot}26 \times 10^{-4}$:
other parameters as in Fig.8

Fig.10 Pressure and film shape

TR 78070

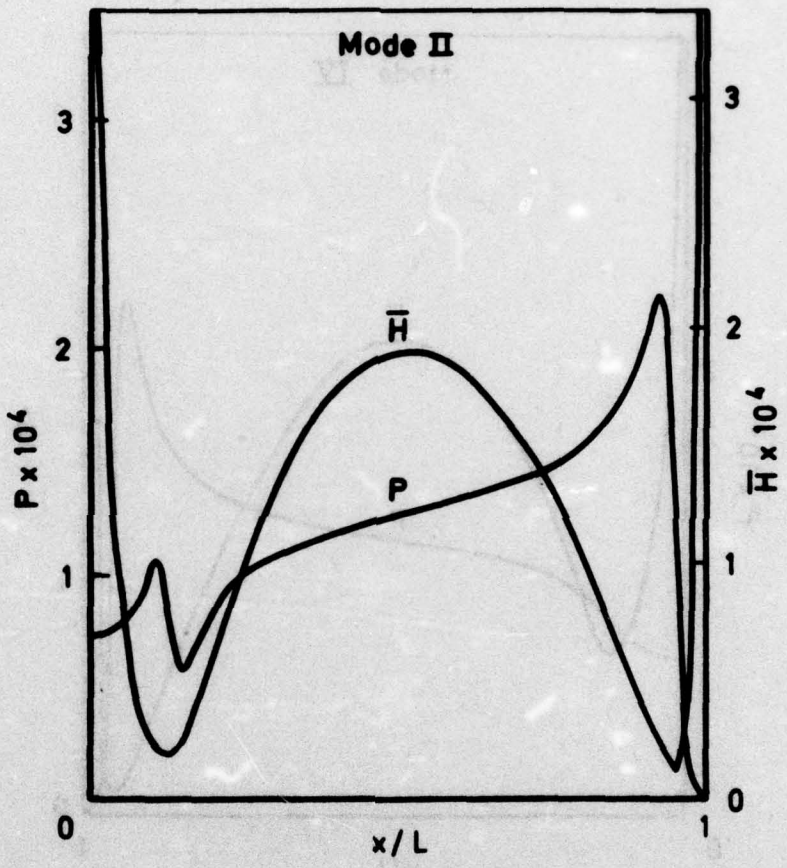

$\bar{U} = 3.5 \times 10^{-11}$; $\bar{H}_0 = 2.21 \times 10^{-4}$; $\bar{W} = 1.16 \times 10^{-4}$;
other parameters as in Fig.8

Fig.11 Pressure and film shape

Fig.12

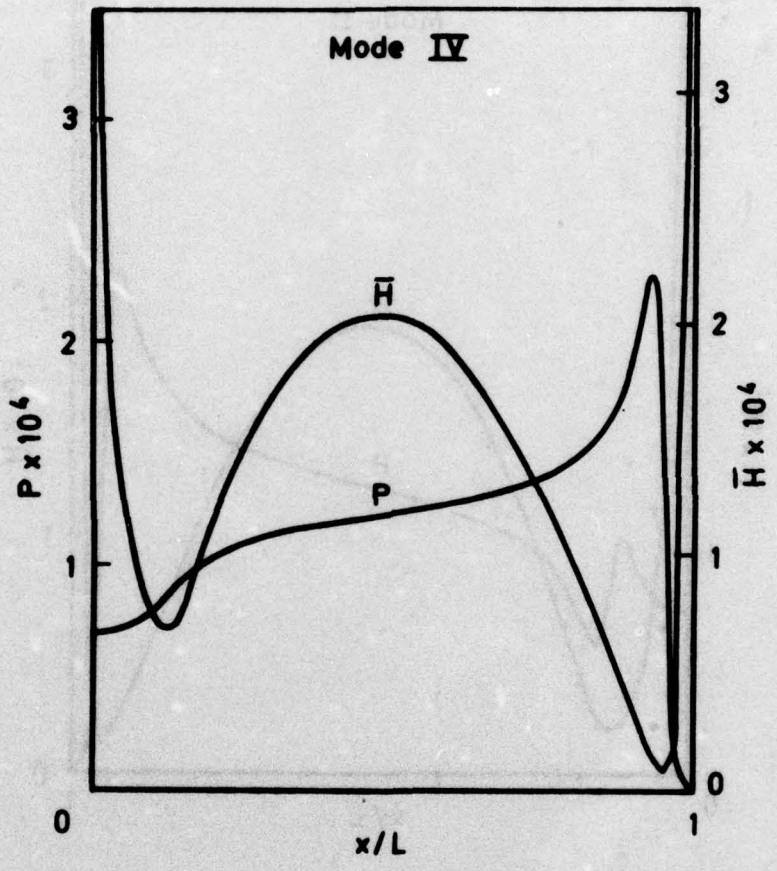

$\bar{U}=2{\cdot}5 \times 10^{-11}$; $\bar{H}_0=1{\cdot}51 \times 10^{-4}$; $\bar{W}=1{\cdot}16 \times 10^{-4}$;
other parameters as in Fig.8

TR 78070

Fig.12 Pressure and film shape

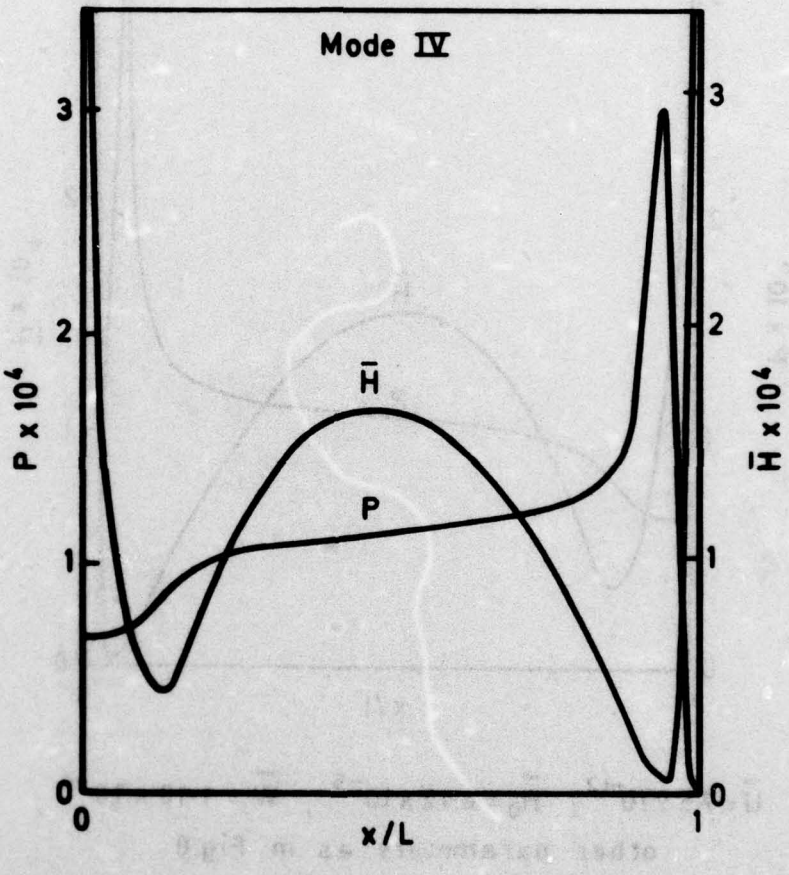

$\bar{U} = 10^{-11}$; $\bar{H}_0 = 5{\cdot}49 \times 10^{-5}$; $\bar{W} = 1{\cdot}11 \times 10^{-4}$; other parameters as in Fig.8

Fig.13 Pressure and film shape

Fig.14

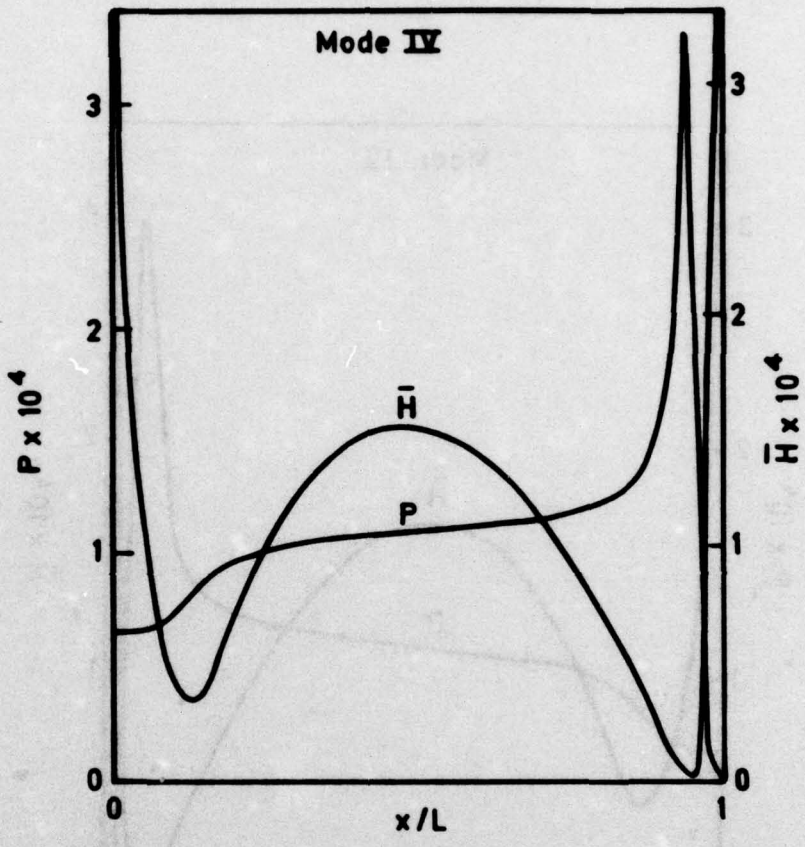

$\bar{U} = 7{\cdot}5 \times 10^{-12}$; $\bar{H}_0 = 4{\cdot}12 \times 10^{-5}$; $\bar{W} = 1{\cdot}10 \times 10^{-4}$;
other parameters as in Fig.8

Fig.14 Pressure and film shape

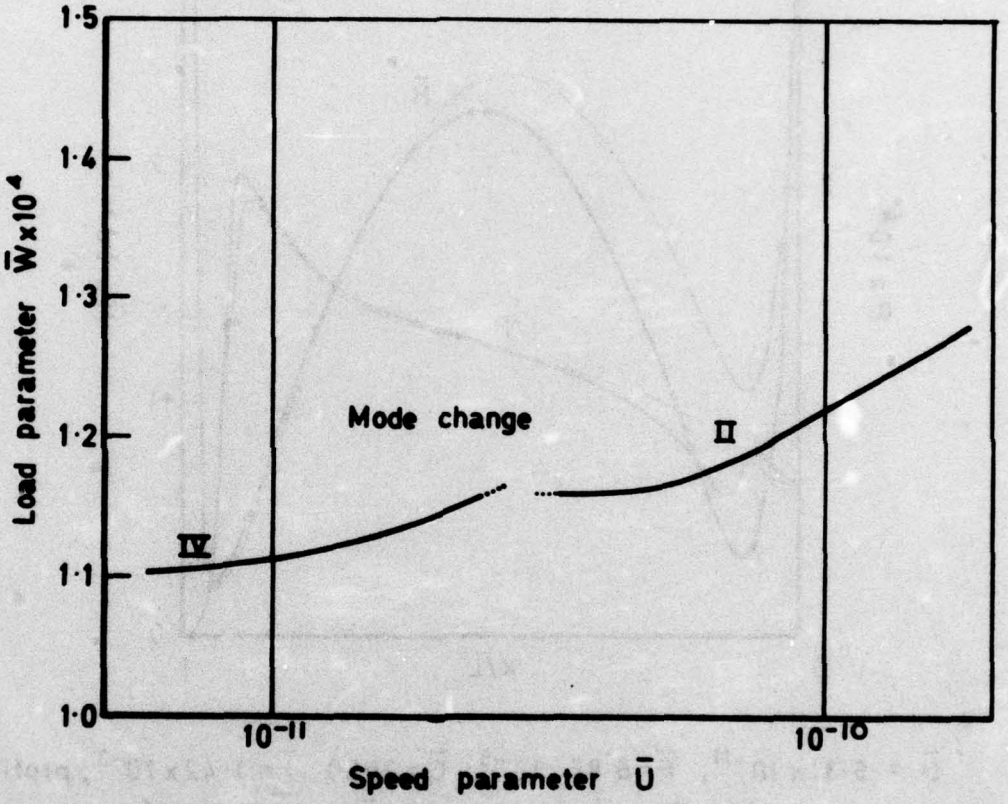

Fig.15 Variation of load with speed for Figs 8–14

Fig. 16

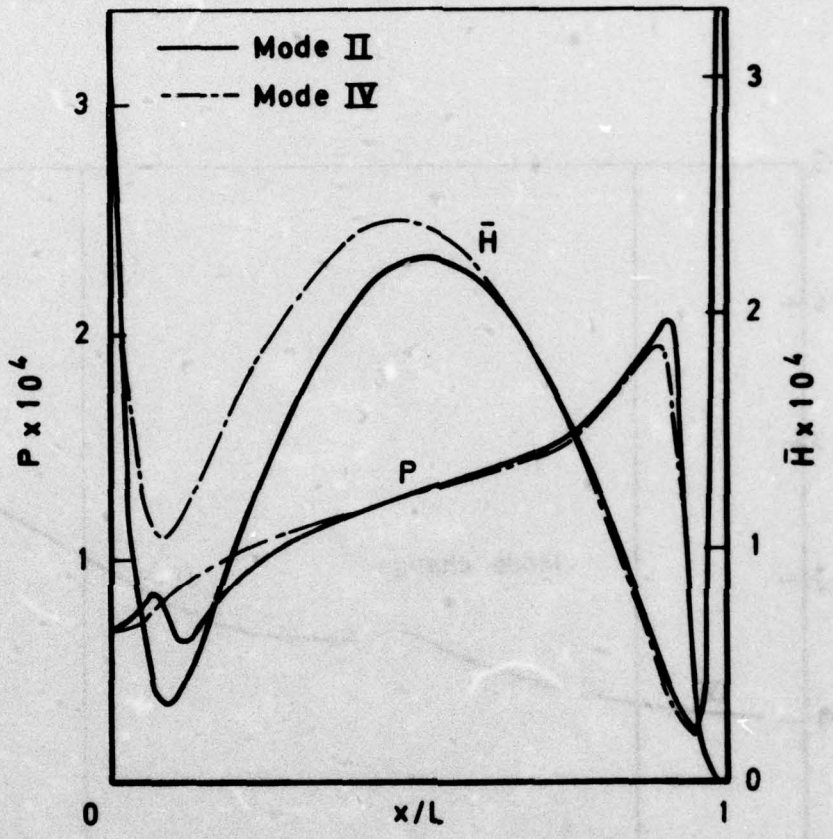

TR 76070

$\bar{U} = 6{\cdot}31 \times 10^{-11}$; $\bar{P} = 6{\cdot}85 \times 10^{-5}$; $\bar{G} = 2060$; $\bar{I} = 1{\cdot}42 \times 10^{-3}$; profile 1

Mode II: $\bar{H}_0 = 4{\cdot}31 \times 10^{-4}$; $\bar{W} = 1{\cdot}18 \times 10^{-4}$

Mode IV: $\bar{H}_0 = 4{\cdot}09 \times 10^{-4}$; $\bar{W} = 1{\cdot}21 \times 10^{-4}$

Fig.16 Alternative solutions of the elastohydrodynamic equations

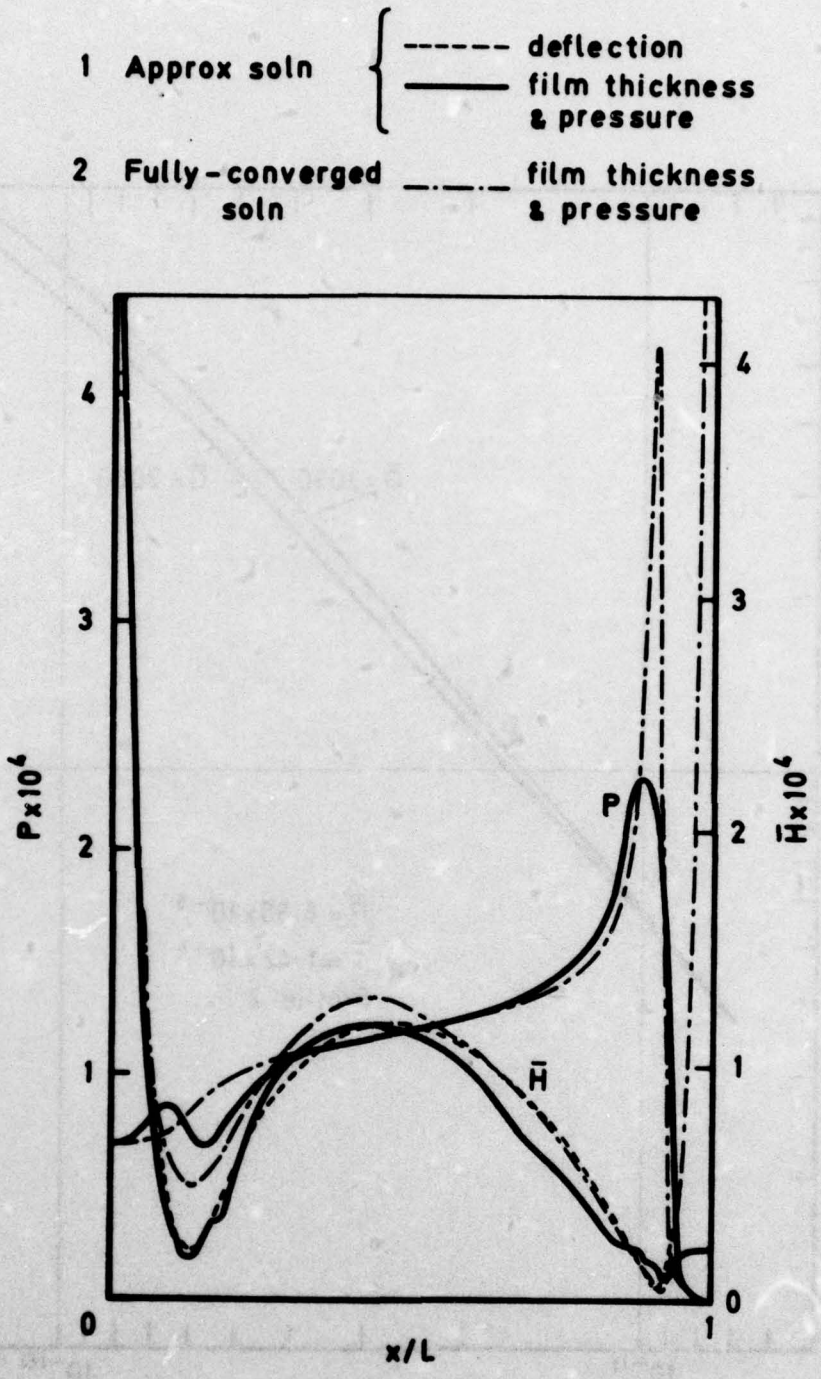

$\bar{U}=10^{-11}$; $\bar{P}=6{\cdot}85\times10^{-5}$; $\bar{G}=2060$; $\bar{T}=1{\cdot}67\times10^{-3}$; profile 3

1 Mode II: manual solution; $\bar{H}_o=1{\cdot}52\times10^{-4}$; $\bar{W}=1{\cdot}08\times10^{-4}$

2 Mode IV: automatic solution; $\bar{H}_o=4{\cdot}60\times10^{-5}$; $\bar{W}=1{\cdot}12\times10^{-4}$

TR 76070

Fig.17 Comparison of manual and automatic solution

Fig. 18

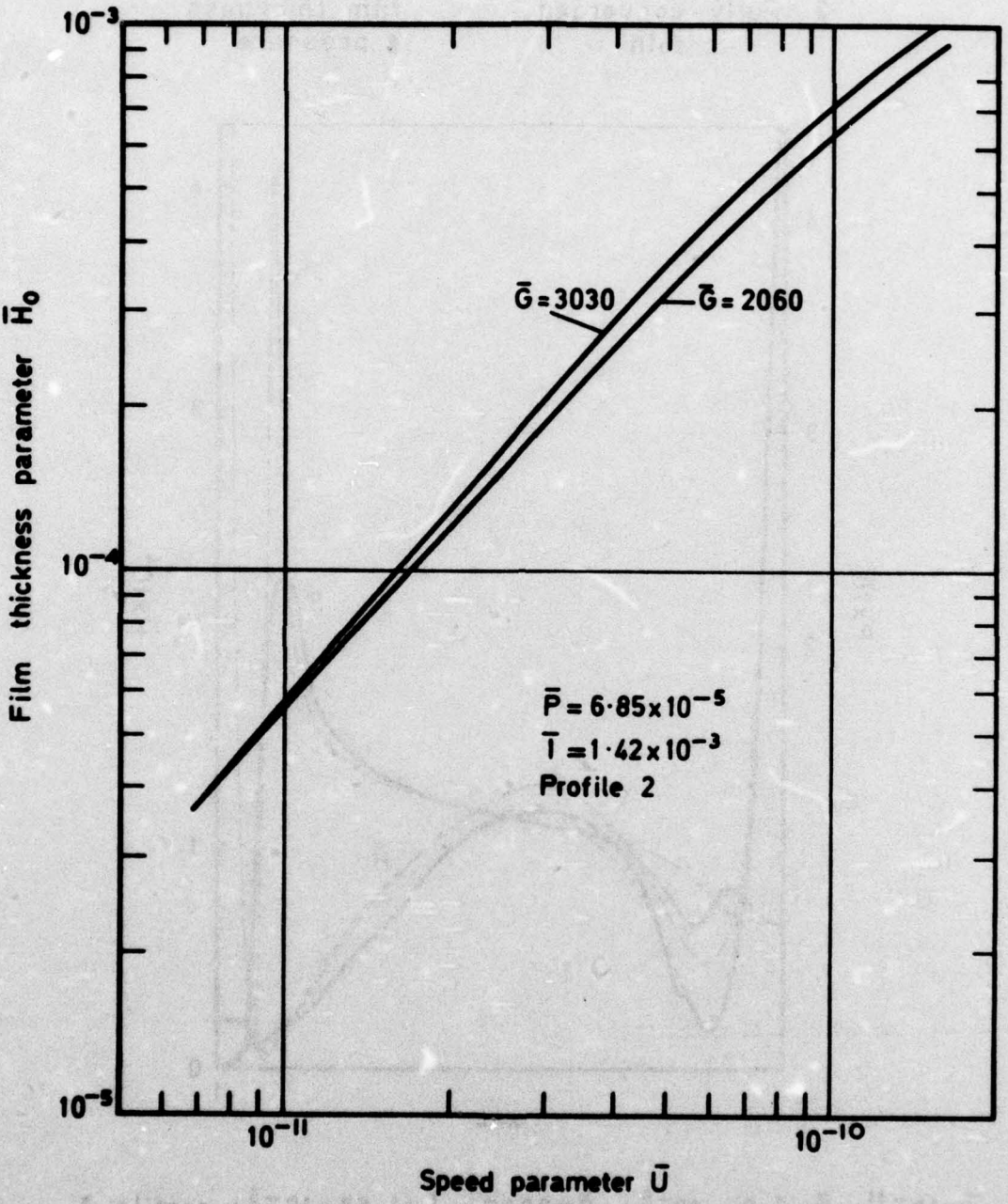

TR 76070

Fig. 18 Variation of film thickness with speed

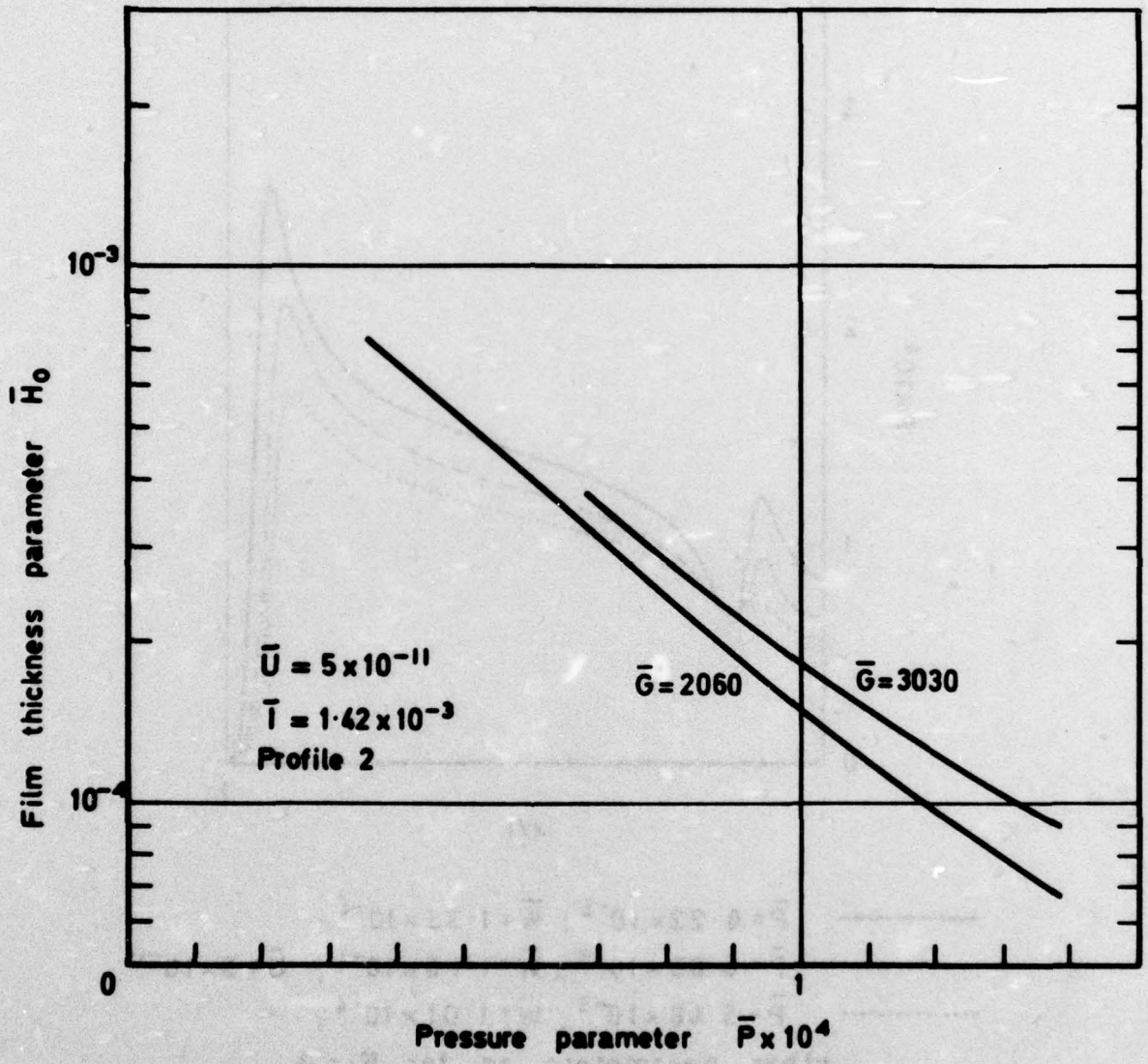

Fig. 19 Variation of film thickness with pressure

Fig. 20

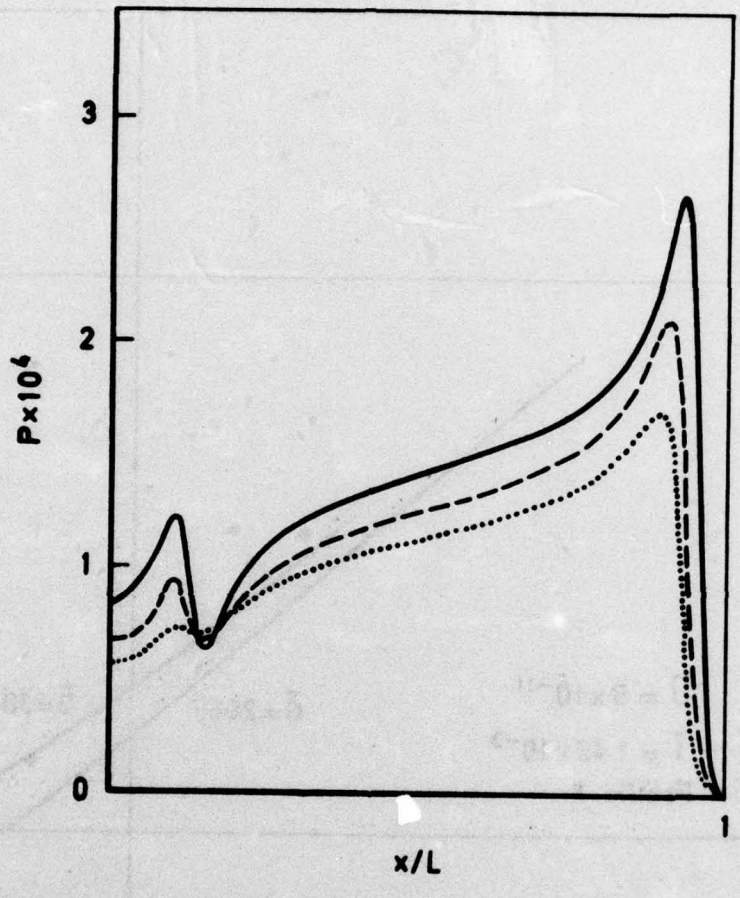

——— $\bar{P} = 8{\cdot}22 \times 10^{-5}$; $\bar{W} = 1{\cdot}33 \times 10^{-4}$;

– – – – – $\bar{P} = 6{\cdot}85 \times 10^{-5}$; $\bar{W} = 1{\cdot}16 \times 10^{-4}$; $\bar{U} = 5 \times 10^{-11}$

..... $\bar{P} = 5{\cdot}48 \times 10^{-5}$; $\bar{W} = 1{\cdot}01 \times 10^{-4}$;

other parameters as for Fig. 8

TR 76070

Fig. 20 Change of pressure profile with $\bar{P}$

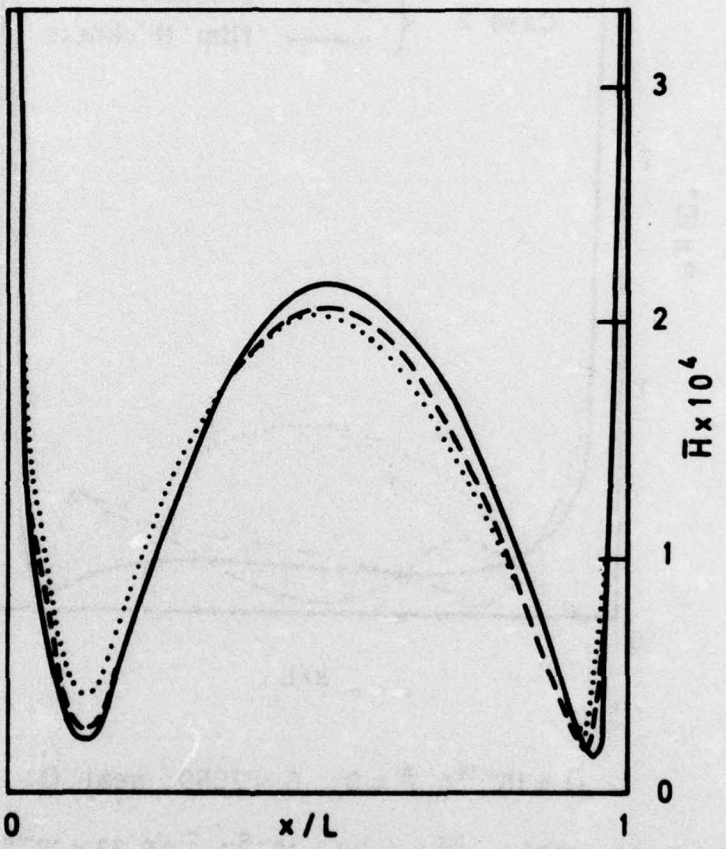

TR 76070

——— $\bar{P} = 8{\cdot}22 \times 10^{-5}$; $\bar{H} = 2{\cdot}42 \times 10^{-4}$;

– – – – $\bar{P} = 6{\cdot}85 \times 10^{-5}$; $\bar{H} = 3{\cdot}19 \times 10^{-4}$; $\bar{U} = 5 \times 10^{-11}$

····· $\bar{P} = 5{\cdot}48 \times 10^{-5}$; $\bar{H} = 4{\cdot}49 \times 10^{-4}$;

other parameters as for Fig. 8

Fig. 21 Change of film shape with $\bar{P}$

Fig.22

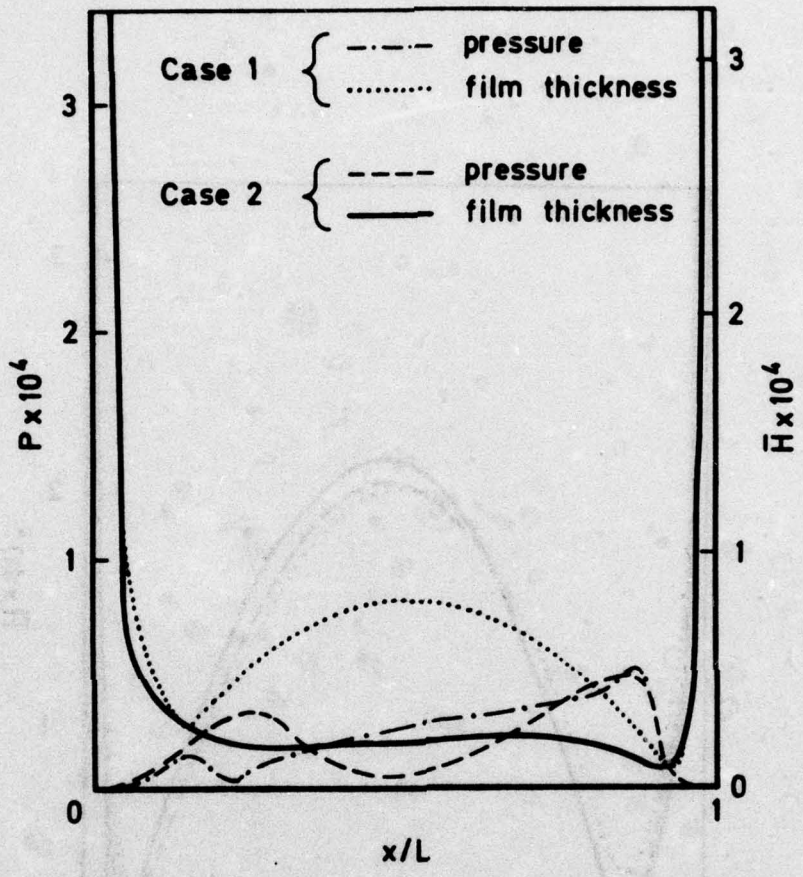

$\bar{U} = 10^{-11}$; $\bar{P} = 0$; $\bar{G} = 2060$; seal B;

Case 1; $\bar{H}_o = 2{\cdot}45 \times 10^{-4}$; $\bar{W} = 2{\cdot}14 \times 10^{-5}$; $\bar{I} = 8{\cdot}33 \times 10^{-4}$; profile 1 (Fig.7)

Case 2; $\bar{H}_o = 2{\cdot}07 \times 10^{-4}$; $\bar{W} = 2{\cdot}21 \times 10^{-5}$; $\bar{I} = 1{\cdot}42 \times 10^{-3}$; profile 3 (Fig.7)

TR 75070

Fig. 22 Manual solutions at $\bar{P} = 0$ (showing how pressure and film thickness can vary appreciably for small changes in interference and profile)

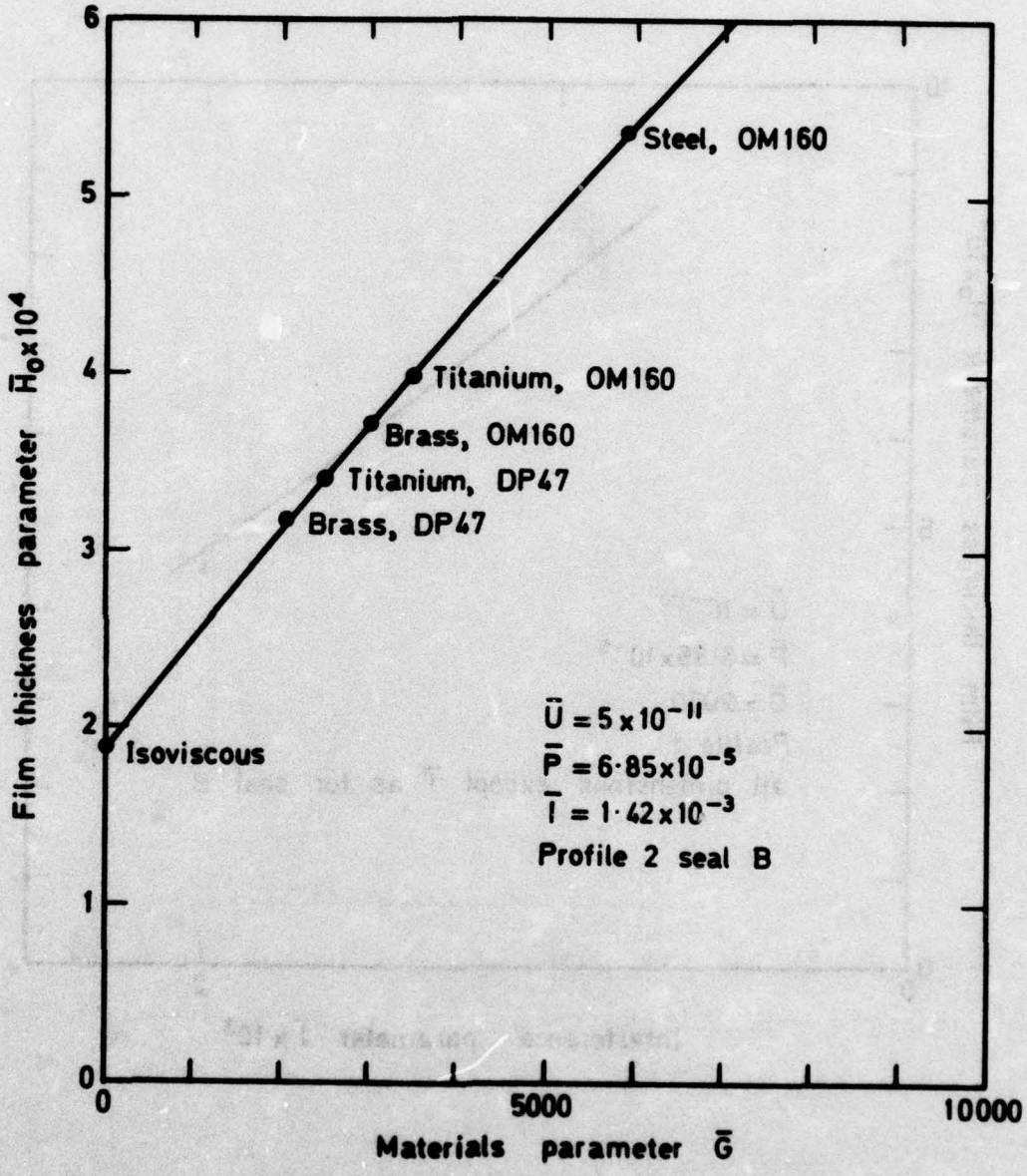

T.R.76070

Fig. 23 Variation of film thickness with $\bar{G}$

Fig. 24

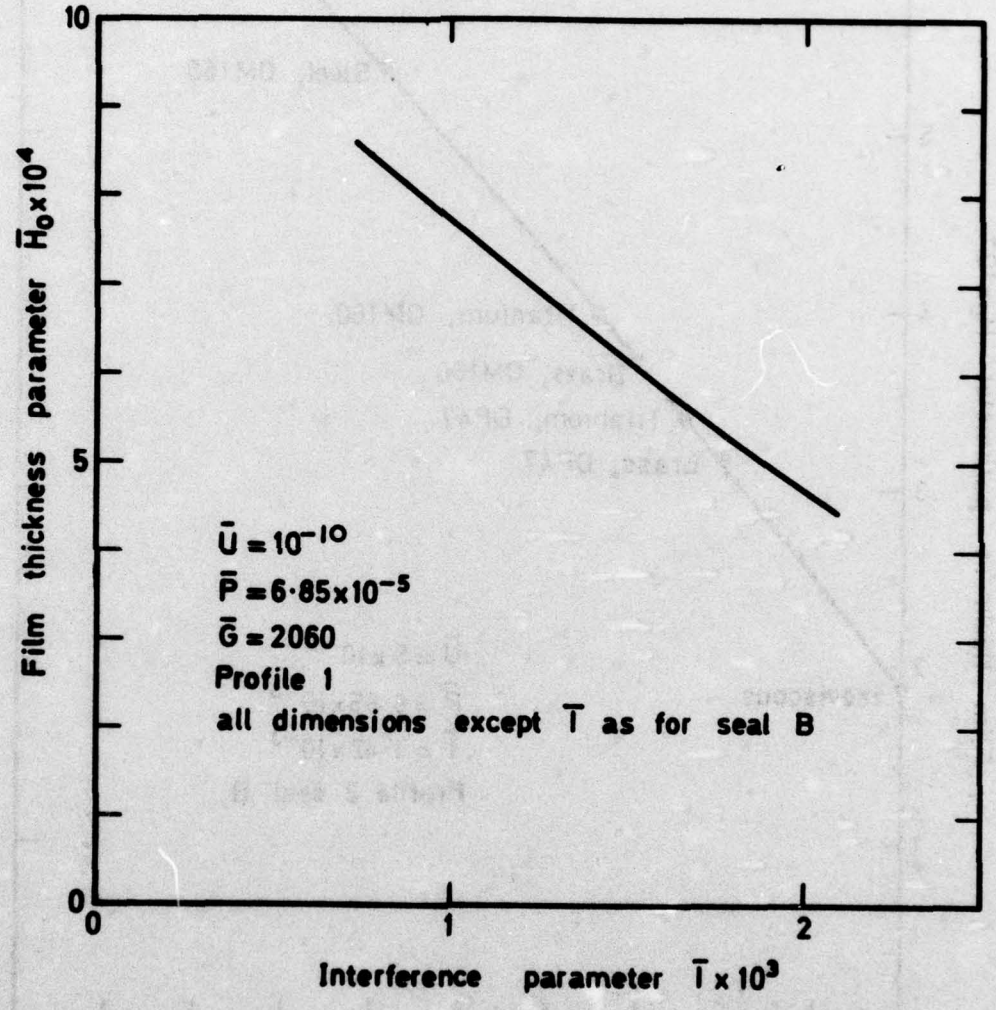

TR 76070

Fig. 24 Variation of film thickness with $\bar{T}$

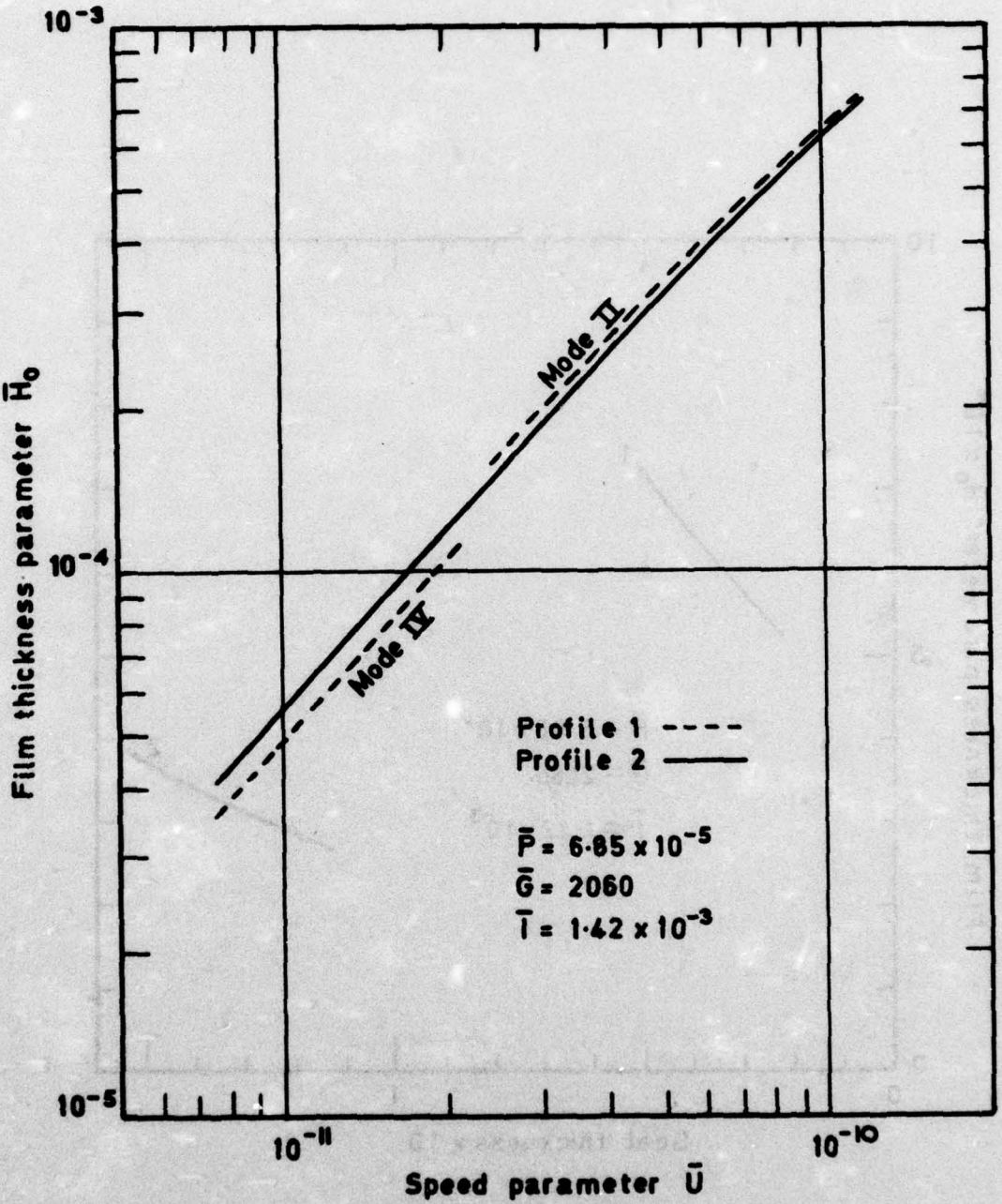

T.R.76070

Fig.25 Effect of profile on film thickness

Fig. 26

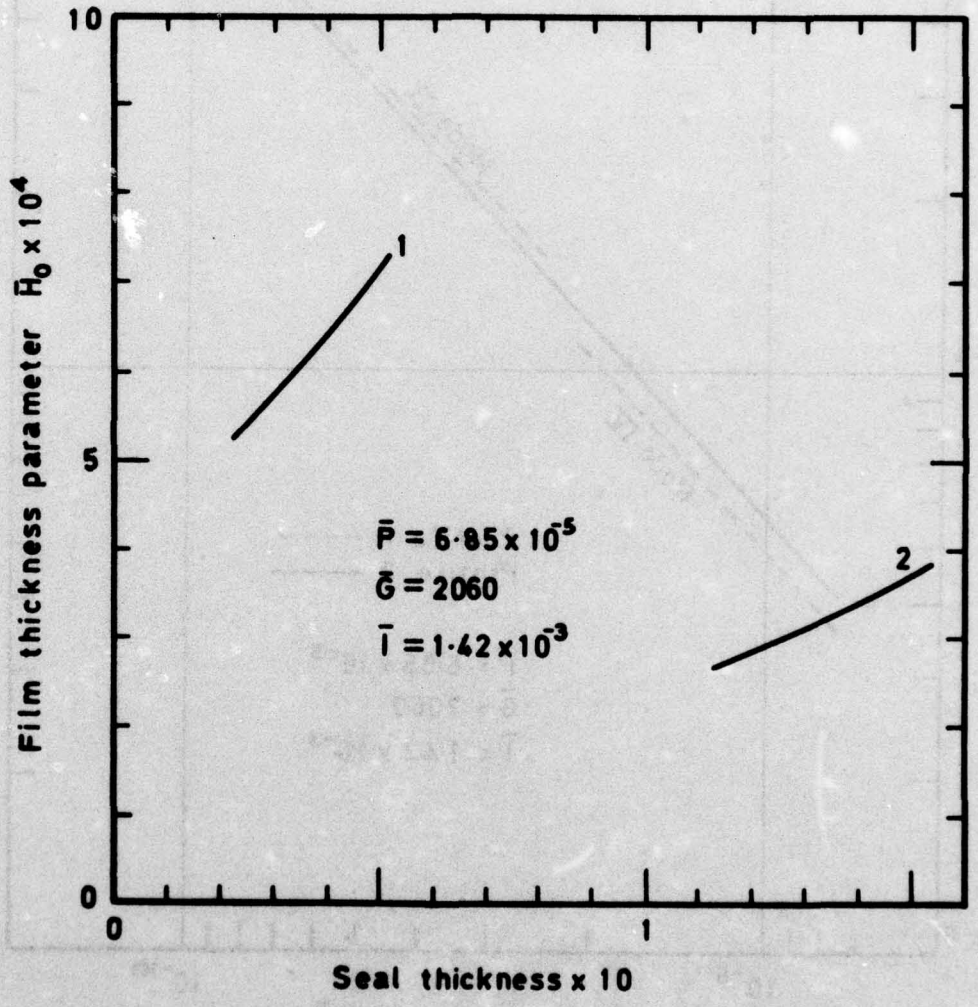

TR 76070

Curve 1 Effect of varying lip thickness t_1/L for fixed t_2/L
Curve 2 Effect of varying root thickness t_2/L for fixed t_1/L
See section 5.6

Fig. 26 Effect of thickness of seal lip and shell on film thickness

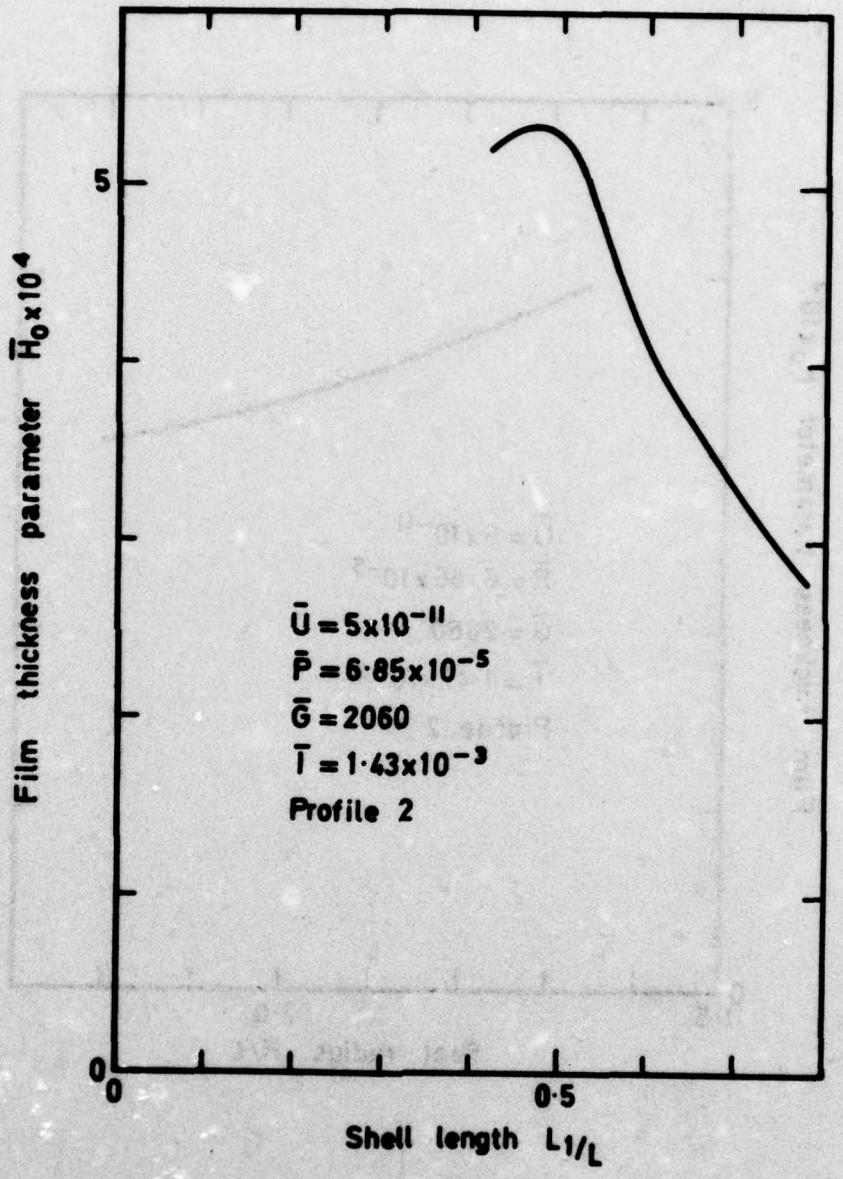

Fig. 27 Effect of shell length on film thickness

Fig. 28

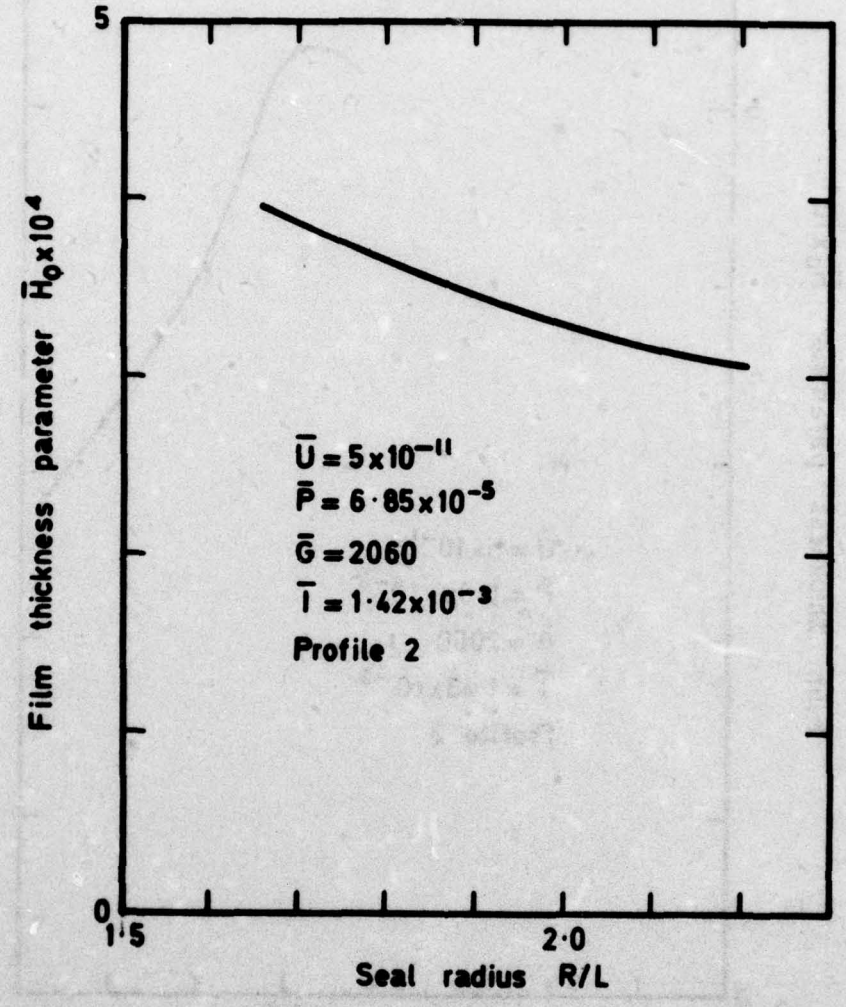

TR 76070

Fig. 28 Effect of seal radius on film thickness

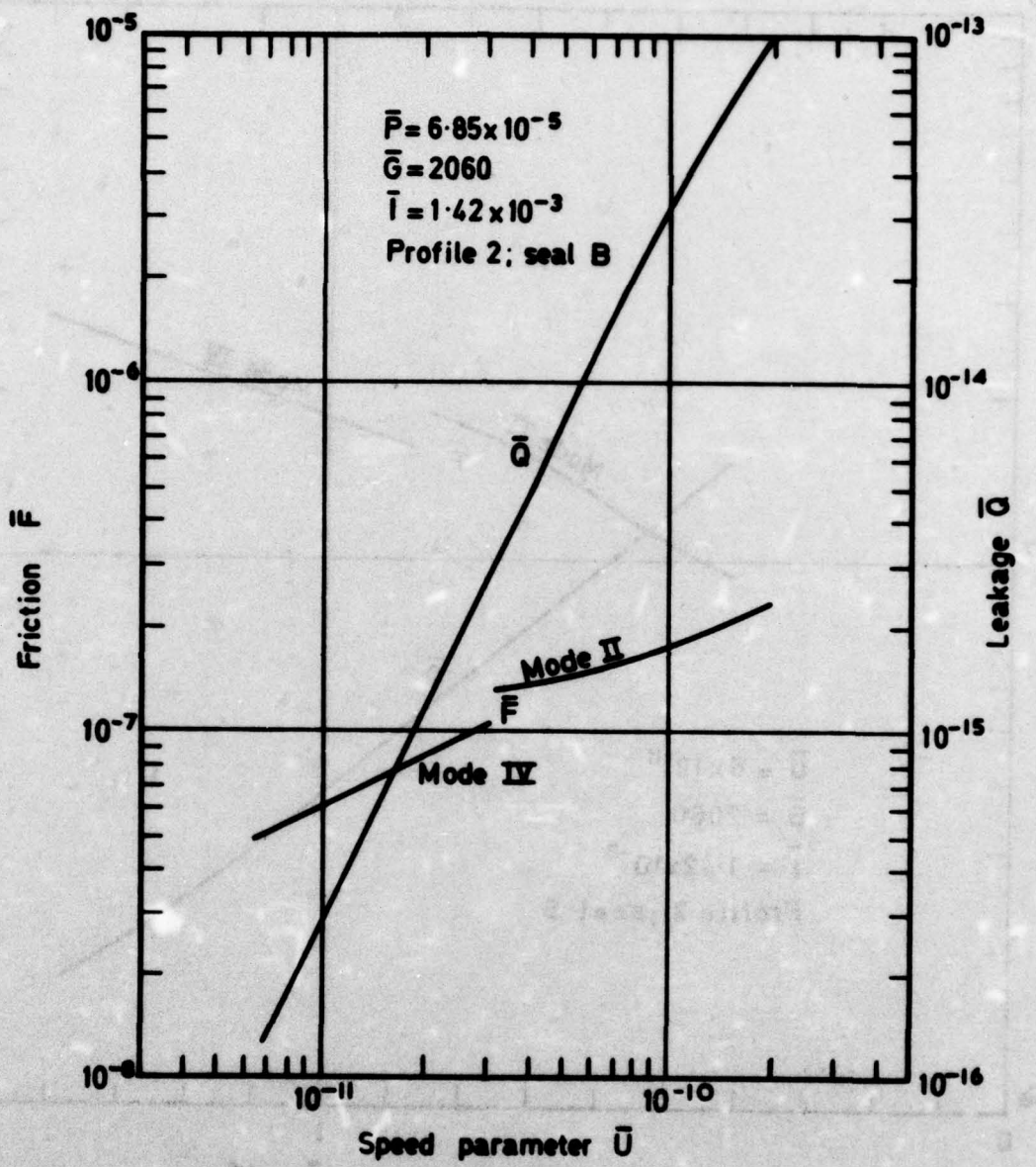

TR 76070

Fig. 29 Variation of friction and leakage with speed

Fig. 30

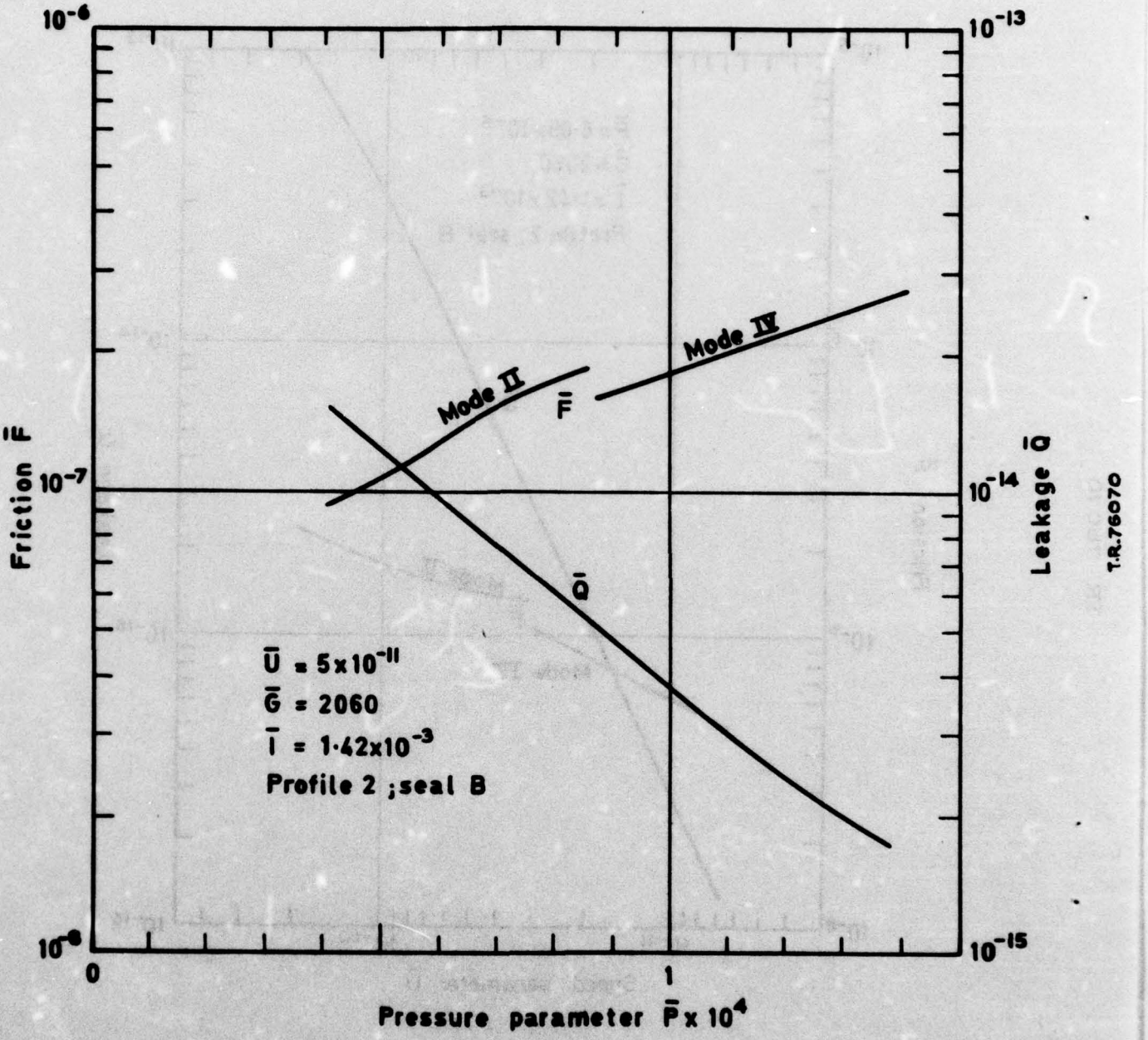

Fig.30 Variation of friction and leakage with pressure

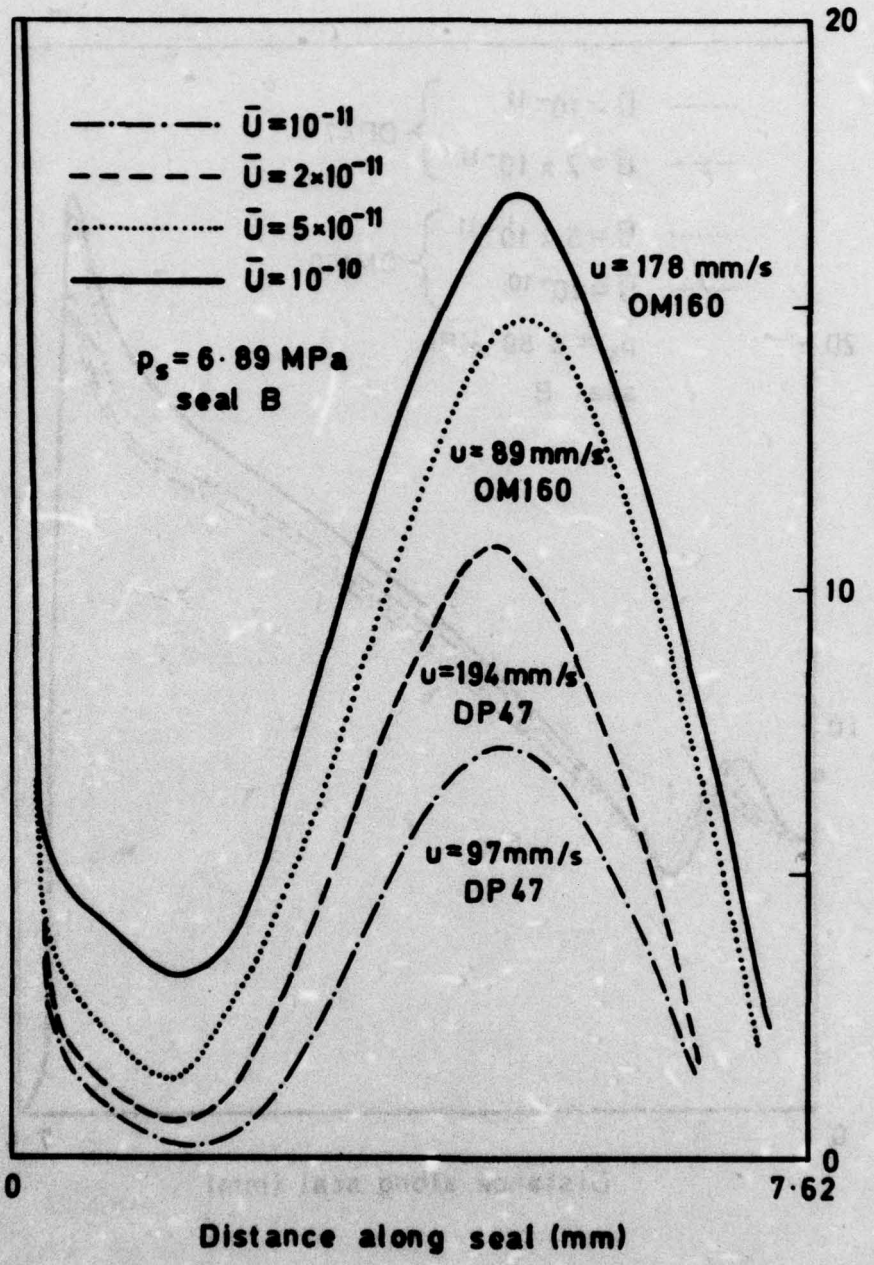

TR 76070

Fig. 31 Measured outstroke oil film shapes

Fig.32

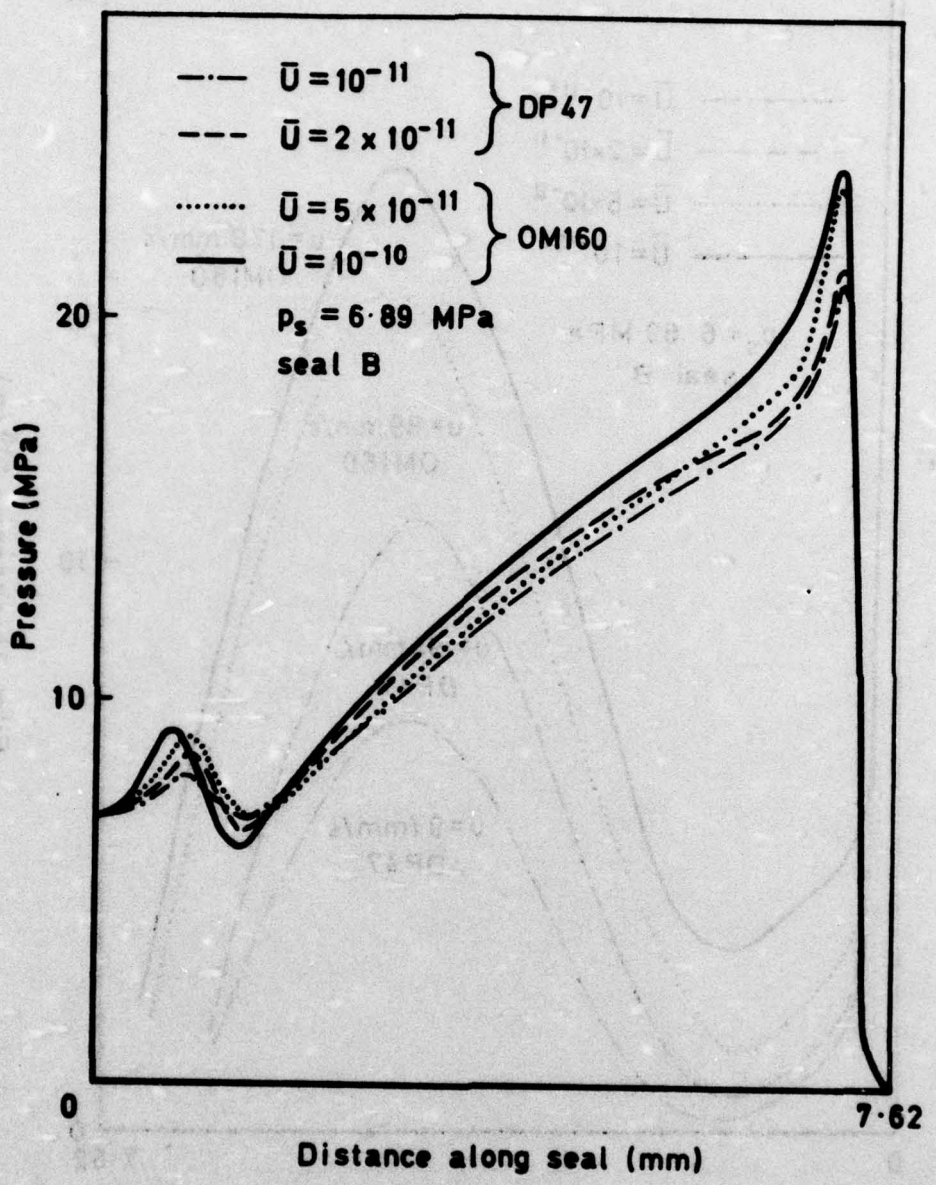

TR 76070

Fig. 32 Measured pressure distributions corresponding to the oil films in Fig. 31

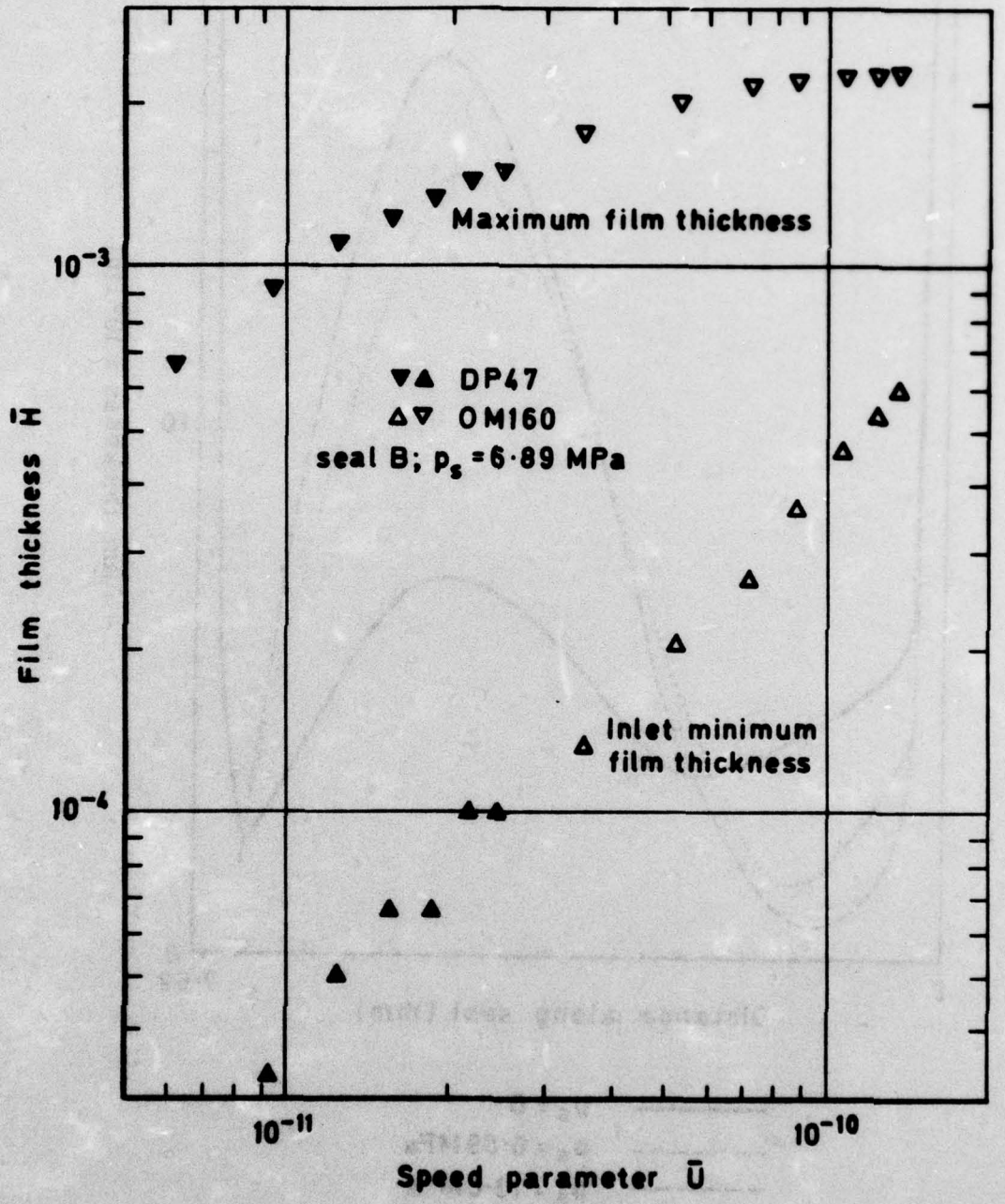

TR 76070

Fig. 33 Variation of film thickness with speed

Fig. 34

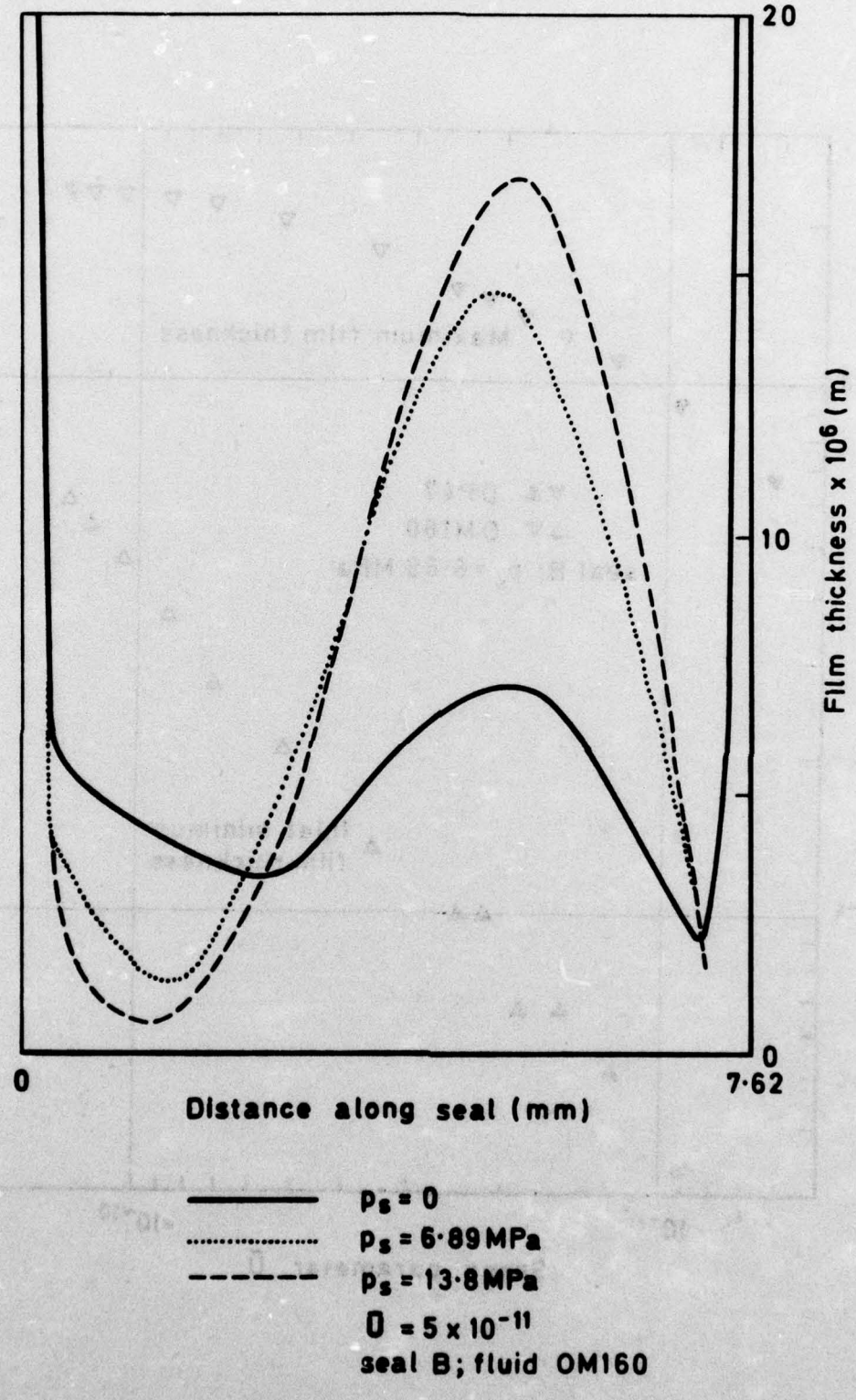

TR 76070

Fig. 34 Change of outstroke film shape with system pressure

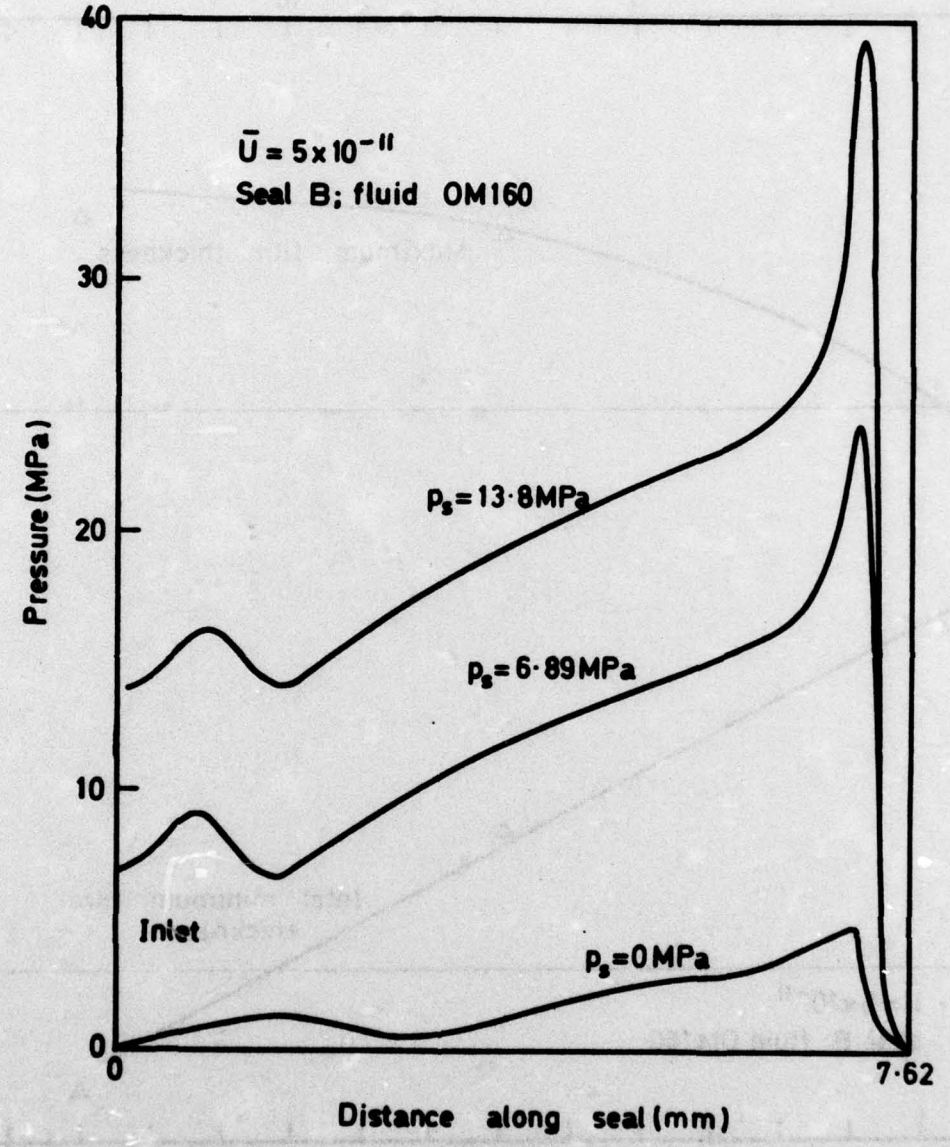

Fig. 35 Change of pressure distribution with system pressure corresponding to the film shapes of Fig. 34

Fig. 36

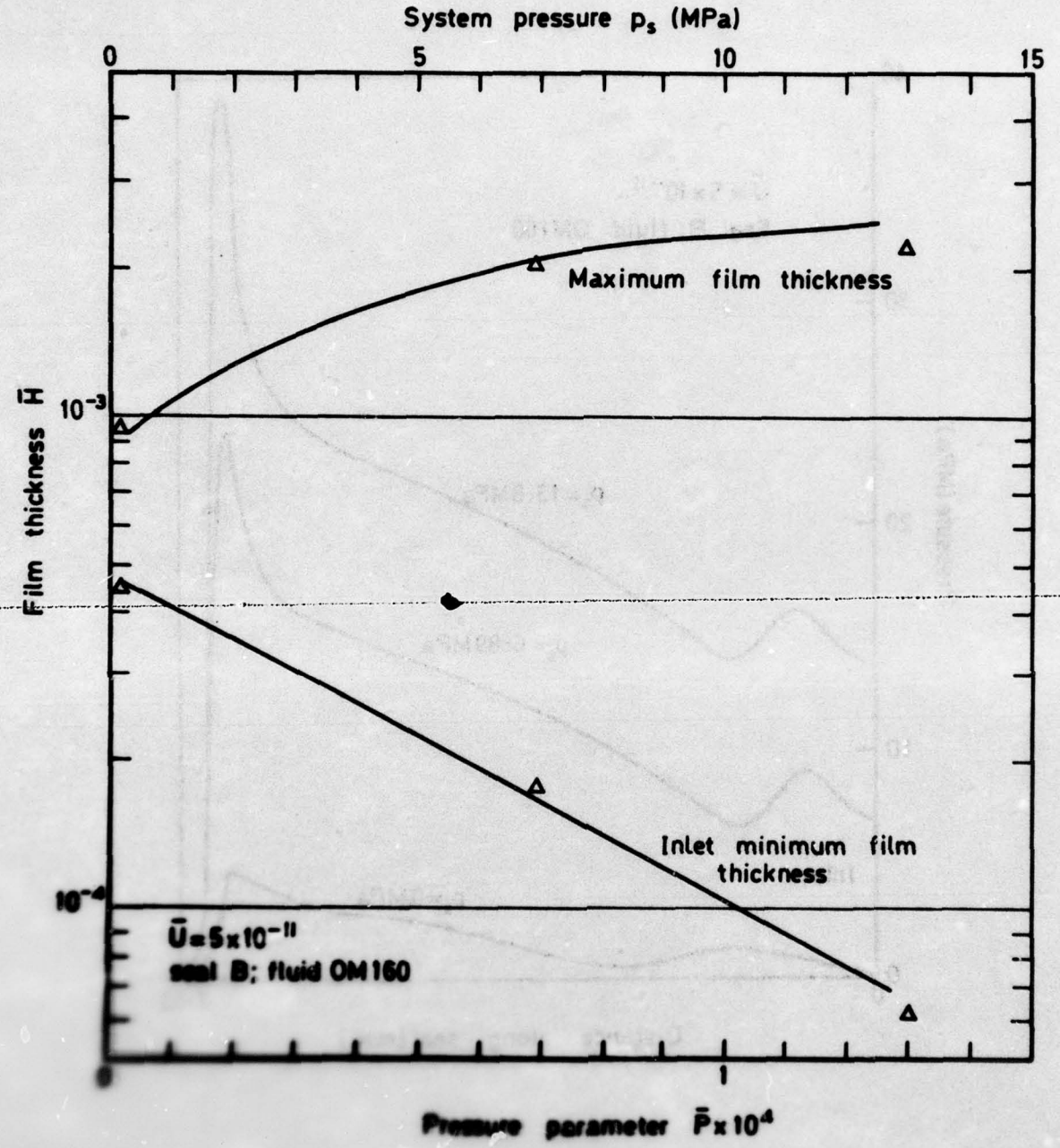

TR 76070

Fig. 37 Film thickness corresponding to Fig. 36

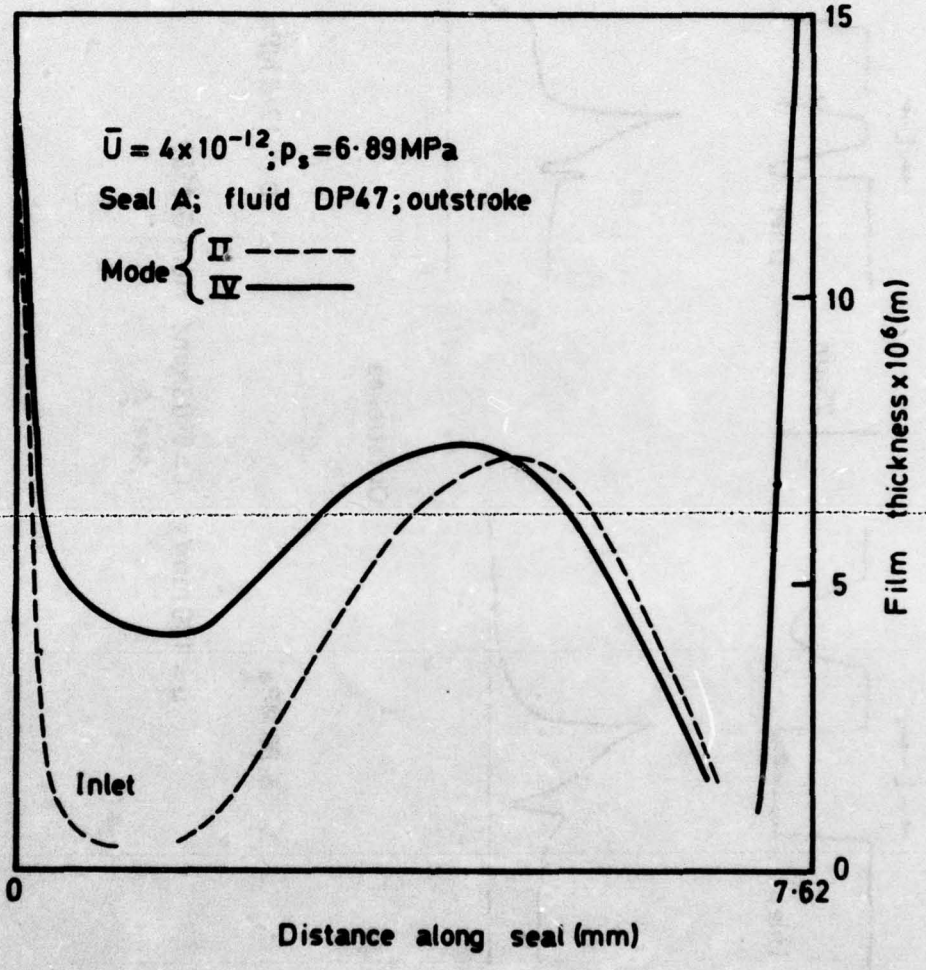

Fig. 37 Different hydrodynamic modes at the same operating conditions

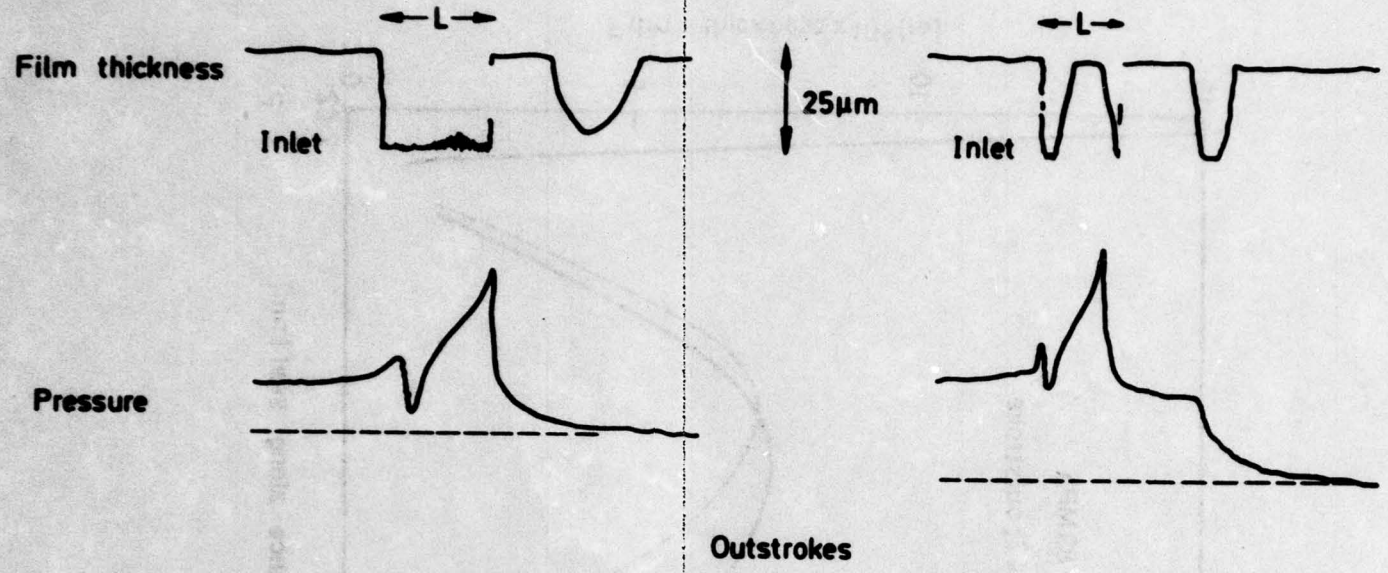

u = 130 mm/s ; L=5·03mm ; fluid OM160
seal A

Fig. 38a & b Effect of reduced lip length L

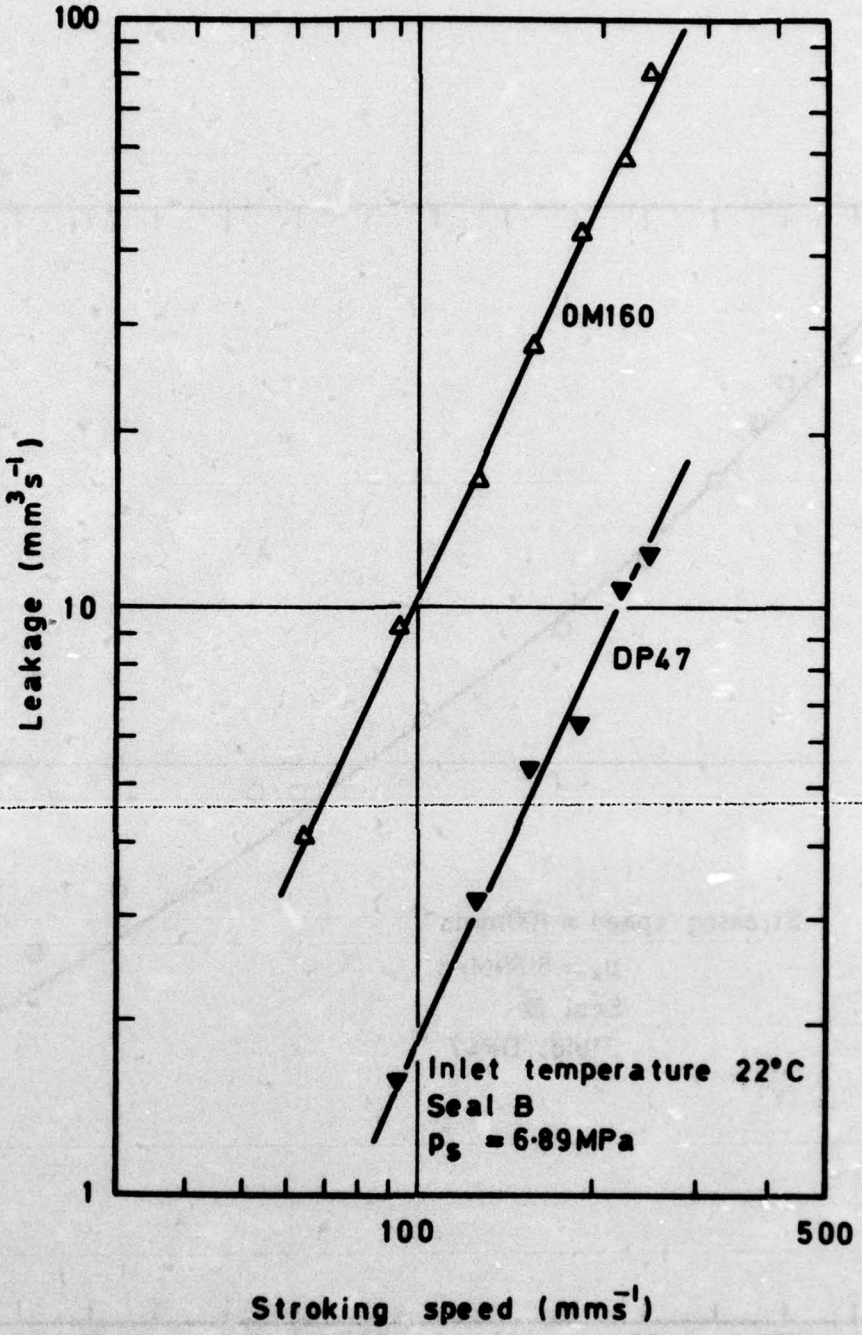

TR 76070

Instananeous leakage values deduced from measured outstroke film thickness

Fig. 39 Leakage

Fig. 40

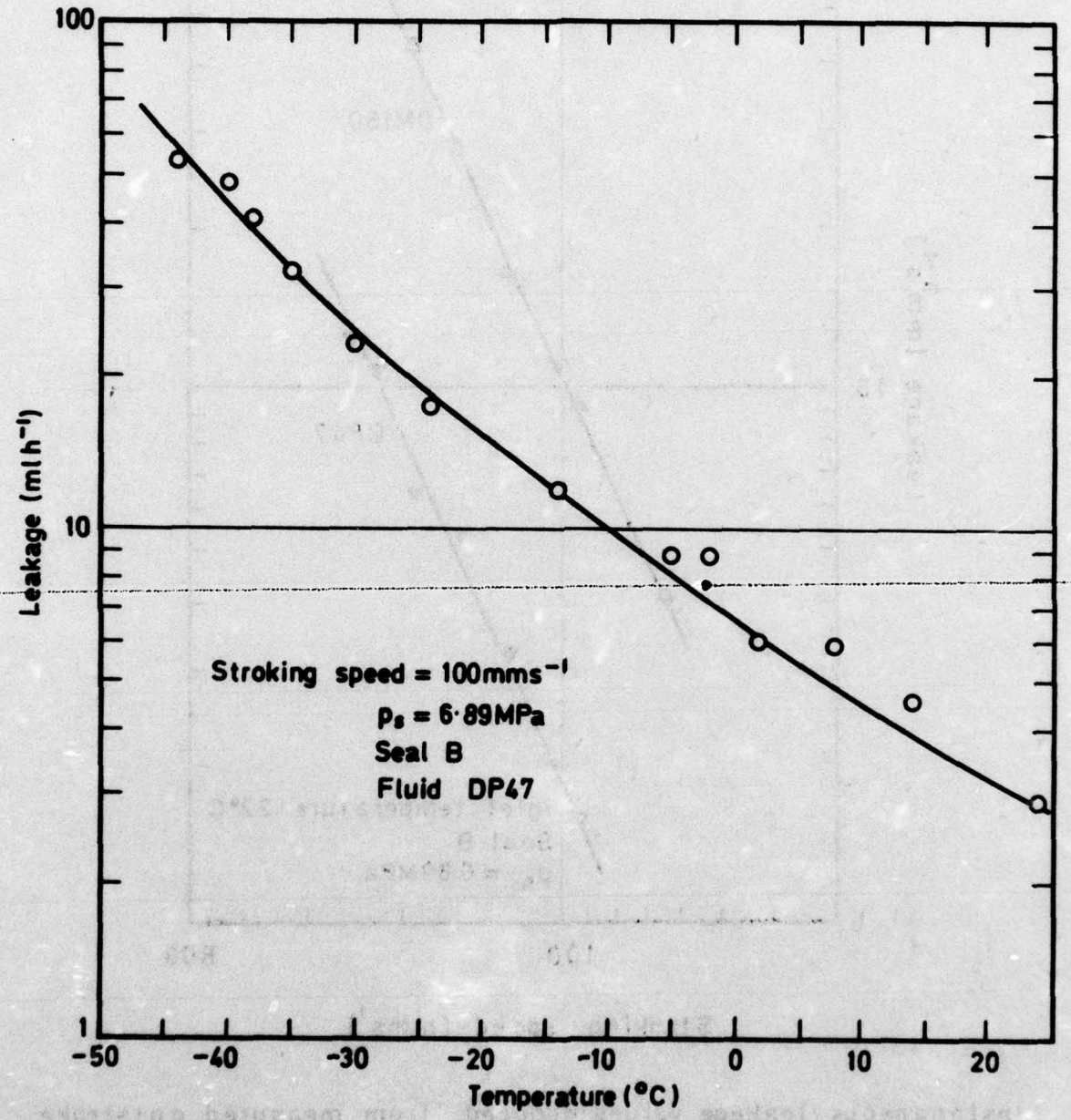

Fig. 40 Variation of leakage with temperature

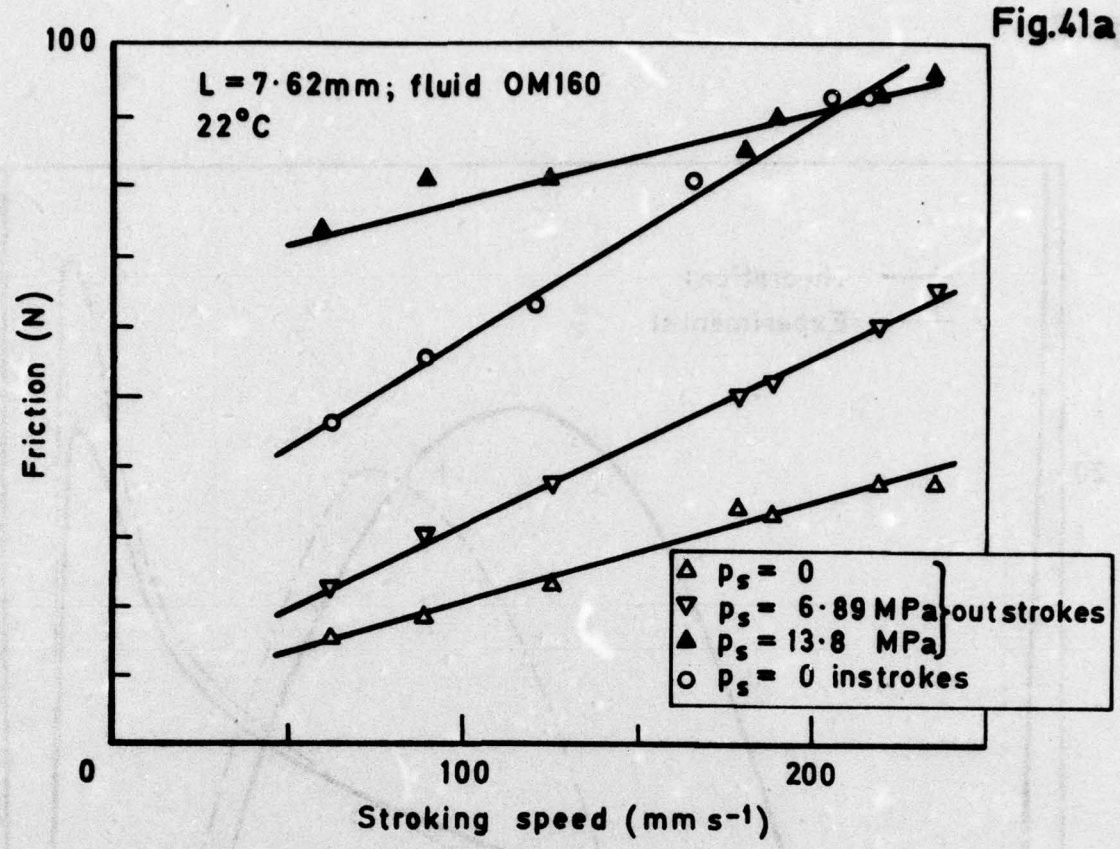

a Friction of seal 'B'

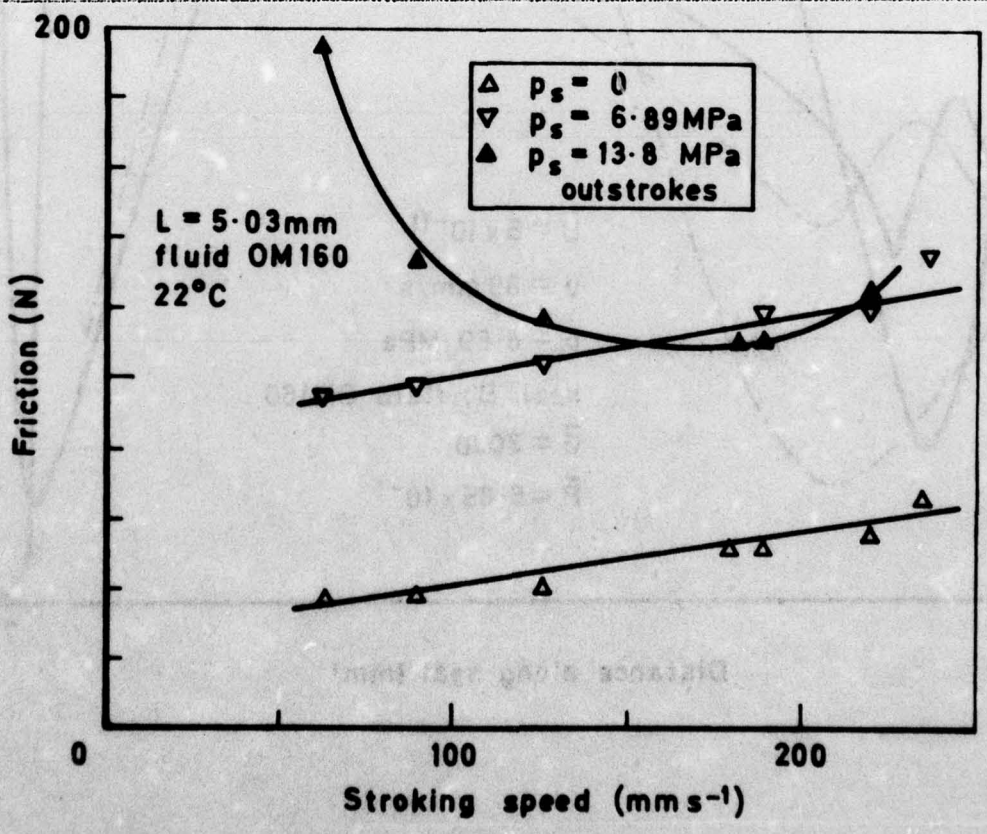

b Friction of seal 'A' with a reduced lip length

Fig.41a & b Friction

Fig. 42

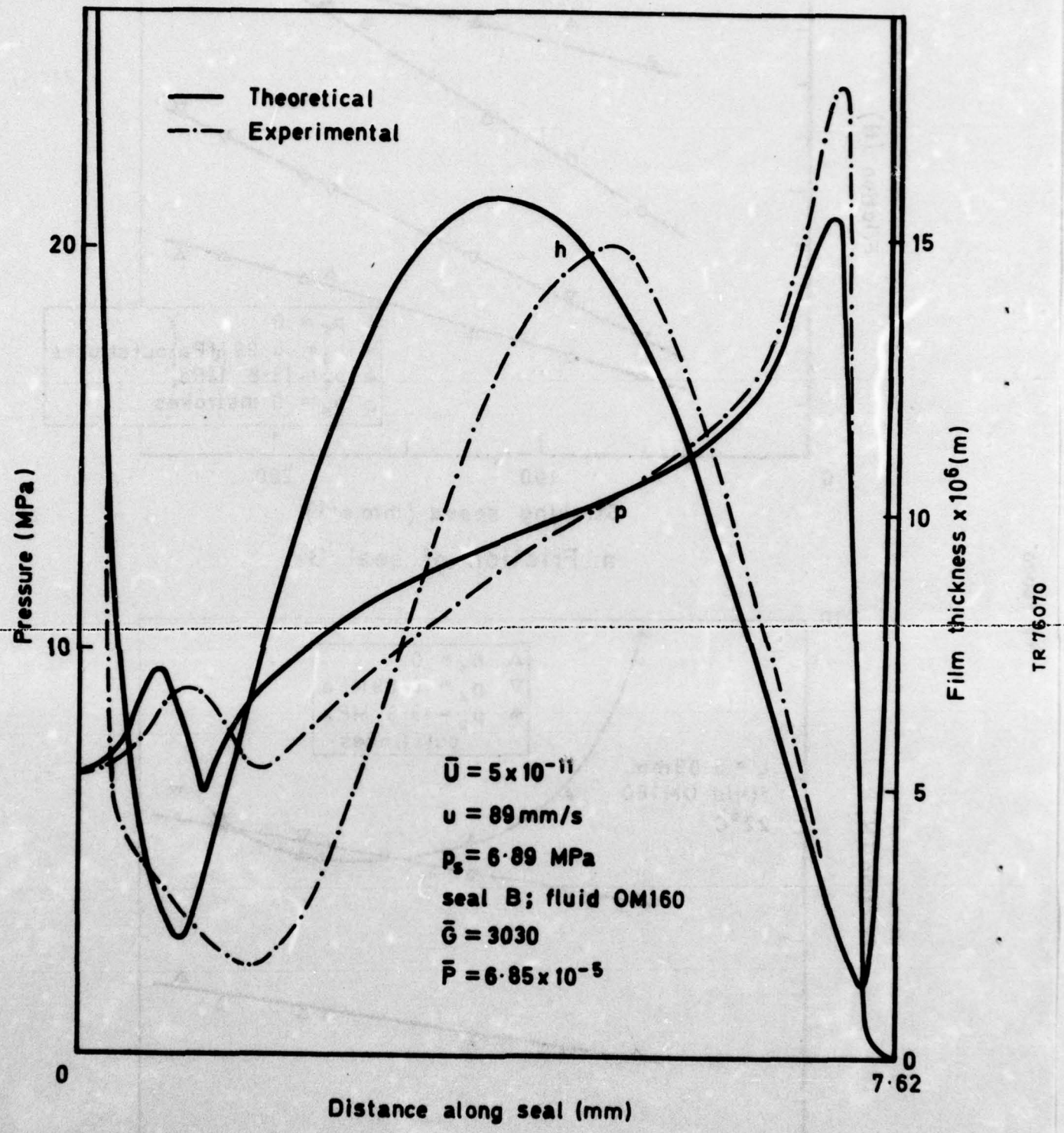

Fig. 42 Theoretical and experimental pressure distribution and film shape

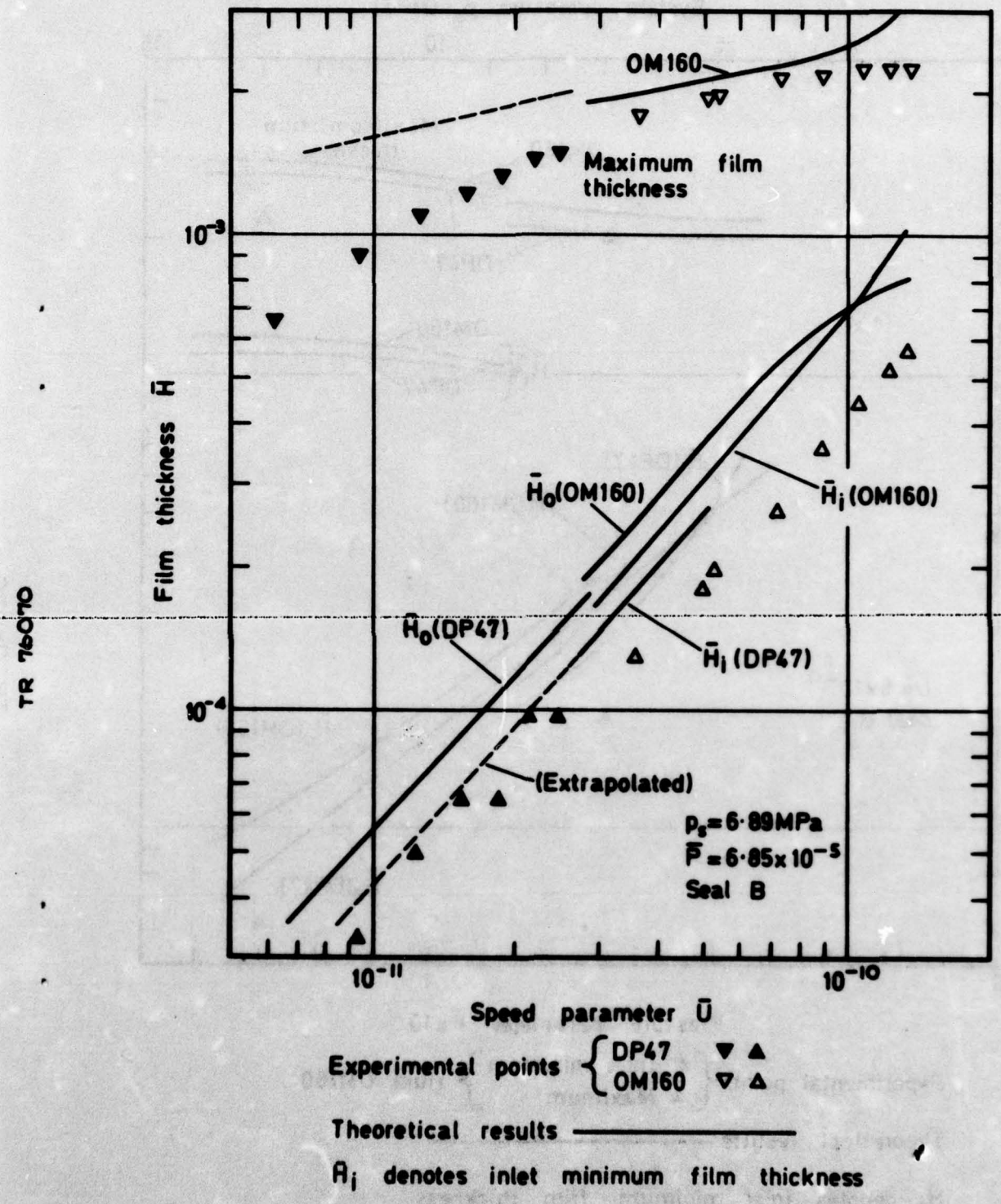

Fig. 43 Theoretical and experimental variation of film thickness with speed

Fig. 44

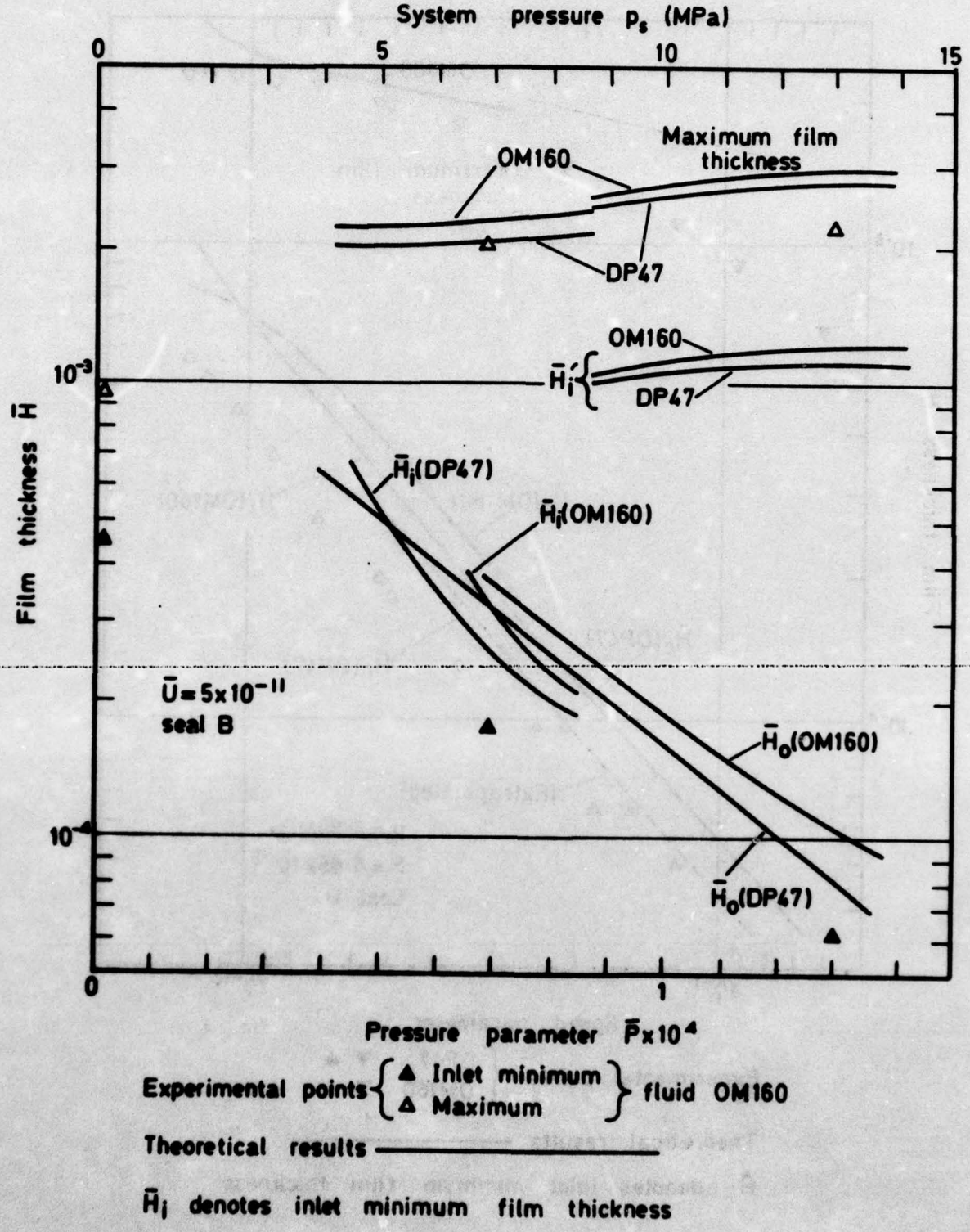

TR 76070

Fig. 44 Theoretical and experimental variation of film thickness with system pressure

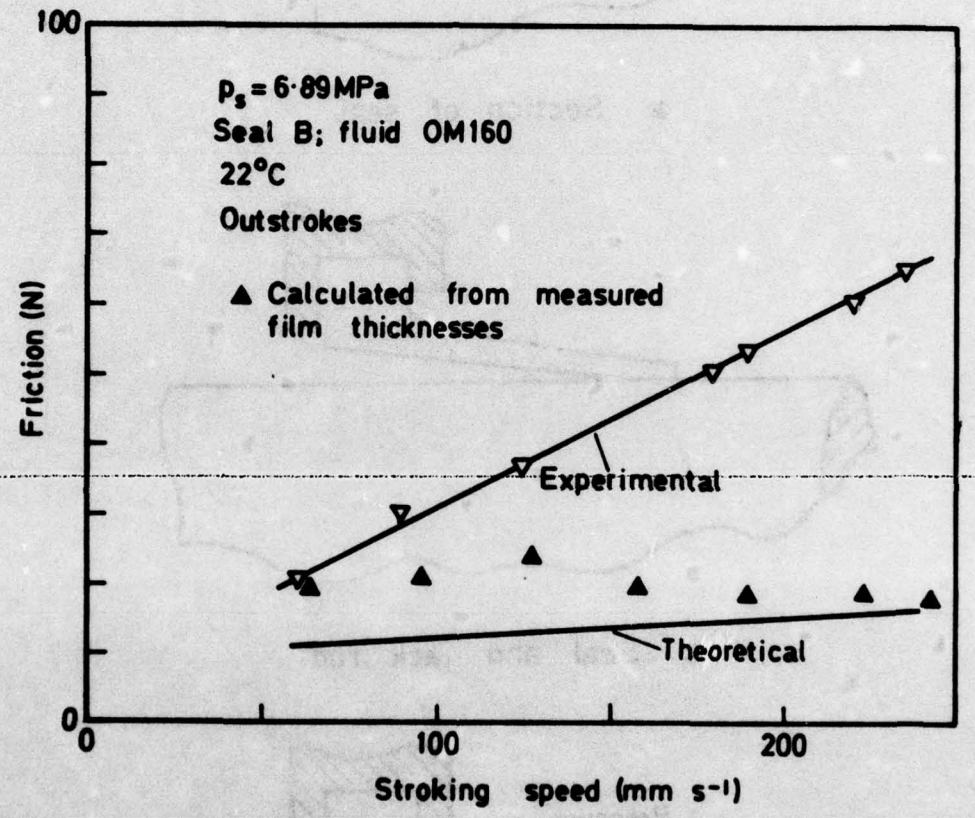

Fig.45 Theoretical and experimental variation of friction with speed

Fig. 46a–c

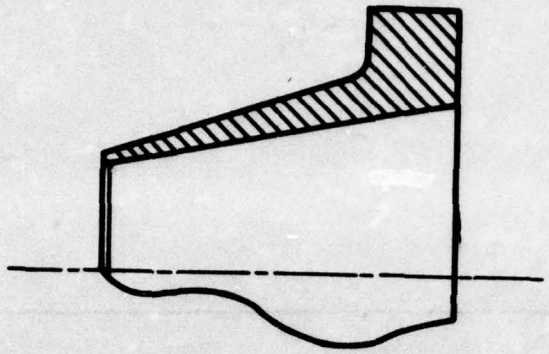

a Section of seal

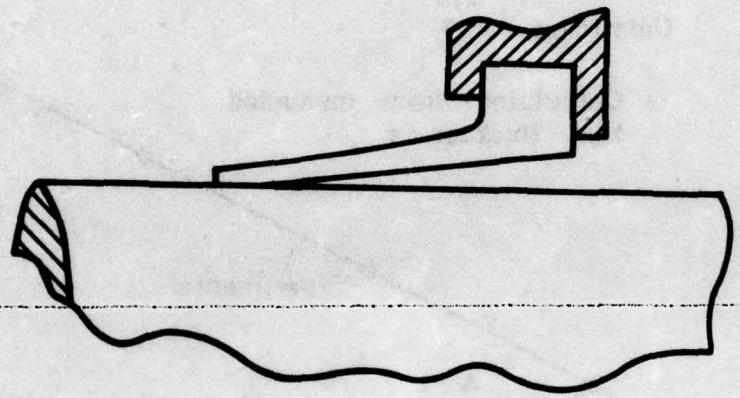

b Seal and jack rod

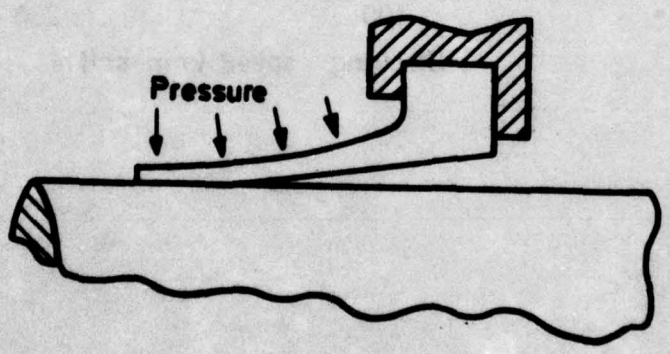

c System pressure acting on seal

TR 76070

Fig. 46a–c Improved seal design